Vol. 49 • No. 10
October 2006

Microwave Journal

Military and Government Electronics

Network-centric Operations and Information Superiority

Airborne X-band Frequency Synthesizer Design

Simple and Complex Frequency Converter Architectures

horizon house®
Founded in 1958

www.mwjournal.com

OCTOBER 2006 VOL. 49 • NO. 10

FEATURES

COVER FEATURE

TECHNICAL FEATURES

Microwave Journal (USPS 396-250) (ISSN 0192-6225) is published monthly by Horizon House Publications Inc., 685 Canton St., Norwood, MA 02062. Periodicals postage paid at Norwood, MA 02062 and additional mailing offices.

POSTMASTER: Send address corrections to *Microwave Journal*, PO Box 3256, Northbrook, IL 60065-3256 or e-mail mwj@omeda.com. Subscription information: (847) 291-5216. This journal is issued without charge upon written request to qualified persons working in that part of the electronics industry, including governmental and university installation, that deal with VHF through light frequencies. Other subscriptions are: domestic, $120.00 per year, two-year subscriptions, $185.00; foreign, $200.00 per year, two-year subscriptions, $370.00; back issues (if available) and single copies, $10.00 domestic and $20.00 foreign. Claims for missing issues must be filed within 90 days of date of issue for complimentary replacement.

Posted under Canadian international publications mail agreement #0738654

Microwave Journal

FEATURES

TECHNICAL FEATURE

TUTORIAL

PRODUCT FEATURES

DEPARTMENTS

Cover photograph by Jim Anderson courtesy of Boeing Co.

STAFF

Publisher: Carl Sheffres
Associate Publisher: Edward Johnson
Editor: Harlan Howe, Jr.
Managing Editor: Keith W. Moore
Technical Editor: Frank M. Bashore
Associate Technical Editor: Dan Massé
Staff Editor: Jennifer DiMarco
Editorial Assistant: Barbara Walsh
Consulting Editor: Howard I. Ellowitz
Consulting Editor: Peter Staecker
Consulting Editor: Dan Swanson
Traffic Manager: Edward Kiessling
Traffic Administrator: Ken Hernandez
Director of Production & Distribution: Robert Bass
Multimedia Designer: Eli Conner
DTP Coordinator: Janet A. MacDonald
Director of Marketing, Publications & Exhibition Group: David J. Metta

EUROPE

Deputy Publisher: Michel Zoghob
European Editor: Richard Mumford
Office Manager: Eugenie Hardy

CORPORATE STAFF

Chairman: William Bazzy
CEO: William M. Bazzy
President: Ivar Bazzy
Executive Vice President: Joan B. Egan
Senior Vice President: David B. Egan
Vice President: Jared Bazzy
CFO: Charles A. Ayotte

Executive Editorial Office:

685 Canton Street, Norwood, MA 02062
Tel: (781) 769-9750
FAX: (781) 769-5037
e-mail: mwj@mwjournal.com

European Editorial Office:

46 Gillingham Street, London SW1V 1HH, England
Tel: Editorial: +44 207 596 8730 Sales: +44 207 596 8740
FAX: +44 207 596 8749

www.mwjournal.com

Printed in the USA

"Ask Harlan," a technical question and answer session with Harlan Howe, Jr., an industry veteran and long-time *Microwave Journal* editor, has been a regular part of our web site (www.mwjournal.com) for almost two years now. In an effort to better combine the editorial content of our magazine with our newly developed and retooled on-line presence, we have decided to develop Harlan's RF and microwave engineering advice into a monthly feature.

How it works: Harlan has selected one question from his "Ask Harlan" column to be featured in the magazine. Please visit www.mwjournal.com/askharlan to provide an answer to this month's featured question (see below). Harlan will be monitoring the responses and will ultimately choose the best answer to the question. Although all of the responses to the featured question will be posted on our web site, we plan to publish the winning answer in the December issue. All responses must be submitted by **November 6, 2006**, to be eligible for the participation of the October question.

The winning response will win a free book from Artech House, along with an "I Asked Harlan!" t-shirt. In addition, everyone who submits a legitimate response will be sent an "I Asked Harlan!" t-shirt.

August Question and Winning Response

The August question was submitted by Larissa Marple from Virginia Tech:

Dear Harlan,

Concerning power amplifiers, what is the highest PAE recorded and what design type achieved that efficiency?

The winning response to the August question is from Robert Kim of Newgen Telecom:

To compare any design method or spec items like PAE, you need to consider other various factors such as operating voltage, operating frequency, modulation type, cost, size, etc., or the comparison may be meaningless because you are talking about two totally different things. If we focused on PAE by ignoring other factors, however, it seems to be 92% with Po=+23 dBm at 3.25 GHz using a pHEMT device with class-E topology, which I read in the April 2004 issue of *RF Design* magazine entitled "Broadband Monolithic S-band Class-E Power Amplifier Design" by Reza Tayrani from Raytheon. Except for Tayrani's work, there have only been a couple of other works involving X-band frequencies that I know of, and they demonstrated relatively poor efficiency, which was around 60% or something, as compared to the expected theoretical 100% efficiency with class-E. As for class-E topology, it was known that Sokal first presented this technique in 1975, and demonstrated 96% PAE at VHF band, but I would put my bet on Tayrani's work considering its operating frequency and impressive high PAE of 92%.

Harlan's response:
A number of people have reported practical PAEs of 60% to 70% at microwave frequencies using class-E topology. For the highest reported number, please see the reader's answer above.

This Month's Question of the Month

(answer on-line at www.mwjournal.com/askharlan)

Arun Kumar has submitted this month's question:

Dear Harlan,

I am involved in Schottky diode mixer design at microwave frequencies. For accurate design, I want to characterize the diode with the help of the text fixture and network analyzer. As the junction resistance varies with LO power level for characterization of the diode how much LO power should I give? Some literature says that the LO power should be such that the rectified current from the diode is in the order of 1 to 1.5 mA. How then should I measure the rectified current through the diode, which is mounted in the test fixture? Please help.

If your response is selected as the winner,
you'll receive a free book of your choice from Artech House.
Visit the Artech House on-line bookstore at www.artechhouse.com
for details on hundreds of professional-level books in microwave engineering and related areas
(maximum prize retail value $150).

CALL FOR PAPERS
IEEE MTT-S International Microwave Symposium
by December 1, 2006

OCTOBER

RADIOTECC 2006
October 18–19, 2006 • Berlin, Germany
www.gerotron.com

28TH ANNUAL SYMPOSIUM OF THE ANTENNA MEASUREMENT TECHNIQUES ASSOCIATION (AMTA 2006)
October 22–27, 2006 • Austin, TX
www.amta.org

NOVEMBER

EUROPEAN CONFERENCE ON ANTENNAS AND PROPAGATION (EUCAP 2006)
November 6–10, 2006 • Nice, France
www.congrex.nl/06a08

DALLAS BASESTATION CONFERENCE
November 7–9, 2006 • Dallas, TX
www.avrenevents.com/dallas2006/

IEEE COMPOUND SEMICONDUCTOR IC SYMPOSIUM (CSICS 2006)
November 12–15, 2006 • San Antonio, TX
www.csics.org

ELECTRONICA 2006
November 14–17, 2006 • Munich, Germany
www.electronica.de

MM-WAVE PRODUCTS AND TECHNOLOGIES
November 16, 2006 • Savoy Place, London
www.iee.org/events/mmwave.cfm

68TH ARFTG CONFERENCE
Nov. 28–Dec. 1, 2006 • Broomfield, CO
www.arftg.org

DECEMBER

IEEE WIRELESS AND MICROWAVE TECHNOLOGY 2006 (WAMICON 2006)
December 4–5, 2006 • Clearwater, FL
http://wamicon.eng.usf.edu

INTERNATIONAL ELECTRON DEVICES MEETING
December 11–13, 2006 • San Francisco, CA
www.his.com/~iedm

ASIA-PACIFIC MICROWAVE CONFERENCE (APMC 2006)
December 12–15, 2006 • Yokohama, Japan
www.apmc2006.org

JANUARY

IEEE RADIO AND WIRELESS SYMPOSIUM (RWS 2007)
January 9–11, 2007 • Long Beach, CA
www.radiowireless.org

IEEE TOPICAL WORKSHOP ON POWER AMPLIFIERS FOR WIRELESS COMMUNICATIONS (PA WORKSHOP)
January 8–9, 2007 • Long Beach, CA
http://paworkshop.ucsd.edu

7TH TOPICAL MEETING ON SILICON MONOLITHIC INTEGRATED CIRCUITS IN RF SYSTEMS (SIRF 2007)
January 10–12, 2007 • Long Beach, CA
www.ece.wisc.edu/sirf07

WCA INTERNATIONAL SYMPOSIUM AND BUSINESS EXPO
January 16–19, 2007 • San Jose, CA
www.wcai.com

FEBRUARY

IEEE INTERNATIONAL SOLID-STATE CIRCUITS CONFERENCE (ISSCC 2007)
February 11–15, 2007 • San Francisco, CA
www.isscc.org/isscc/

APRIL

IEEE RADAR CONFERENCE 2007
April 17–20, 2007 • Waltham, MA
www.radar2007.org

JUNE

IEEE MTT-S INTERNATIONAL MICROWAVE SYMPOSIUM AND EXHIBITION
June 3–8, 2007 • Honolulu, Hawaii
www.ims2007.org

Workshops & Courses

"Leading Insight" Application Workshops

■ **Topics:** Ansoft's "Leading Insight" Application Workshops for High Performance Design provide attendees with an excellent opportunity to exchange ideas and learn from experts in the design of high performance electronics. Presentations and interactive poster sessions by invited speakers together with Ansoft's technical staff will cover: IC design and verification; signal- and power-integrity simulation; RF, microwave and antenna design; and advanced packaging, SIP and SOC design.
■ **Sites:** Asia, North America, Europe
■ **Dates:** Oct. 17–Dec. 5, 2006
■ **Contact:** For more information, visit www.ansoft.com/leadinginsight/papers.cfm.

COMSOL Users Conferences

■ **Topics:** Two conferences in the US (along with 14 others throughout the world) combine hands-on training along with presentations from users and COMSOL technical staff. Attendees will learn about the latest COMSOL products, discover the expanding range of applications possible with COMSOL Multiphysics, while making contacts and getting hands-on training.
■ **Sites:** Boston, MA; Las Vegas, NV
■ **Dates:** Oct. 22–24/26–27, 2006
■ **Contact:** For more information, visit www.comsol.com/conference/2006.

Design Troubleshooting, Failure Analysis and Prevention in Electronic Circuits

■ **Topics:** This course covers techniques for troubleshooting design problems both in the laboratory and in field installations. Each technique is discussed in depth, including how to apply it and how to interpret results. Participants learn how to locate and deal with the sources of noise that cause problems in designs, including noise-related reliability problems in system, board and device design. For more information, visit www.unex.berkeley.edu.
■ **Site:** San Francisco, CA
■ **Date:** October 26, 2006
■ **Contact:** UC Berkeley Extension, 1995 University Avenue, Berkeley, CA 94720 (510) 642-4151 or e-mail: course@unex.berkeley.edu.

Far-field, Anechoic Chamber, Compact and Near-field Antenna Measurements

■ **Topics:** This course presents the state-of-the-art in antenna measurements, including far-field, anechoic chamber, compact and near-field measurements. The course also includes range evaluation and compensation techniques and microwave holography. For more information, visit www.pe.gatech.edu.
■ **Site:** Atlanta, GA
■ **Dates:** November 6–10, 2006
■ **Contact:** Georgia Institute of Technology, Professional Education, PO Box 93686, Atlanta, GA 30377 (404) 385-3500.

Reverberation Chamber Theory and Experiment Short Course

■ **Topics:** This course is designed for engineers and technicians who will be involved in radiated emission or immunity testing of commercial or military systems using reverberation chambers. The theory portion will cover the statistical nature of reverberation chamber testing. The experiments include typical measurement techniques, calibration, immunity, emission and pulse testing in reverberation chambers.
■ **Site:** Stillwater, OK
■ **Dates:** November 13–17, 2006
■ **Contact:** For more information, visit http://rc-course.okstate.edu.

Microwave Measurements for Emerging Technologies

■ **Topics:** This 1½ day course covers microwave measurement fundamentals, including vector network analysis, scattering parameters, power and thermal noise. Practical issues such as cables, fixtures, probes and on-wafer measurements are covered. More advanced measurement topics are also covered including microwave measurements for optoelectronic applications and scattering-parameter uncertainty analysis. For more information, visit www.arftg.org.
■ **Site:** Broomfield, CO
■ **Dates:** November 28–29, 2006
■ **Contact:** David Walker, NIST, M.S. 813.01, 325 Broadway, Boulder, CO 80305 (303) 497-5490 or e-mail: dwalker@boulder.nist.gov.

ELECTRONICA 2006 PREVIEW

From **14–17 November** the **New Munich Trade Fair Center** will be the meeting place and communications platform for the global electronics industry as it opens its doors for *electronica 2006*. The sector's premier global event and world's leading trade show for electronics covers the complete spectrum of electronics and showcases the latest trends and developments. *electronica 2006* has the tagline-Components, Systems and Applications-emphasising the fact that although the event is focused on components and systems it also recognises the importance of the increasingly wide range of applications where electronics are being employed.

As regulars to this biannual event will know it is vast and a visit takes some planning, so hopefully this preview will be of help. Occupying 152,000 m^2 of floor space across 14 halls, more than 3000 exhibitors will be presenting their latest products and system solutions. The organizer is expecting to welcome over 75,000 electronics professionals with a strong international mix and build on *electronica 2004* when the percentage of international exhibitors climbed to 57 percent and the number of international attendees rose to 44 percent.

The event encompasses the full range of electronics components and systems currently available and under development, including semiconductors, power supplies, interconnection devices, and test and measurement equipment. It will also focus on emerging technologies and high growth applications in the automotive, wireless, embedded systems, and microtechnology and nanotechnology sectors by offering clusters within the trade show halls with dedicated exhibition areas including topic-oriented platforms for speaker presentations.

ELECTRONICA WIRELESS

Comprising the Wireless Congress 2006: Systems & Applications (15–16 November in the International Congress Center Munich), the forum and the exhibition in Hall A4, 'electronica wireless' will present the latest wireless technologies and applications. The congress will be examining all the technical aspects of current and future wireless technologies, focusing specifically on industrial applications. It will also provide an insight into the latest applications, security aspects, certification and approval problems, and measurement technology, along with standards and market opportunities.

ELECTRONICA AUTOMOTIVE

At the electronica automotive Conference (13–15 November at the ICM), in the forum and in the exhibition area in Hall A6, 'electronica automotive' will present the latest developments, innovations and trends in automotive electronics. Carmakers, their suppliers and international manufacturers of automotive electronics components will present state-of-the-art products and outline visions for the future.

ELECTRONICA EMBEDDED

Hot topics from the world of embedded technology will be presented at the electronica embedded Conference Munich (14–15 November at the ICM), in the forum and in the exhibition located in Hall A6. The exhibition has expanded again this year, with software playing a significant role. The main focus will be on embedded software engineering, embedded test and verification, small embedded systems (8 and 16 bit) and complex embedded systems.

ELECTRONICA MICRONANOWORLD

The industry platform for microtechnology and nanotechnology is 'electronica MicroNanoWorld,' which will be making its debut at electronica. It will use the exhibition in Hall A2 and forum to spotlight components, systems and applications based on microtechnology and nanotechnology. Topics include RF-MEMS, optical MEMS and bio-MEMS, packaging for MEMS and microsystems as well as MEMS sensor technology, micromotors, micropositioning and microtransmissions. Also, the co-located Multicore Conference (14–15 November at the ICM) will be covering the topic of multicore technology.

In summary, *electronica 2006* covers all sectors of the electronics industry in what is the world's leading trade fair featuring the industry's major players. It also offers complementary conferences, practice-oriented user forums and panel discussions. So, if it's electronics you are interested in then *electronica 2006* is the place to be. For more information, visit: www.electronica.de.

electronica 2006
components | systems | applications

EVENT DETAILS

electronica 2006 — Components, Systems and Applications
Venue: The New Munich Trade Fair Center, Munich, Germany
Dates: Tuesday 14 November to Friday 17 November
Opening Hours: 09.00 to 18.00 daily

CONFERENCES

Venue: International Congress Center Munich (ICM)

By logging onto:
www.global-electronics.net/id/23514/cubesig/404f9bc662f07e6f12ea0310e49d9972 and pre-registering you will be able to:

- Save on the price of admission to the fair.
- Receive a free ticket for use on all Munich public transport to the Trade Fair Center valid on the day(s) of your visit.
- Plus the opportunity to enter a draw offering the top prize of a weekend with a Jaguar E-Type worth approximately €850!

Network-centric Operations and Information Superiority: Current Trends of Key Enabling Technologies

Defence and security authorities around the world are presently pursuing the idea of Network-centric Operations as the key to efficiently identifying and fighting potential threats. For defence applications this is well accepted, but now civil governmental organisations are also using this approach for security applications. The basic idea is to network the available resources and combine the collective capabilities. The enabling elements include: a high performance information grid with access to all appropriate sources; actors/weapons and other countermeasures with speed of response and high precision; automated command and control (C2) processes enabling high speed decision making and assignment of resources; and integrated sensor grids closely coupled in time to the command and control processes and actors/weapon systems. ***Figure 1*** shows Network-centric Operations building on information grids.

Since information gathering forms the basis and the start of the decision making process, sensors play a vital role in employing the concept of Network-centric warfare. The decisive trends in this field will be considered later in this article, together with the equally important subjects of data processing, communications and electronic warfare. In all phases advanced electronics provides the basis for enabling these capabilities.

RADAR SENSORS

When it comes to all weather sensing, radar systems are the most important sensors for any platform. The emergence of compact MMIC technology in the '90s has lead to a revolution of radar systems with regard to capabilities and architecture—the Actively Electronically Scanned Array (AESA) radar. In Europe the AESA radar technology was initially developed and demonstrated in the AMSAR[1] program. Operational evidence is proven in high resolution Synthetic Aperture Radar (SAR) such as the multinational SOSTAR,[2] with excellent results, and the launch of AESA SAR for space is imminent with the TerraSAR[3] satellite. Today, the fourth generation of radar front-end technology is being used in radars such as the CAESAR prototype, a compact multi-function fighter radar.[4]

Typically, AESA radars are based on a fully modular architecture—the antenna contains several thousands of transmit/receive modules (TRM)—and consists of a number of identical modules, including exciters and processors. All active RF components are solid state and have a much higher intrinsic reliability than conventional HVT (high voltage tubes)-based

Heinrich Daembkes
EADS Defence Electronics

Fig. 1 Network-centric Operations building on information grids (illustration: EADS).

pulse-Doppler radars. The result is significantly enhanced availability (> factor of 10) due to higher reliability in conjunction with graceful degradation.

Besides the architectural benefit, equally important is that AESA radars offer a new class of operational capabilities such as the highest flexibility in beam scanning and beam forming. GaAs TRMs generate typically 46 dBW of radiated power per square meter of antenna area. In conjunction with very thin antenna arrangements (allowing typically larger antennas), AESA radars have the highest power-aperture product of any radar system, supporting the detection of very small objects at large ranges. Some of the present limitations of GaAs concerning maximum output power and incident damage power will be overcome by the gallium nitride (GaN) components, presently under development.[5]

Power levels up to 20 W per HPA will become feasible for multi-octave bandwidths up to 20 GHz, while for narrow band X-band the 50 W level becomes realisable. The high energy band gap of GaN will also enable the operation of amplifiers at high supply voltages, reducing some of the present operational constraints. For switches recent results of RF MEMS switch technology have shown very low insertion loss and high isolation with multi-octave performance. This technology may be used for SPDT switches and phase shifters, for example, in SAR and seeker head applications.

Besides the superior equivalent incident radiated power (EIRP) AESA radars offer very large RF bandwidths (> 1 GHz), quasi-instantaneous beamsteering and fully digital beamforming.[6] In Homeland Security missions, AESA airborne surveillance radars can provide SAR image resolutions down to < 30 cm in all weather conditions. As an example, ***Figure 2*** shows a high resolution radar image taken with X-band radar.

Another key feature is the potential for aperture sharing and concurrent operation—for example, simultaneous SAR and Moving Target Indication (MTI)—for searching different directions simultaneously. Besides airborne applications, AESA radars are also being used on ships such as the German frigate F 124 APAR,[7] for ground applications (MEADS)[8] and space borne platforms (TerraSAR and TanDEM-X).

The long-term trend will lead us to radar sensors which can be more highly integrated into airborne structures allowing for wide field-of-view and also to a multi-function sensor which can be shared between radar, communication and EW tasks. Targeted are planar (1D) or conformal (2D) active antenna arrays with very low installation depth and a low number of RF and mechanical interfaces at a small antenna curve radius.

Figure 3 shows a standardized modular transmit/receive module as employed in today's AESA applications. A key element of this architecture is a very small tile-type transmit/receive module (module size for X-band: 15 × 15 × 5.6 mm) comprising the complete

▲ *Fig. 2 High-resolution radar image taken with an X-band radar (photo: EADS).*

▲ *Fig. 3 Standardized modular transmit/receive module as employed in today's AESA applications (photo: EADS).*

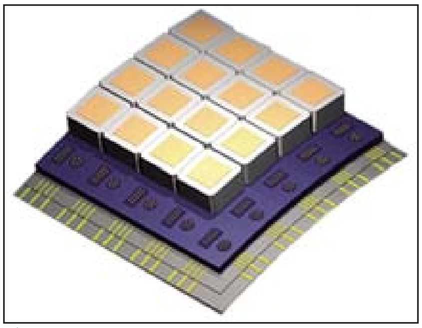

▲ *Fig. 4 Advanced T/R modules applied to 2D curved structure integrated antennas (drawing: EADS).*

TRM, control electronics and radiating element.[9] These antennas will fit perfectly in the outside skin of complex structures such as an aircraft even at positions that could not be utilised before (for example, wings, gear, fin or cabin), while at the same time avoiding increasing the radar cross section. Advanced T/R modules applied to 2D curved structure integrated antennas are shown in ***Figure 4***.

DATA LINKS

Data links are the vital interconnects between the different elements of the network. Typically, wireless links are used alongside fixed installations and, from the RF-point of view, require similar technologies as described earlier. The upcoming UAV applications will crucially depend on them. The technical trend in this field is also towards total digitalization. This will affect the signal processing part first, but also very quickly the HF-front-end too. The digital-analogue transition is moving close to the antenna front-end[10] and this will enable waveforms, protocols and applications which are not currently feasible.

One of the keywords is Software Defined Radio (SDR)[11] based on a defined Software Common Architecture (SCA). This approach must be combined with very capable, flexible, digital programmable and very wideband HF hardware. The latter is not yet in place. The spectrum to be covered in the future will need to be from 2 MHz up to the high gigahertz region (more than 60 GHz). This is quite a challenge as the power needed will be over 200 W at low volume and weight.

A very good performing example of today's state-of-the-art is the MIDS Link 16 power amplifier of the Multi-functional Information Distribution System-Low Volume Terminal (MIDS-LVT), an advanced Link-16 command, control and communication (C^3) system.[12]

A further challenge for data links is to provide secure protected communication and to combine more than one data link. This task has been solved in the Wideband Protected Data Link (WPDL), which is operational in the German Kleinfluggerät ZielOrtung (KZO) drone and in the French System Intermédiaire de Drone MALE (SIDM).[13] It combines a wideband link up to 10 MHz and a highly secured command and control data link. Both are uniquely protected by a smart combination of various methods and inherently organize themselves, including the steering of the directed antennas and the GPS-independent localisation of the drone.

With regards to the industrialization and production of data links, three aspects are of particular relevance: limitations due to the International Traffic in Arms Regulations (ITAR), obsolescence of components and the emerging materials. Due to ITAR it will be important for the Europeans to have access to all crucial parts themselves. This is particularly valid as communications move to higher frequencies like Ka-band. Regarding obsolete components there will be a convergence of commercial and military technologies, provided that the emerging market can offer enough and suitable standard components. Finally, modern materials like GaN and SiGe need to be mastered at the series production level.

ASSESSING ELECTRONIC THREATS

Significant changes are emerging in the field of electronic warfare. Postulated scenarios during the Cold War assumed a sophisticated threat from radar-guided weapons, both surface-to-air and air-to-air. Today's asymmetrical warfare scenarios, however, generally assume that an organized, long-range radar-controlled air defence system can quickly be rendered ineffective by a combination of stealth, heavy jamming and physical attack. Once air superiority is achieved, the only air defence assets available to the asymmetrical enemy are those that can be easily concealed and constantly moved around to avoid detection. Typically, such assets will be highly mobile radar-directed SAMs and AAA backed up by larger numbers of EO-guided weapons. Similar scenarios are unfortunately also valid for homeland security and therefore require comparable systems.

In these scenarios, electronic warfare has three major roles:

- to provide blanket, detailed and real-time battlefield data on the enemy's actions and intentions, including all kinds of intelligence, especially communications intelligence (COMINT).

▲ *Fig. 5 EHEP sensor on Global Hawk UAV (photo: EADS).*

- to completely deny the enemy the full or selective use of the electromagnetic spectrum for target detection, weapon guidance and especially for communication.
- to provide own forces with a highly reliable self-protection in the event of a successful weapon launch.

In the asymmetrical and especially security related scenario only selective use of these roles may apply, that is, only very selected domains of the EM-spectrum have to be surveyed or to be made unusable.

ELECTRONIC SURVEILLANCE

The task of electronic surveillance is increasingly being taken over by unmanned aircraft. Thanks to the bandwidth and range of modern data links, the Signal Intelligence (SIGINT) operators can directly control the aircraft receivers in the complete safety of their ground station, no matter how dangerous the mission. An example of such a system is the EADS EHEP sensor shown in a prototype form on the Northrop Grumman GlobalHawk UAV[14] in ***Figure 5***. In its operational configuration, this sensor represents an extremely wideband, long-range ELINT/COMINT surveillance asset that can be rapidly deployed anywhere in the world.

ELECTRONIC ATTACK

Electronic jamming of hostile radar sensors is an essential element of any Suppression of Enemy Air Defence (SEAD) strategy. Currently, in the West only the US seems to have significant RF jamming assets in the form of the EA-6B Prowlers, which themselves are nearing the end of their operational life. Because of this, several NATO countries are actively pursuing independent Stand-off Jammer (SOJ) programs based on fighter aircraft, business jets or transport aircraft platforms.

The core of any modern SOJ is a wideband, multi-bit Digital RF Memory (DRFM) capable of following even the most agile radar threat radar. Modern DRFM technology allows multi-gigahertz bandwidth to be achieved with integrated technique generation in small and economical packages. One core element here is the availability of high speed broad bandwidth ADCs. Today 10-bit resolution at 3Gs/s are state-of-the-art.[16]

Equally important is the transmitter system, which determines the range, number of simultaneous threats and the jamming effectiveness of the SOJ. In the past, vacuum tube technology was the only real option available, but today, solid-state broadband phased arrays based on GaN power sources offer an attractive alternative targeting the > 100 W output level. ***Figure 6*** shows the development of output power versus time for single MMICs, with an inset photo of a 23 W GaN MMIC.

ELECTRO-OPTICAL SELF-PROTECTION: UV AND IR TECHNOLOGIES

Today, IR-guided weapons constitute the most serious threat to any aircraft, military as well as civil. Not only are they highly survivable even in an unsymmetrical conflict, but they have also proliferated all over the world and are now in the hands of many terrorist and insurgent forces.

The key to effective IR missile protection is a reliable missile warning system capable of controlling flare dispensing or an IR jamming turret. There are three missile warning technologies: RF detection using pulse-Doppler radar; UV detection of the missile plume; and IR detection of the missile plume. Radar-based warning systems have the advantage of providing time-to-go measurement, but they generally lack the spatial coverage and angular precision of optical warners.

UV missile warners are most widely used due to their low cost, compact construction and relative freedom from false alarms. An example of this type of warner is the MILDS AN/AAR-60 UV warner currently in worldwide operation on many different types of helicopter and fixed-wing aircraft. This detector works by looking for the UV component radiated by the missile plume in the solar-blind region. The main advantage of this approach is that there is practically no natural background interference in this band that can cause false alarms. As an example, ***Figure 7*** shows the MILDS AAR-60 missile warner in the NH90 configuration.

Although UV warners are adequate for most applications, potentially longer ranges can be achieved by detecting the much stronger IR component in the missile signature. In the past, the achievable performance of IR warners was limited by strong IR background clutter caused by the sun, fires, explosions and so on. Extracting the missile signature in this environment requires very high sensor resolution and enor-

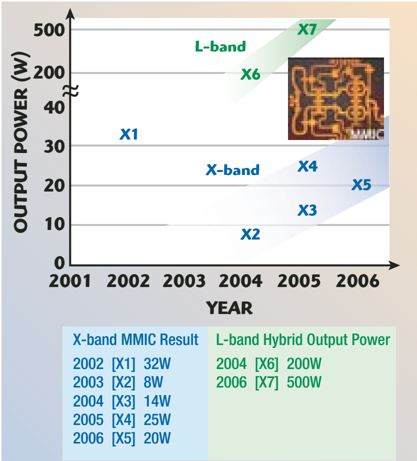

▲ *Fig. 6 Development of output power vs. time for single MMICs (inset photo of 23 W GaN MMIC) (illustration: EADS).*

▲ *Fig. 7 MILDS AAR-60 missile warner in the NH90 configuration (photo: EADS).*

mous computing power. Recent advances in both computing power and sensor technology have triggered several IR missile warner programs, perhaps the most advanced of which is the French/German MIRAS multi-colour IR warner for the A400M transport aircraft. These new-generation warning systems have the potential to exploit the range advantages of IR detection while at the same time achieving a very low false alarm rate.

LASER WARNING

Laser-guided missiles are of great concern especially to air forces because they are growing in proliferation and virtually immune to known countermeasures. Platform survivability can, however, be greatly increased by warning the crew of laser illumination in time for them to take evasive countermeasures.

Laser warning systems must combine high sensitivity with an extremely large dynamic range. They must also be capable of detecting even single pulses and indicating the threat bearing with a high degree of precision. A particular problem for laser detectors is that of multiple reflections which can falsify the angle measurement of the actual pulse. Many different concepts have been implemented to solve these problems, ranging from diode arrays to delay-line detectors. A newer and more precise measurement method is provided by the Harlid detector,[15] which is capable of dual-band detection and high precision angle measurement in a single, compact TO5 housing.

ACTIVE IR COUNTERMEASURES

Directed IR Countermeasures (DIRCM) represent a highly effective counter to IR-guided missiles. Both lamp-based and laser-based DIRCM systems are available or in development. Compared with flares, these systems are covert, effective against most missile countermeasures and have an essentially unlimited reload capability.

DIRCM systems rely on a missile warning system to perform initial detection and hand off the threat to a jamming turret. This turret then illuminates the missile seeker with a suitably modulated, high power IR beam, which induces an error into the missile tracking system. To be effective against the newest generations of staring missile seekers, a DIRCM must be capable of both multi-spectral jamming and very high power on target, in order to saturate or even physically damage the sensor element. This approach has been extensively investigated in the frame of the French/German FLASH DIRCM program.[17]

COMPUTERS: THE DIGITAL HEART

In every case, the managing and controlling element of all the systems that have been mentioned in this article is a computer. Depending on the application, different names are used, such as controller, avionics computer, or signal/data processor. For all 'mobile applications' the key requirement besides the computing performance is the power consumption and the heat removal concept. In many applications the limits of available technologies are stressed, requiring sound compromises between hardware capability and software solutions.

With the effort being put into software (SW) development currently easily exceeding that being put into hardware (HW), architectures with a fixed interface ('API') between application SW and HW-related SW is becoming standard. This allows users to transfer existing code from one platform to the next, which is especially pertinent with regards to the very short lifetime of Commercial Off The Shelf (COTS) components.

Specific trends today are:

- the transfer of as much functionality as possible into one computer while demanding a very high reliability, which requires a very low temperature inside the computer.
- the use of standardized, but very high performance COTS components to comply with the system requirements. Due to cost reasons and the short lifecycles of leading-edge technologies specific computer chip developments are avoided and benefit is taken from the power of other driver markets. Today the game market is dominant with unprecedented performance.
- increasingly demanding certification rules for safety critical systems, such as aviation or traffic applications. Civil certification standards are entering the military field, for example with the A400M program. Wherever possible, standardized and certified but modular solutions are preferred, leading to families such as Modular Mission Avionic Computers (M^2AC).

Very high end performance computers are being developed for the processing of high speed, high volume data, like the radar computer for the Eurofighter (CAPTOR). They are typically realized as array or cluster computers based on ruggedized standard processor chips. Here particularly, the multi-core processor chips of the new game generations will have a strong impact. Environmental impacts like radiation effects or single electron upset (SEU) events are, however, establishing very severe barriers for the use of technologies with line widths below the 120 nm range. New protection or correction mechanisms will be required and are under development.

CONCLUSION

Gaining information superiority is heavily based on the use of leading-edge technologies. This comprises all areas of electronics: From advanced high frequency materials and circuits to new integrated antenna structures, optical sensors and actors from IR up to UV, digital hardware from simple digitalisation up to highest end ADCs with the continuous need for even more performance, including signal processing and medium to high end computing performance. This, together with the refinement of algorithms and advanced software technologies, has lead to a new generation of networked systems offering unprecedented capabilities. It also means that the effort for research and development as well as for the industrial implementation of these achievements, that is, the ability to manufacture these new systems in a reliable and cost-efficient way, will grow tremendously. As a consequence, increasingly, only companies with a broad technology basis—and the economical power to sustain it consistently—will be able to take the lead in driving technology. ■

ACKNOWLEDGMENTS

Without the contribution of the following colleagues this article would not exist:

H.P. Feldle, C. Hamilton, H. Brugger, A. Bader, L. Belz, U. Pietzschmann, A. Domann, W. Neuhaus and U. Schneider.

References

1. H. Hommel and H.P. Feldle, "Current Status of Airborne Active Phased-array Radar Systems and Future Trends," *Proceedings of the European Radar Conference EuRAD 2004*, Amsterdam, The Netherlands, October 11–15, 2004, pp. 121–124.
2. M. Kirscht, "Core Electronics for SOSTAR-X," *Proceedings of the 5th European Conference on Synthetic Aperture Radar*, Ulm, Germany, May 25–27, 2004.
3. R. Werninghaus, "The TerraSAR-X Mission," *Proceedings of the 6th European Conference on Synthetic Aperture Radar*, Dresden, Germany, May 16–18, 2006.
4. W. Holpp, "The Future of Radar has Begun," *Military Technology*, Issue 7, 2006, pp. 100–102.
5. P. Schuh, et al., "20 W GaN HPAs for Next Generation X-band T/R-Modules," *Proceedings of the IEEE IMS*, San Francisco, CA, 2006.
6. M. Younis, C. Fischer and W. Wiesbeck, "Digital Beamforming On-receive-only for Radar Applications," *Proceedings of the German Radar Symposium*, Bonn, Germany, Sept. 3–5, 2002, pp. 213-217.
7. A.B. Smits and P. v. Genderen, "The APAR Multi-function Radar-system Overview," *Proceedings of IEEE International Symposium on Phased-array Systems and Technology*, October 14–17, 2003, pp. 241-246.
8. www.defenseindustrydaily.com/2005/06/34b-development-contract-signed-for-meads/index.php.
9. R. Rieger and H.P. Feldle, "Advanced T/R Module Technology for SAR Applications," *Proceedings of the 6th European Conference on Synthetic Aperture Radar*, Dresden, Germany, May 16–18, 2006.
10. I. Aoki, et al., "Fully integrated CMOS Power Amplifier Design Using the Distributed Active-transformer Architecture," *IEEE Journal of Solid-State Circuits*, Vol. 37, No. 3, March 2002, pp. 371–383.
11. COMMON STAFF TARGET (CST) for the Tactical Communications-Software Defined Radio; Lt. Col. Zimmermann, 5th Draft, 16 May 2006.
12. I. Aoki, et al., "A Fully Integrated 1.8 V, 2.8 W, 1.9 GHz CMOS Power Amplifier," *Radio Frequency Integrated Circuits (RFIC) Symposium*, June 2003, pp. 199–202.
13. "AV Data-links, Tasks, Types, Technologies and Examples," North Atlantic Treaty Organization (NATO), Research and Technology Organization (RTO), RTO Educational Notes 9 (*Development and Operation of UAVs for Military and Civil Applications*), April 2000.
14. EuroHawk Nordholz Demonstration: "Global-Hawk Passes German Test," Flight International, 11 November 2003; "Global Hawk Completes German Tests," *Jane's Defence Weekly*, 12 November 2003.
15. E.G. ALTAS, EADS Product Brochure, "ALTAS 2Q-Advanced Laser Threat Alerting System, 2 Quadrant," August 2005.
16. EADS Internal Development Using SiGe Technology.
17. EADS Product Brochure, "Flying Laser Self-defence Against Infrared Seekerhead Missiles," April 2006.

Prof. Dr.-Ing. Heinrich Daembkes *studied electrical engineering at the Technical University in Aachen, Germany. After a short period as a young design engineer at Telefunken Radio and TV Systems he took a position at Duisburg University, where he worked on GaAs-based FETs and HEMTs. In 1983 he received his PhD degree on this topic (summa cum laude). Then he started a research career at the AEG Research Centre in Ulm, Germany, working on InP HBT-based optoelectronic receiver ICs, followed by GaAs and SiGe-based technologies and ICs. Until 1996 he was vice president for high frequency electronics at Daimler Research Centre with responsibility for advanced high frequency semiconductor technologies (SiGe, GaAs, InP), optoelectronics, packaging and mm-wave radars. In parallel with this he also became professor at the University of Ulm in 1995. A year later he became a co-founder and CEO of United Monolithic Semiconductors (UMS), a joint venture between Thales and EADS on GaAs-based MMICs, which he turned into a successful commercial enterprise. Since 2003 he has been with EADS Defence Electronics, where he is presently vice president of system and software engineering. He is also active in several organizations including the IEEE and EuMA.*

Harris Corp. Team Achieves Milestone in FAA Telecommunications Program

Harris Corp. announced that it has completed the installation and check out of all the equipment and services required for the transition of 24 major hubs to the new FAA Telecommunications Infrastructure (FTI) network. The transition moves an important portion of voice communication, flight data and weather information to the safest and most secure network operating within the civil sector of the US government. Harris will continue to transition the remaining 137 legacy network hubs to the more cost-effective FTI network over the next 18 months.

"The conversion of these major hubs from the legacy network to FTI will help the FAA more rapidly achieve its safety, security and cost-saving goals for the program," said John O'Sullivan, FTI program vice president for the Harris Government Communications Systems Division. "We specifically targeted some of the largest hubs for upgrading this quarter and will continue to convert other sites—many of which are located at major FAA locations—as we complete the transition to the more modern, more efficient FTI network. These network hubs are located near major metropolitan areas such as Seattle, Atlanta, Minneapolis/St. Paul, Denver and Washington DC."

The FAA has already issued disconnect orders for 14 of the 24 legacy network hub sites and is positioned to issue orders for the remaining 10 sites in accordance to its goal for the current year. Legacy network hubs carry circuits that support 90 percent of the FAA facilities to be upgraded through the FTI program. Targeting the replacement of these network hubs will accelerate the conversion of the more costly legacy circuits to FTI, generating millions of dollars in savings to the FAA. The FTI network also features enhanced safety and security, providing intrusion detection and a security feed directly to the FAA security center for seamless security threat assessment.

During the 15-year FTI program, Harris is upgrading and improving telecommunications and operations functions at more than 4400 FAA facilities nationwide, providing the FAA with a safer, more efficient network that is expected to save hundreds of millions of dollars in operating costs over the life of the program. FTI equipment has now been installed and accepted at more than 1650 FAA facilities and more than 7000 operational services have been accepted and are in service nationwide. Harris remains committed to completing the work associated with all major nodes by December 2007.

Harris is leading a team of top telecommunications companies consisting of AT&T, BellSouth Corp., Qwest Communications International, Sprint, Verizon Communications and Raytheon Technical Services. The team is consolidating the services carried on FAA legacy networks including the Leased Interfacility National Airspace System (LINCS), the Data Multiplexing Network, the Bandwidth Manager and the National Aviation Data Interchange Network into an integrated telecommunications infrastructure. Requirements include replacing more than 20,000 circuits, upgrading switching and routing services, improving network monitoring and control, implementing a state-of-the-art security system and providing network engineering services.

Northrop Grumman Tests Confirm Performance of Advanced EHF Array

The downlink phased-array antenna developed by Northrop Grumman for the Advanced Extremely High Frequency (EHF) military satellite communications payload has completed range tests that confirmed performance predictions. The company will provide the Advanced EHF payloads to Lockheed Martin, prime contractor for the Advanced EHF system.

Test results demonstrated antenna gain and coverage performance in excess of requirements. The downlink phased-array antenna, which sends signal to ground terminals, will be the first of its kind to operate at 20 GHz in space. Advanced EHF will significantly increase capacity and connectivity over the legacy Milstar system through new phased-array antennas, advanced microelectronics, and efficient waveforms and protocols.

"The downlink phased array test was a key step in Advanced EHF payload flight production," said Gabe Watson, vice president of the Advanced EHF payload program for Northrop Grumman's space Technology sector. "Phased-array antennas are essential to our commitment to deliver protected and assured communications with increased capacity and connectivity to the US military."

The Advanced EHF system will provide global, highly secure, protected, survivable communications for all warfighters serving under the US Department of Defense. Lockheed Martin is currently under contract to provide three Advanced EHF satellites and the mission control system to its customer, the MILSATCOM Joint Program Office, located at the Air Force Space and Missile Systems Center, Los Angeles Air Force Base, CA.

Lockheed Martin Announces Team for Secure Border Program

Lockheed Martin's Secure Border Initiative (SBInet) solution will present the Department of Homeland Security (DHS) with a balanced mix of people, process, technology and infrastructure in order to gain full operational control of the country's borders, the corporation said. The solution was shaped by the company's eight team members, each chosen for specific expertise in areas relevant to homeland and border security. The

SBInet program is a comprehensive multi-year plan to secure America's 6000 miles of borders.

"Our team is composed of companies that are actively participating in cornerstone programs for DHS, protecting America's ports of entry in the air, on the water and on the ground," said Jay Dragone, vice president, Homeland Security Programs. "Collectively, we offer a wealth of experience in border control and security, infrastructure and integrated communications—with a strong history of successful past performance on critical national programs. Our SBInet solution will result in a flexible system that provides an integrated common operational picture at the agent, station, sector and headquarters level and is tailored to the needs of the individual user."

Lockheed Martin's proposed solution is focused on two factors: 1) ensure operational success and safety by understanding and meeting the critical needs of agents and officers, and 2) ensure program success by creating a strategic plan to measurably enhance control of the borders while maximizing use of existing capabilities. The SBInet solutions include: a performance-based approach to monitor real-time progress; an open business model that provides continuous competition; an extensive investment program to ensure day-one program execution, early capability delivery, risk reduction efforts and continued development technologies; an experienced stakeholder advisory council; and intelligence-driven operations to maximize resource efficiency and effectiveness.

Lockheed Martin's partner companies include Accenture, Advanced Technology Systems, HDR, Harris Corp., High Performance Technologies Inc., Parson Corp., Science Applications International Corp. and Sandler & Travis Trade Advisory Services. The assembled team's relevant experience on critical national security programs includes: Deepwater, US-VISIT, Customs and Border Protection Automated Environment, TCA's Strategic Airport Security Roll-out Program, New York Metropolitan Transit Authority's electronic security project and security for the 2004 Olympics in Greece. Like SBInet, these programs require the development, management and deployment of very large, complex systems as well as the connection of field staff with each other and to regional and headquarters locations.

In addition to its larger partner companies, Lockheed Martin has actively solicited the participation of small businesses throughout the country for the program. The company held industry days in seven communities and established a small business web portal to identify qualified small businesses to supply services, technology and product capabilities that would augment the corporation's SBInet solution. To date, more than 612 small businesses have responded, including minority and women-owned, Native American, service disabled veteran and veteran-owned businesses.

"We've built our solution on an open business model providing partnership and results, not selling products," added Dragone. "Throughout the program, we believe it will be essential to engage with small businesses, in order to assess new innovations to keep the borders secure in the face of changing security needs." ■

Alcatel to Acquire Nortel's UMTS Business

As part of its strategy to further strengthen its UMTS market position and expand its global leadership in broadband access, Alcatel has signed a non-binding Memorandum of Understanding (MoU) with Nortel to acquire its UMTS radio access business (UTRAN) and related assets for $320 M. The acquisition is subject to the execution of a definitive agreement and other closing conditions. The parties are targeting to complete the transaction in the fourth quarter of 2006. Alcatel has emphasised that it has and will continue to involve Lucent in the conclusion and implementation of this project in order to achieve the most efficient fit within the combined company.

The proposed acquisition would enhance Alcatel's mobile radio expertise and product portfolio with technology and products that enjoy strong recognition among leading operators. The company also intends to benefit from significantly strengthened research and development capabilities, amongst the most advanced in the world, with the scale and know-how to lead innovation in broadband wireless access, especially in HSxPA and 3G Long-Term Evolution (3G LTE), fully leveraging its expertise in multi-standard radio solutions and software defined radio technology.

Under the transaction, Alcatel intends to acquire Nortel's UMTS radio access technology and product portfolio, associated patents and tangible assets as well as customer contracts. It is anticipated that a significant majority of employees of Nortel's UMTS access business will be transferred to Alcatel.

Philips Semiconductors Becomes NXP

To mark its independence from Royal Philips, Philips Semiconductors will move forward as NXP. The name change follows an agreement between Royal Philips and Kohlberg Kravis Roberts & Co. (KKR), Bain Capital, Silver Lake Partners, Apax and AlpInvest Partners NV that will see the consortium take an 80.1 percent stake in the semiconductor operation with Philips retaining a 19.9 percent interest. NXP is Europe's second largest semiconductor company and a global top 10 player.

Explaining the origins of the name, Philips Semiconductors CEO Frans van Houten, said, "NXP stands for Next Experience. Put simply, we're enabling the next generation of consumer entertainment products. In order to emphasize the rich heritage which NXP gained from 53 years as part of Royal Philips, the NXP name will be supported by the tagline founded by Philips."

van Houten confirmed that NXP will continue its current business renewal strategy, which has been underway for 18 months and has contributed to sustained profitability and cost savings as a strong foundation for the future. The new shareholders support the continuation of the strategy of NXP, which is driving for leadership in five markets on which the company focuses: automotive, identification, home, mobile and personal, and multimarket semiconductors. This will be achieved through investment of €1 B in R&D, the asset light manufacturing strategy, a strong customer focus, the enormous talent base among its 37,000 employees and the continued Business Renewal Program.

EU Approval for Saab Microwave Systems

Following the original announcement in June, the EU commission has approved Saab's takeover of the former Ericsson microwave company and the formation of the new business unit, Saab Microwave Systems. It has approximately 1250 employees and the business unit now forms part of the Systems and Products business segment within Saab. It has over 50 years of experience within radar development and has supplied more than 3000 radar systems in over 30 countries. This creates new and sustainable business opportunities for Saab.

Saab Microwave Systems supplies radar systems for the Gripen fighter and the acquisition enables the company to create scope of action to secure continued development of the Gripen programme. Moreover, the advanced airborne surveillance system, complete with the company's Erieye radar for Saab 2000 aircraft, is already established on the international market.

"The acquisition of Saab Microwave Systems is a strategically important, long-term deal and one of the most important in Saab's history," said Åke Svensson, Saab CEO. "It gives us access to unique know-how in sensor technology."

Echoes of Success for QinetiQ

QinetiQ has won a £1.4 M contract to develop a novel radar target simulator to emulate realistic radar echoes from targets such as missiles, aircraft, small surface craft and submarine periscopes. The contract includes provision for initial trials to evaluate interaction between the Radar Research Target Generator (RRTG) and the UK ARTIST (Advanced Radar Technology Integrated System Testbed) radar system. The RRTG will then be used to extensively test and evaluate the performance of ARTIST. The contract is due to be completed by December 2007 and be delivered two thirds of the way through the current ARTIST programme.

QinetiQ's digital signal processing technology and Roke Manor Research's analogue radio frequency hardware will be used in the RRTG development. In addition to testing ARTIST, the technology will be used for auditing, acceptance and through-life testing of in-service and future radar systems.

Andrew Sleigh, QinetiQ's group managing director for defence, said, "As radar systems become more capable and adaptive, so the radar acceptance process becomes more complex and expensive. The versatility of the RRTG allows easy manipulation of target characteristics and scenarios, making it an extremely effective method of testing radar capability without the huge expense of conducting real-time trials with physical targets."

EADS Deploys Combat Centre in Germany

For the first time, the German Air Force has at its disposal a Deployable Control & Reporting Centre (DCRC) for the military surveillance of airspace and for the tactical command and control of air force units thanks to EADS and Frequentis GmbH, Vienna. The companies jointly developed the DCRC on behalf of the Federal Office for Information Management and Information Technology (IT-AmtBw). Thanks to the DCRC, a deployable combat operations centre will be added to the four stationary Control & Reporting Centres (CRCs) already in service in Germany.

EADS is responsible for equipping the workstations and for the operations centre electronics—German Improved Air Defence System II (GIADS II)—while the communications equipment required for the DCRC was supplied by Frequentis. GIADS II assists the user in the tactical command and control of aircraft and air defence units by evaluating the information provided by military and civil radar sources. The software assists the operators in the task of generating an accurate presentation of the air situation.

Specific incidents are announced via an alarm system so that countermeasures can be initiated rapidly and effectively. Tactical datalinks connect the system to the NATO Integrated Air Defence. Flight plan and radar data from civil air traffic control are also fed into the system. During operation, all the data can be recorded for time-displaced replay and analysis as required.

To ensure that the DCRC is capable of serving as a mobile combat operations centre in international missions, it contains an integrated interface for the exchange of air situation data with the Airborne Early Warning & Control system (E-3A). This makes the system ideal for the tactical command and control of air force units in multinational as well as joint and combined operations. ■

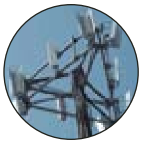

New Competitors Will Threaten Established Navigation Device Vendors

The enormous market expansion and related price war in the consumer navigation market is no longer new. What has changed is that the attempts at production segmentation and the additional revenue streams for the most competitive portable segment are increasingly arriving in the form of network-connected services. Over the past few years, higher-end models have offered such features as test-to-speech and real-time traffic information. But, as even these features are incorporated into the most inexpensive products by generic device manufacturers, connectivity is becoming the last bastion of feature differentiation. "By next year, simple one-way traffic information over satellite radio will be found even on the lowest-price portable navigation devices sold for under $300," says ABI Research principal analyst Dan Benjamin. "The big players in the portable navigation market are going to see increased competition, not just from me-too products offered by the classic consumer electronic vendors, but also from thin-client specialized vendors such as TeleNav and Wayfinder. The thin-client players will be able to advertise perpetually updated maps and POI, and lower up-front costs due to reduced storage and processing needs. We expect on-board portable navigation vendors to follow TomTom and offer more connectivity, but with a focus on premium traffic information and location database updates." Benjamin also believes that some of the newest market entrants, big names like Philips and Sony, could be in for a rude market awakening. "Established navigation names like Magellan have been forced to clear out their products through discounters and Navman is publicly up for sale. If they come in to compete on brand instead of price or features, I would not be terribly optimistic. This market is comparable to the audio player market before the iPod. Many had products, but it was the service component in iTunes that separated Apple's offering from the pack."

Triple-band UMTS Handsets Drive RF Components

Strategy Analytics, the global research and consulting company, has released "Popular UMTS Multi-band Combinations: Implication for Radio Components," from its RF and Wireless Components Service, which assists radio component companies in targeting their design resources to expected market trends. The need for handsets that can operate in UMTS and legacy GSM modes across multiple regions will drive shipments of handsets with as many as seven or more bands. Operator decisions on which band to support in these handsets have already started to set the development course for suppliers of radio components. This research, based on regional spectrum allocations and the plans of leading wireless operators, assesses which combination of frequency bands will emerge as most significant as UMTS matures. With knowledge of these bands and careful design, suppliers of radio components can minimize the number of transceivers and front-end modules that they will have to develop to address the future handset market. "By focusing on the most popular bands, radio component designers can target the needs of high volume markets or select niches best suited to their company's capabilities," notes Stephen Entwistle, vice president of the Strategic Technologies Practice at Strategy Analytics. "The leading suppliers do not have the luxury of developing unique transceivers and front-end modules for each and every possible combination of bands," adds Chris Taylor, director of the RF and Wireless Components Service. "Instead, they are attempting to develop a small suite of products that can address as many combinations of bands as possible, particularly the ones that they believe will emerge in high volume."

Mobile WiMAX Sales Will Surpass Fixed WiMAX in 2008

In the past year, the stationary form of WiMAX (fixed WiMAX or 802.16-2004) has seen steady adoption in the marketplace. But the mobile version, 802.16-2005, will be here sooner than many people think. To be technically and economically viable, mobile WiMAX ICs must hit "sweet spots" on a number of parameters. Vendors who find them quickly will outpace those who do not. "ABI Research sees fixed WiMAX sales hitting peak in 2007 and then leveling off," says principal analyst Alan Varghese. "Mobile WiMAX will start to see deployments in 2007 and the crossover point between the two will be late in 2008. Considering that it takes a year to design ASICs and then more time to design them into end-equipment, vendors up and down the value chain need to be discussing the required tradeoffs in their strategy meetings now." Performance, power consumption and cost requirements for WiMAX ICs become much more challenging on the mobile platform. MIMO will be required, but it means increased circuitry, so IC vendors will have to trade off MIMO performance for die area, power usage and price. The ASP for the WiMAX RF is about $15 and for the baseband about $23; the total is more than the BOM for a low tier device, so considerable cost reduction is needed. WiMAX IC companies such as Beceem Communications and Runcom would seem to be very well placed, since they bypassed fixed WiMAX and went straight to the mobile platform. But they are being shadowed by companies such as Redpine Signals, RF Magic, Sequans, Sierra Monolithics, Telecis and Wavesat, which have honed their skills through deployments in fixed WiMAX. Competition will also come from giants such as Fujitsu and Intel that understand the mobile platform intimately, all the way from RF to applications.

ABI Research's new study, "WiMAX Semiconductors: Fixed and Mobile WiMAX: RF and Baseband Chips for Network Infrastructure and CPE," discusses these issues in detail, examining market drivers for WiMAX, business models, fixed and mobile WiMAX deployment schedules worldwide, and details of RF and baseband chipset architectures, power consumption, process technologies, integration roadmaps and ASPs.

Booming Trailer Tracking Market Growth to Continue

Markets for electronic trailer tracking hardware and services are booming, according to a new study from ABI Research. Worldwide subscriber numbers will see a strong, prolonged growth through the end of the decade, and in North America, the percentage of trailers tracked will more than triple. Growth is already very strong: worldwide subscriber numbers have almost doubled since the previous year. According to analyst Steve Bae, several factors have converged to produce this strong growth: "Trailer tracking hardware costs have fallen significantly while products and services have become more sophisticated. Customers are more aware of the technologies and many see electronic tracking as an efficient solution to maximize productivity of trailers and resources." This rapid expansion is seeing many vendors enter the market and some players chalking up big wins. A good example is GE, which recently acquired Wal-Mart as a trailer-tracking customer. The retailer placed an order for 46,000 units. When the fit-out is complete by the end of this year, GE will have more than doubled its market share, putting it on a nearly equal footing with other leading vendors such as Qualcomm, SkyBitz and Terion. As in any fast-growing market with new vendors, consolidation can be expected and not all will survive. There are two parts to the trailer tracking equation: hardware and services. Most of the market value is on the on-going provision of services and these can range from basic tracking of a trailer's location and status, to multiple sensor connections, integration and monitoring parameters such as the temperature of refrigerated trailers. "By the end of this decade," says Bae, "trailer tracking stands to be integrated with other commercial telematics solutions." ■

INDUSTRY NEWS

▲ Dave Sherman

■ **Dave Sherman** passed away on July 16, 2006, in Wildomar, CA. Sherman was employed at Lark Engineering in June of 2001 as vice president of sales and marketing and was promoted in September 2002 to executive vice president. A provider of inspiration and motivation for the company's sales reps, he was also heavily involved with Lark's marketing and ad campaigns. A catalyst in many venues, he inspired and implemented effective techniques that continue to be utilized daily.

■ **L-3 Communications** announced that it has agreed to acquire **Nova Engineering** for $45 M in cash, plus an additional purchase price not to exceed $10 M that is contingent upon Nova's future financial performance. The business is expected to generate annual sales of approximately $40 M for the year ending December 31, 2007, and will be included in L-3's Command, Control, Communications, Intelligence, Surveillance and Reconnaissance (C3ISR) reportable segment. The acquisition is expected to be completed in the third quarter of 2006, subject to customary closing conditions, and to be slightly accretive to L-3's earnings for 2006.

■ **Sirenza Microdevices Inc.** announced that it has signed a definitive agreement to acquire **Micro Linear Corp.**, headquartered in San Jose, CA. Under the terms of the agreement, 0.365 of a Sirenza share will be issued for each Micro Linear share, subject to potential adjustment. Based on Micro Linear's fully diluted shares outstanding and Sirenza's closing price on August 14, 2006, the transaction is currently valued at approximately $45.6 M.

■ **Planar Electronics Technology** announced the recent acquisition of **Planar Filter Co.** This acquisition will allow Planar Electronics Technology to continue supplying filters, switch filter banks and filter assemblies to the RF/microwave community.

■ **The Micromanipulator Co.** announced that **Flywheel Ventures**, a New Mexico-based venture capital firm, has acquired a majority interest in the company for an undisclosed amount from its current owner, the California Institute of Technology (Caltech). In addition to the transfer of interest, the company will also receive a direct $1 M cash infusion from Flywheel to support future growth and acquisitions. Terms of the transaction were not disclosed.

■ **E2G Partners LLC**, Cincinnati, OH, announced it completed the acquisition of the assets of **Tampa Microwave Lab Inc.** (TMLI), a provider of microwave products for satellite communication systems. The company will continue to do business under its current name at its current facilities in Tampa, FL.

■ **QUALCOMM Inc.** announced that it will acquire San Diego, CA-based **Qualphone Inc.**, a provider of IP-based Multimedia Subsystems embedded client software solutions for mobile devices and interoperability testing services. The acquisition of Qualphone's products and resources will help QUALCOMM further accelerate the delivery of multimedia-capable, feature-rich 3G solutions on top of the emerging IMS and multimedia domain architectures to WCDMA/UMTS and CDMA2000® markets.

■ **Unity Wireless Corp.** closed its acquisition of **Celletra Ltd.**, an Israel-based supplier of coverage enhancement solutions for 2G and 3G wireless networks. Terms of the acquisition were unchanged from the initial terms announced on July 19, 2006.

■ **Ducommun Inc.** announced that its Ducommun Technologies Inc. (DTI) subsidiary has opened and begun production in its new manufacturing facility in Thailand. Initial production supports DTI's high performance and high reliability commercial microwave switches to service the growing demands in the US and other international markets. The facility is located in Saraburi, approximately two hours north of Bangkok. DTI is developing the site to accommodate future expansion of the facility as required to meet the growing needs of the marketplace.

■ **Freescale Semiconductor** is expanding its India operations with a new 100,000 square-foot facility in Bangalore to support Freescale's research and development in software for wireless technologies. This follows the company's recent acquisition of a 300,000 square-foot campus in Noida to support expansion plans.

■ **Cree Inc.** announced that its newly opened 230,000 square-foot engineering and production facility in Research Triangle Park, NC is operational. The new facility is producing the company's advanced electronic devices based on silicon carbide and gallium nitride.

■ **Andrew Corp.** has opened a new manufacturing facility in the Czech Republic for the production of base station antennas for wireless operators in the Europe, Middle East and Africa (EMEA) region. The new Brno plant is a significant expansion of Andrew's European presence and enhances the company's ability to support locally the network requirements of customers in the region. The facility is closely tied to the EMEA product design center in Scotland that Andrew established in 2005 to provide region-specific design, qualification and system specification services.

■ **NuSil Technology**, a manufacturer of silicone-based materials for healthcare, aerospace, electronics and photonics, announced that it has opened its first technical support office in Asia. This office will specialize in the areas of optoelectronics and electronic packaging, served by the company's Lightspan products and its line of low outgassing electronic packaging materials, respectively. T.Y. Lim, the application engineer heading the office in Penang, Malaysia, will support all of NuSil's customers, distributors and representatives in Asia.

■ **Ansoft Corp.** announced that Nexxim,® the company's circuit simulation software for high performance IC design and signal integrity analysis, has been accepted into the **Cadence Design Systems Inc.** Connections® Program. The integration of Nexxim into the Cadence Virtuoso® Analog Design Environment allows designers of complex DigitalRF CMOS ICs and GaAs/SiGe RFICs to gain access to Ansoft's new circuit simulation technology, without the costs and risks associated with changing design methodologies.

■ **The Ethernet Alliance**, an industry group dedicated to the continued success and expansion of Ethernet technology, announced that the **Institute of Electrical and Electronic Engineers** (IEEE) 802.3 working group has formed the Higher Speed Study Group (HSSG) to evaluate the requirements for the next generation of Ethernet technology.

■ **PSI-TEC Corp.** announced that it has established a co-location agreement with a New Jersey-based micro-optics company. The agreement has allowed PSI-TEC scientists to establish a pre-production line in order to test and integrate its organic materials into waveguide devices and system prototypes as a first step toward product commercialization.

■ **Keithley Instruments Inc.** announced a new partnership agreement with **TestMart Inc.** The agreement authorizes TestMart to present a catalog of Keithley's precision test and measurement equipment as well as government marketplace services for Keithley to meet the needs of federal customers.

■ **picoChip** announced it has signed a development partnership agreement with **China GrenTech**. Based on picoChip WiMAX software-upgradeable technology, China GrenTech will develop radio frequency solutions. The two companies will work together in the joint development to complete WiMAX solutions targeted at the wideband wireless access market.

■ **M2 Global Technology Ltd.** announced that it has been awarded AS9100 certification. M2 Global has met the stringent requirements necessary for this international aerospace quality system standard for aerospace industry suppliers, ensuring customers that the company meets the highest quality standards.

■ **Innovative Micro Technology** (IMT), a contract manufacturer for MEMS, announced that it has received ISO 9001:2000 certification from Det Norske Veritas. The formal certification reflects IMT's commitment to continuous process improvement and delivering the highest level of quality and customer satisfaction.

■ **K&L Microwave Inc.**, part of Dover Corp.'s Microwave Products Group,® has received ISO 14001 certification for its Environmental Management System (EMS). Implementing an ISO-certified EMS greatly improves the company's ability to manage environmental issues, and demonstrates sound environmental management.

■ **JFW Industries** announced that it complies with the RoHS Directive 2002/95/EC. The company has completed the implementation of all required changes in its production and purchasing departments and its engineers have approved all new RoHS compliant materials, components and finished products. In the future, JFW will continue to offer non-compliant versions of all products for customers that require it.

■ **Aperto Networks** announced that its PacketMAX™ family of customer premise equipment has achieved WiMAX Forum™ certification.

■ **Modular Components National** (MCN), headquartered in Forest Hill, MD, marks its 25 year milestone in the design and development of microwave products and technology. Over the last 20 years, MCN has continued to expand manufacturing operations in Forest Hill, as well as increased capacity through acquisitions. In 2006, MCN will begin construction of a new 50,000 square-foot manufacturing facility on a recently acquired six-acre site adjacent to corporate headquarters in Maryland. This purchase follows over $3 M of capital equipment purchases over the last three years.

■ **Dow-Key Microwave Corp.**, part of Dover Corp.'s Microwave Products Group,® was named a Lockheed Martin Corp. STAR Supplier award winner within the Electronic Systems business area.

■ **Jacket Micro Devices Inc.** announced that the US Patent and Trademark Office has issued US Patent No. 7,068,124 — "Integrated Passive Devices Fabricated Utilizing Multi-layer Organic Laminates." This patent was awarded to JMD's founders for their invention of a key technology used in JMD's Multi-layer Organic (MLO™) packaging and module production process.

■ **RFMD**® announced that the company has commenced mass production shipments of its RF3159 linear EDGE power amplifier to **Samsung Electronics** for use in at least 15 EDGE-enabled handsets.

FINANCIAL NEWS

■ **Silicon Laboratories Inc.** reports sales of $123.5 M for the second quarter ended July 1, 2006, compared to $107.2 M for the same period in 2005. Net income for the quarter was $10.1 M ($0.18/per diluted share), compared to a net income of $15.6 M ($0.28/per diluted share) for the second quarter of last year.

■ **ANADIGICS Inc.** reports sales of $40.2 M for the second quarter ended July 1, 2006, compared to $23.9 M for the same period in 2005. Net loss for the quarter was $2.8 M ($0.06/per share), compared to a net loss of $9.1 M ($0.27/per share) for the second quarter of last year.

■ **Superconductor Technologies Inc.** reports sales of $5 M for the second quarter ended July 1, 2006, compared to $8.6 M for the same period in 2005. Net loss for the second quarter was $22.7 M ($1.82/per diluted share), compared to $2 M ($0.19/per diluted share) for the second quarter of last year.

■ **WJ Communications Inc.** reports sales of $12.4 M for the second quarter ended July 2, 2006, compared to $4 M for the same period in 2005. Net loss for the second quarter was $1.3 M ($0.02/per diluted share), compared to a net loss of $7.8 M ($0.12/per diluted share) for the second quarter of last year.

PERSONNEL

■ EMS Technologies Inc. announced that **Gerald Hickman**, senior vice president and general manager of its EMS *Wireless* division, is retiring from the business. Paul Domorski, president and chief executive officer, reported that the company has begun a search for Hickman's replacement, and that Domorski would act as the division's general manager in the interim period.

■ **Robert "Tony" Grimes** has been named president of Continental Electronics. Grimes is responsible for all day-to-day operations and brings a background in business management and program planning for wireless products. Grimes's background includes more than 20 years of engineering design, marketing and sales, organizational development and presidential leadership. He comes to Continental after serving as president of TRAK Microwave Corp. and on the board of directors for Radyne Corp.


▲ Gary Moore

■ **Gary Moore** has been promoted to the position of vice president of sales and marketing for EMC Technology and Florida RF Labs. Moore has been associated with Florida RF Labs for over 18 years and EMC since 2001. In his previous position as director of sales — Americas, Moore made a substantial and significant positive impact on both businesses. Prior career positions he has held include director of sales and marketing at Delta Electronics Mfg. Corp. and regional sales manager for Solitron/Microwave.

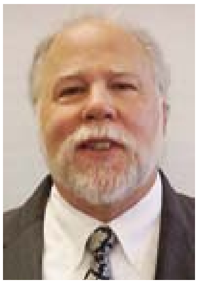
▲ Gregg Pollack

■ Palco Connector Inc., an affiliate of the Phoenix Co. of Chicago, has announced the appointment of **Gregg Pollack** as director of sales and marketing. Located in Naugatuck, CT, Palco is a designer and manufacturer of RF and microwave coaxial connectivity solutions. These include a full range of catalog and custom connectors, cable assemblies and integrated coaxial subassemblies. Pollack brings extensive experience in the RF and microwave industry to this position. He may be reached at (603) 431-1414 or e-mail: gpollack@palcoconnector.com.

■ The Georgia Tech Research Institute (GTRI) has named **William Melvin** as director of its Sensors and Electromagnetic Applications Laboratory (SEAL). He replaces Robert Trebits, who retired in May after a distinguished 35-year career with GTRI, including 15 years as director of SEAL. An expert in signal processing and aerospace radar systems, Melvin has been with GTRI for eight years, most recently as director of SEAL's Adaptive Sensor Technology Project Office.

REP APPOINTMENTS

■ **Digi-Key Corp.** and **Amphenol**® Connex Connector Corp. announced the signing of a global distribution agreement. Amphenol Connex designs, manufactures and distributes RF connectors, interfaces, crimp tools and accessories. Among Amphenol Connex products stocked by Digi-Key are its RF connectors, including BNC, SMA, TNC and N-type connectors along with corresponding tools and accessories. These products are available for purchase directly from Digi-Key through both its print and on-line catalogs.

■ **Tundra Semiconductor Corp.** announced that it has signed **Avnet Electronics Marketing Americas** as a value-added distributor in North America, expanding Tundra's product and support delivery to customers in the region. Avnet will now promote, supply and support Tundra System Interconnect products throughout North America.

■ **SemiconductorStore.com**, a design-oriented eCommerce site that is helping design engineers research and buy electronic components on-line, announced that it has signed an agreement to add **Integrated Device Technology Inc.** (IDT™) to its expanding on-line offering. Under the terms of the agreement, SemiconductorStore.com is authorized to promote and sell the complete lineup of products from IDT to their worldwide customer base of design engineers and procurement professionals.

■ **Reactel Inc.**, a manufacturer of RF and microwave filters, multiplexers, switched filter banks and sub-assemblies to the commercial, military, industrial and medical industries, announced the appointment of **T & E Repco** as the company's representative in FL, GA, AL, NC, SC and TN. For more information about T & E Repco, please visit www.microwaves.com/t&erepco.html or call Ernie DeVita at (561) 630-7330.

■ **TRAK Microwave Corp.** announced the appointment of **Castle Microwave Ltd.** as the company's exclusive sales representative in the United Kingdom. Castle Microwave will represent TRAK products including RF and microwave multi-function assemblies, frequency sources and converters, ferrite and signal control devices, and time and frequency systems. Castle Microwave can be contacted at +44 (0)1635 271300 or e-mail: sales@castlemicrowave.com.

■ **Mica Microwave** announced the appointment of **Novacom Microwave Ltd.** as its exclusive sales representative in the United kingdom, Scotland and northern Ireland.

Novacom Microwave can be contacted at Unit 6, The Green, Nettleham Lincoln, LN2 2NR +44 1522 751 136, fax: +44 1522 754408 or e-mail: sales@novacom-mwave.com.

■ **Modelithics Inc.** announced that it will be represented in Scandinavia by **MTT Components & Systems AB**, a division of AGETO AB located in Täby, Sweden.

■ **MI Technologies** announced it has selected **Actions and Services** to provide sales and **Cal Info Mesure** to provide service for the company's line of RF and microwave test and measurement products to customers in France.

■ **Nu Horizons Electronics Corp.** announced the expansion of the company's North American distribution agreement with **Micrel Inc.** into Greater China. In addition to North America, this partnership now includes demand creation and fulfillment of Micrel's analog, high bandwidth and Ethernet products in Hong Kong, China and Taiwan.

■ **DesignAdvance™ Systems Inc.**, a developer of innovative design automation software for users of EDA and MCAD tools, announced its entrance into the Chinese PCB design market with the appointment of **Shenzhen EDA Technologies Co. Ltd.** as a distribution partner. Shenzhen EDA Technologies, an engineering software company, provides industry-specific solutions to the PCB and IC markets.

WEB SITES

■ **Labtech Ltd.** has launched a new look web site (www.labtechmicrowave.com) to promote its wide range of products and enhance its customer service. The broadband microwave components and microwave manufacturing specialist supplies the defense, space, SATCOM and telecommunication markets. The site features the latest company news, data sheets and product sheets on its portfolio, including the new range of thin dielectric material (TDM) modules, low cost standard amplifiers and detector log video amplifiers (DLVA). Also, a customer access portal is being developed to provide real time order status information.

■ **Networks International Corp.** (NIC) announced the launch of the company's new corporate web site at www.nickc.com. The new site reinforces NIC's commitment to expand its brand name and provide a dynamic environment for its customers to understand its products and capabilities.

■ **Chelton Telecom & Microwave** has launched a brand new web site (www.chelton-tm.com) that focuses on its complete portfolio of RF and microwave systems and components. Detailed information is given on the company's five product ranges—systems, diodes and modules, RF filters and duplexers, ferrite devices, and waveguides. From the Home Page users can easily search for products under specific applications—telecom, space, defense and medical—individual product ranges, technologies or frequencies.

DESIGN OF BIAS TEES FOR A PULSED-BIAS, PULSED-RF TEST SYSTEM USING ACCURATE COMPONENT MODELS

In this article, a design of custom bias tees to be used in a pulsed-bias, pulsed-RF measurement system is described. The bias tee design is such that the DC path allows bias pulses to pass through to the device unchanged, while still allowing RF measurements at as low a frequency as possible. The use of accurate component models led to a successful simulation-based development of a bias tee with a (three-port) frequency response that allows accurate pulsed S-parameter and pulsed IV measurement results to be achieved in the desired bandwidth.

This article describes the design of a bias tee for a pulsed-bias, pulsed-RF test system. The cut-off frequency of the DC path was raised to allow pulsing of the bias signal. The theory of bias tee design for pulsed measurements is first presented. The simulation results for the design without the use of component models are presented, followed by simulation results obtained using accurate parasitic models for the inductor and capacitor used. The simulation results are then compared with S-parameter measurements obtained using a TRL calibration and found to show good agreement. Finally, illustrations of the accurate use of the bias tees in performing both pulsed IV and pulsed S-parameter measurements are provided.

Fig. 1 Bias tee circuit.

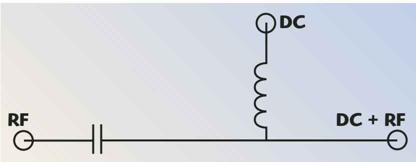

BIAS TEE DESIGN

A typical bias tee circuit consists of an inductor and a capacitor, as shown in ***Figure 1***. The function of the bias tee is to simultaneously allow a DC bias voltage and an RF test signal to be applied to the port of a transistor during measurement. For example, in an S-parameter measurement system, the DC bias is applied at the port labeled "DC," and the RF test signal from the vector network analyzer is applied to the port labeled "RF." At the RF + DC port, both the RF and DC voltages are applied to the device.

CHARLES BAYLIS
University of South Florida
Tampa, FL
LAWRENCE DUNLEAVY
University of South Florida and Modelithics Inc.
Tampa, FL
WILLIAM CLAUSEN
Modelithics Inc.
Tampa, FL

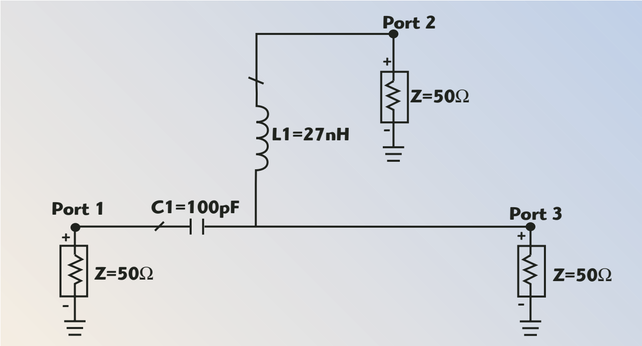

Fig. 2 Circuit with ideal components and without microstrip lines used in simulation.

The purpose of the inductor is to prevent the RF signal from entering the DC path, and the purpose of the capacitor is to keep the DC signal from entering the RF path. The inductor and capacitor should be designed such that the upper cut-off frequency of the low pass DC path is lower than the lower cut-off frequency of the high pass RF path. If this is true, then the lower cut-off frequency of the RF path containing the capacitor (considering the inductor to be an open circuit) is given by

$$f_{c,AC} = \frac{1}{2\pi RC} \qquad (1)$$

where R is the total resistance seen at the capacitor terminals. In this case, the termination at the RF port is 50 Ω and the termination at the RF + DC port is large (either the input or output impedance of the device) in normal operation but will be 50 Ω in the bias tee test setup. In operation, however, the value of the input resistance will be fairly large, changing the cut-off frequency. However, in a 50 Ω test system, 50 Ω is the impedance at all test ports. This setup will be used for the purpose of benchmarking the behavior of the device through measurement and simulation. Thus, R = 50 + 50 = 100 Ω for this case.

The cut-off frequency of the DC path, assuming that the capacitor appears as an open circuit, is given by

$$f_{c,AC} = \frac{R}{2\pi L} \qquad (2)$$

In this case, R is equal to the sum of the impedance presented by the bias equipment and the input impedance to the device under test. For a 50 Ω test system, R = 50 + 50 = 100 Ω.

The outstanding factor for a pulsed bias tee design is that the cut-off frequency of the DC path must be high enough to allow the pulsed bias signal to proceed unabated from the DC to the RF + DC ports. In this case, the smallest pulse length to be used for pulsing the bias is approximately 100 ns. The frequency content of this pulse is a (sin x)/x function centered at a frequency of $1/(100 \times 10^{-9}) = 10$ MHz. Thus, the upper cut-off frequency of the bias network should be greater than 10 MHz, large enough that the entire frequency content of the pulse can pass through the DC path without distortion; this will allow the integrity of the pulse shape to be maintained.

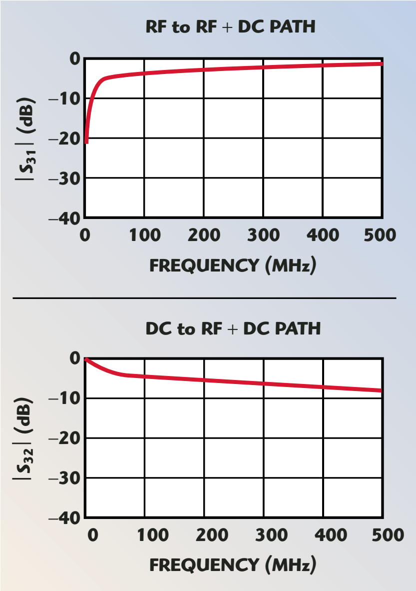

▲ *Fig. 3 Simulated S-parameters for the ideal circuit.*

Initial values for the inductor and capacitor were chosen and simulations containing ideal elements were performed to ensure the selection of component values that will provide adequate cut-off frequencies for the DC and RF paths. The simulations were performed using Agilent Technologies' Advanced Design System (ADS). The simulation circuit and results for ideal component values of C = 100 pF and L = 27 nH are shown in ***Figures 2*** and **3**, respectively. For these component values, the 3 dB cut-off frequency of the RF path is shown to be 151 MHz and the cut-off frequency of the DC path is shown to be 61 MHz.

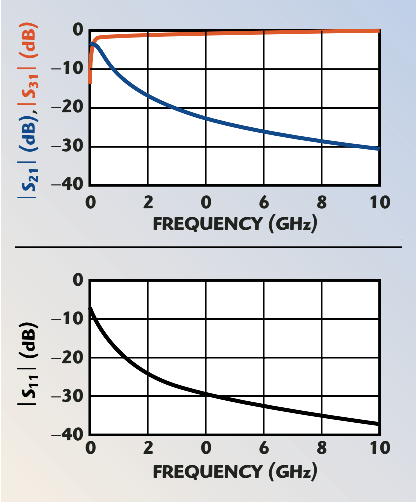

▲ *Fig. 4 Simulated S-parameters for the ideal circuit.*

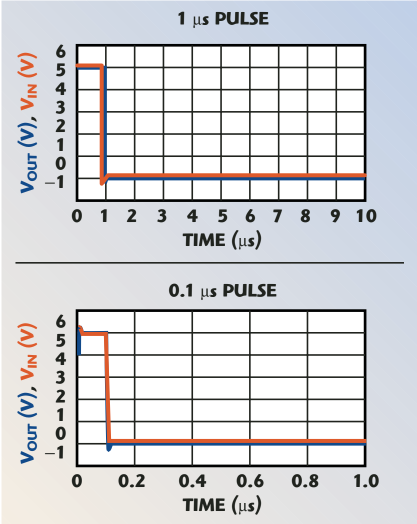

▲ *Fig. 5 Simulated transient results.*

SIMULATION RESULTS

Simulations were performed for the selected component values L = 27 nH and C = 100 pF. The simulation was performed at three different levels. At each level, both S-parameters

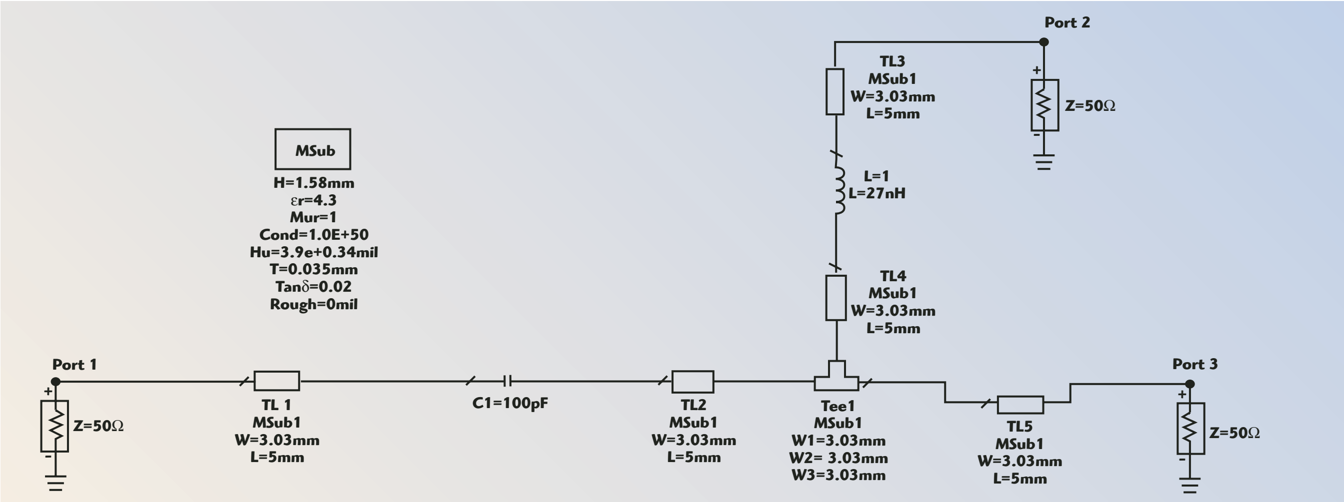

Fig. 6 Simulated circuit with microstrip lines and ideal components.

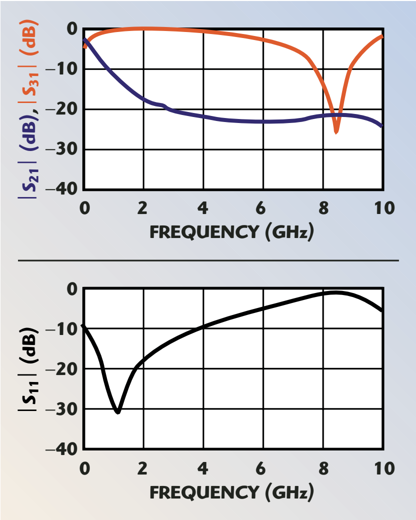

Fig. 7 Simulated S-parameters for the circuit with microstrip lines.

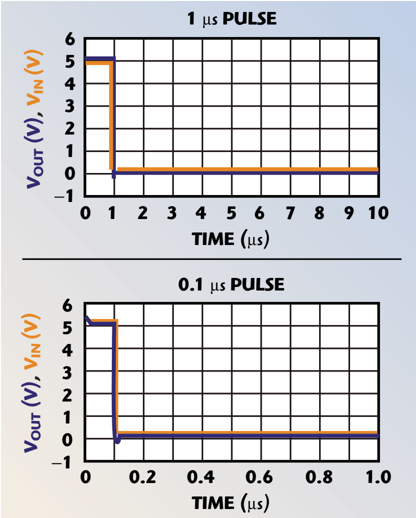

Fig. 8 Simulated transients from DC to RF + DC ports for the circuit with microstrip lines.

and transient simulations were run. The purpose of the S-parameters simulation is to ensure that the RF path of the bias tee passes the signal while the DC path does not at RF frequencies. The transient simulation is used to show that the pulse can accurately reach the RF + DC port without being significantly distorted in the time domain. Three levels of simulation were incorporated into this effort: (1) ideal components and no transmission lines; (2) ideal components with microstrip (FR-4 substrate) transmission lines; and (3) lumped component parasitic models developed by Modelithics, combined with microstrip transmission line models built-in to Agilent ADS. The first level was used to assess the opti-

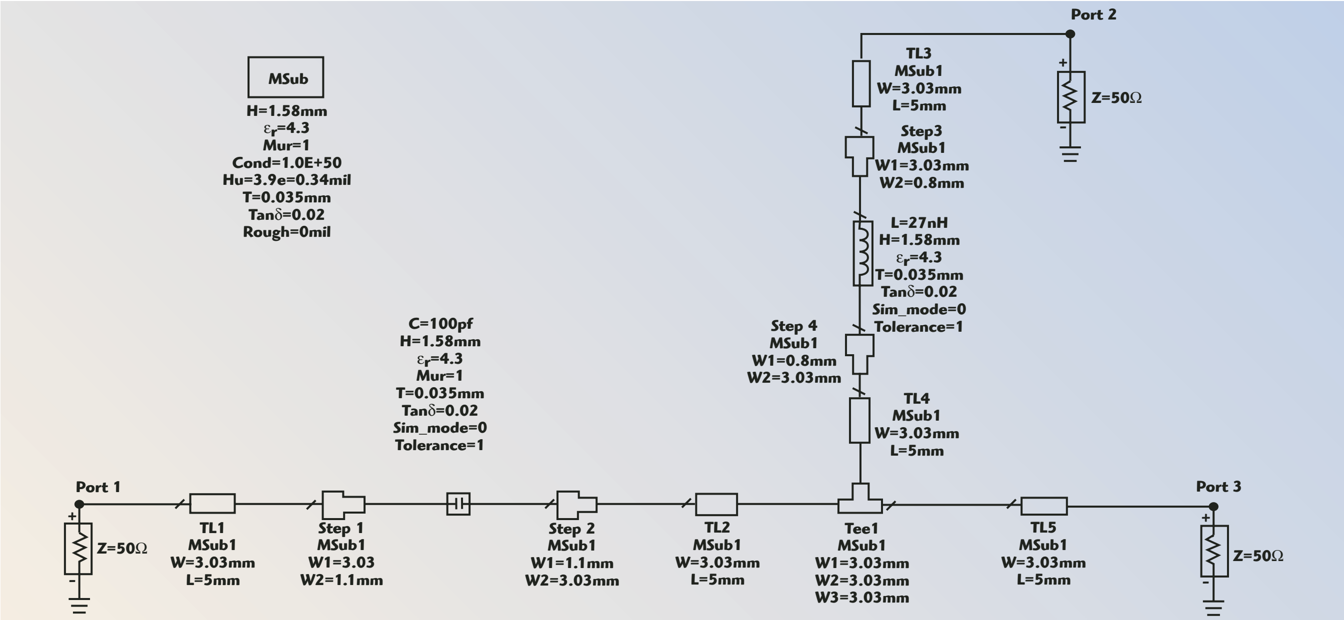

Fig. 9 Simulated circuit with parasitic models for lumped components and microstrip lines.

mum inductance and capacitance values, as shown in the previous section; the second and third levels are used to view non-idealities introduced by the substrate (second level) and component parasitics (third level).

For the first-level schematic, the simulation results are displayed in ***Figures 4*** and ***5***. They show that the S-parameter results are as desired. From approximately 500 MHz and above, S_{31} is high (which means that most of the input signal is getting to the RF + DC output) and S_{21} is low (very little signal is going from the RF port to the DC port). Also, S_{11} is below approximately –20 dB for all frequencies greater than approximately 1.7 GHz. These results show that the choice of component values seems reasonable for a large RF passband. The transient simulation reveals whether the bias tee will allow accurate transmission of pulses from the DC port to the RF + DC port. The results show that a 1 μs square pulse sent from the DC port appears virtually undistorted at the RF + DC port, and a 0.1 μs pulse also goes through the system with only minimal overshoot at the rising and falling edges of the pulse. Since 0.1 μs is short enough for isodynamic measurements, it appears that this bias tee is designed correctly with regard to the DC path passband.

The next step was the incorporation of microstrip lines into the simulation. Ideal components, however, were still used for the inductor and capacitor, as shown in ***Figure 6***. The substrate parameters used in the

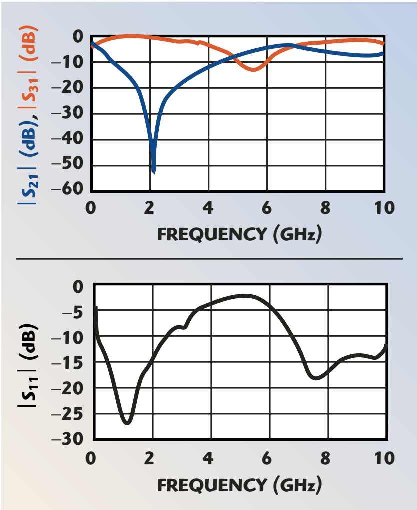

▲ *Fig. 10 Simulated S-parameters for the circuit with parasitic models for lumped components and microstrip lines.*

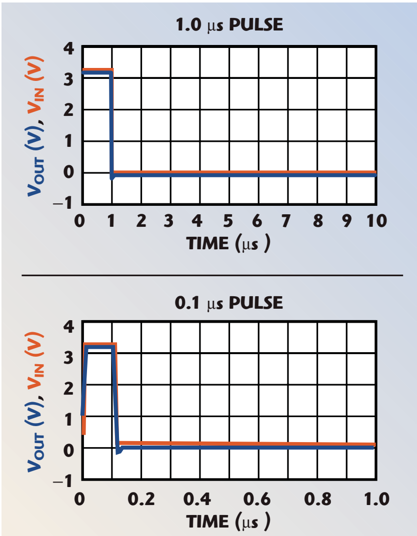

▲ *Fig. 11 Simulated transients from DC to RF + DC ports for the circuit with microstrip lines and parasitic lumped components models.*

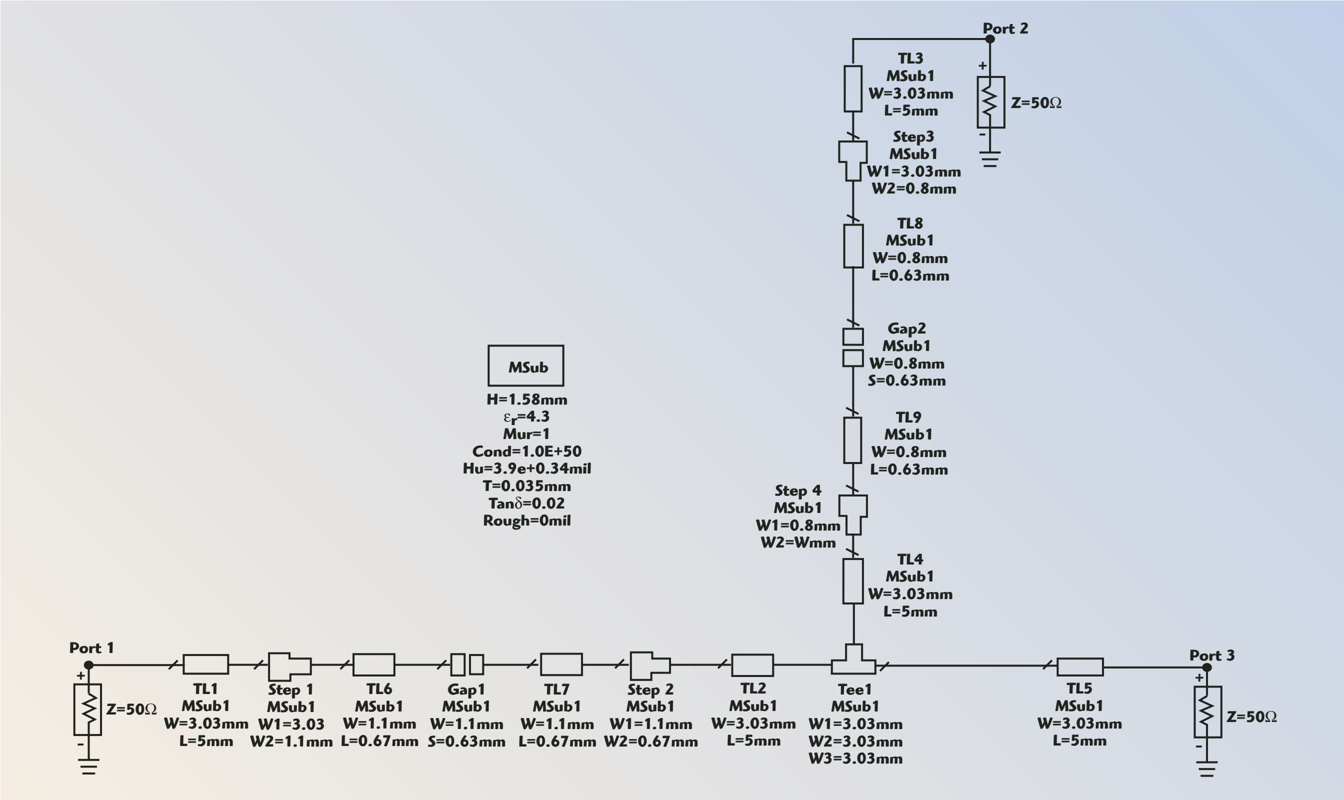

▲ *Fig. 12 ADS schematic for layout generation.*

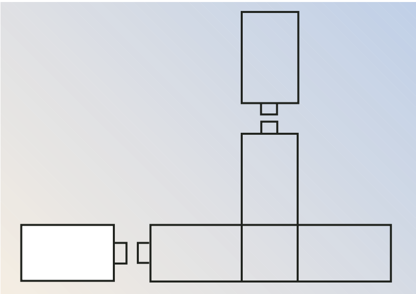

▲ *Fig. 13 Bias tee layout for FR4 milling.*

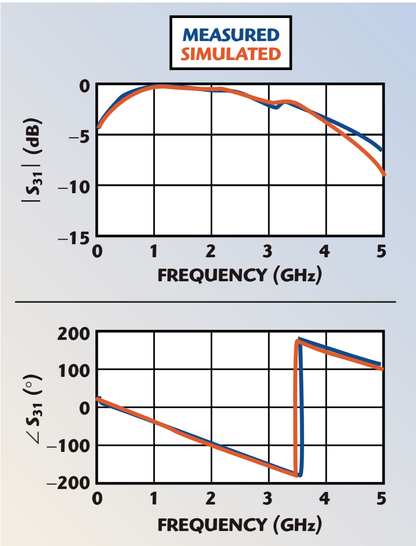

▲ *Fig. 14 Measured and simulated S_{31} (RF to RF + DC transmission).*

"MSUB" element are those for the FR-4 substrate to be used in milling the circuit. ***Figure 7*** shows the S-parameters simulation results for the microstrip circuit. While the circuit behavior is still close to ideal up to approximately 5 GHz, there is a steep drop in S_{31} at approximately 8 GHz. In addition, the input match becomes worse as the frequency increases, reaching a peak at the same location as the notch in S_{31}. However, these simulations indicate that the bias tee should be useful in applications up to 6 GHz. The transient simulations are shown in ***Figure 8***. Excellent pulse integrity is obtained at the RF + DC port.

Finally, the simulations were performed using detailed models for the components to be used in the circuit: a TDK 27 nH size 0603 inductor and an ATC 100 pF size 0603 capacitor. The models include the bond pads, so these were not included in the microstrip components. However, it is necessary to include these bond pads in the schematic for the layout generation.

Figure 9 shows the schematic used for the simulation. ***Figure 10*** displays the S-parameters simulation results. The plots show that the response concerning the RF to DC port and RF to RF + DC port transmissions is adequate at frequencies below 4 GHz. However, at 4.5 GHz, more transmission is occurring from the RF port to the DC port than from the RF port to the RF + DC port. In addition, the input match at this frequency is relatively poor, as evidenced in the S_{11} plot. These non-ideal effects are due to the component parasitics, since the microstrip line elements added in the second simulation stage did not cause such effects at these frequencies. They will limit the frequency range for which the bias tee will be able to be accurately used in S-parameter measurements. ***Figure 11*** shows the transient simulation results for the bias tee. It appears that the height of the pulse at the RF + DC port is slightly lower than at the input. This is likely due to the non-ideal resistance of the components that is included in the models but is not taken into account in the ideal component definitions used for the simulations whose results were previously displayed. The use of three levels of simulation has shown that both the transmission line elements and the parasitic effects of the components have a substantial impact on the S-parameters simulation results. With the addition of the transmission line elements and component models, it was seen that some non-ideal effects are expected to occur above 4 GHz.

LAYOUT AND FABRICATION

The bias tees were constructed by mounting the components on a 59-mil thick FR4 substrate. The circuit board was fabricated in the University of South Florida (USF) Wireless and Microwave Instructional (WAMI) Laboratory. The layout for milling was generated using a schematic in Advanced Design System with the components replaced by bond pads and a small gap. The bond pads were not part of the previous schematics used for simulation because the effects of the bond pads were included in the models for the simulations. The schematic used to generate the layout is shown in ***Figure 12*** and the layout generated by ADS for milling is shown in ***Figure 13***.

S-PARAMETER MEASUREMENTS OF BIAS TEES

To test the accuracy of the models in predicting the behavior of the bias tees, S-parameter measurements were performed over a frequency range of 40 MHz to 6 GHz using an Anritsu 37397C "Lightning" vector network analyzer. A through-reflect-line (TRL) calibration was used for the measurement. The 59-mil FR4 standards used for this calibration have coaxial-to-microstrip adapters at each port. The length of the standards was measured in the USF laboratory. The through standard was measured to be 10.00 mm, while the delay standard was measured as 18.64 mm. The open was offset by half of the through standard line length. The calibration was performed using the Multical Software created by the National Institute of

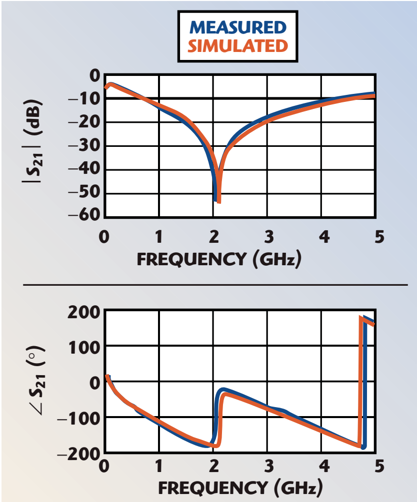

▲ *Fig. 15 Measured and simulated S_{21} (RF to DC transmission).*

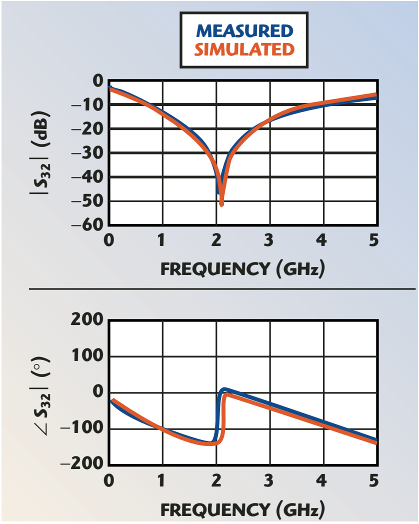

▲ *Fig. 16 Measured and simulated S_{32} (DC to RF + DC transmission).*

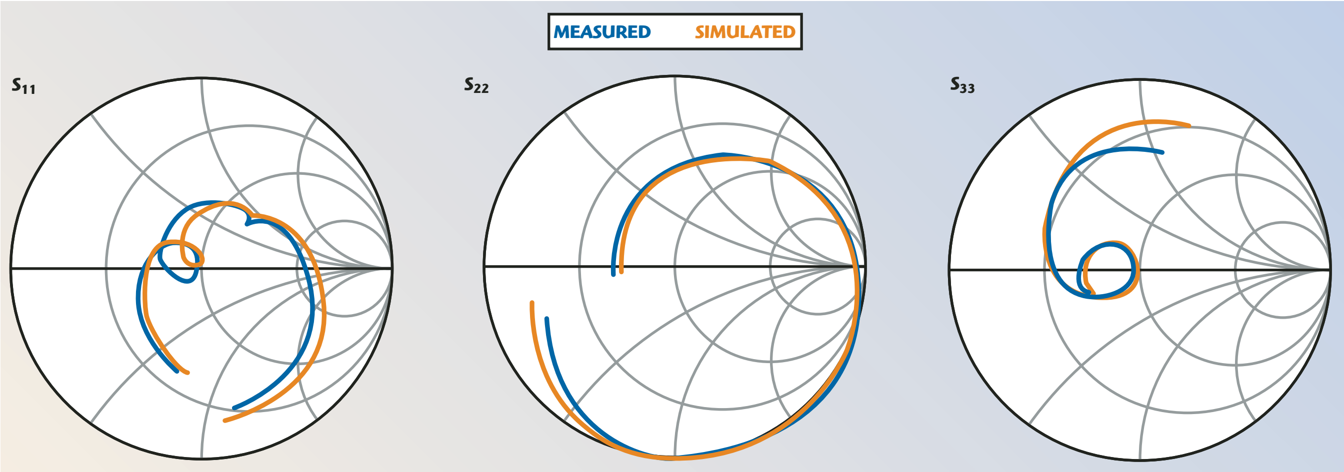

▲ *Fig. 17 Measured and simulated S_{11}, S_{22} and S_{33} (F = 40 MHz to 5.0 GHz).*

Standards and Technology (NIST). A reference impedance of 50 Ω and an effective relative permittivity of 3.3 were used. The reference plane was set to be 5 mm from the center of the through, placing it at the beginning of the microstrip line, just on the microstrip side of the coaxial-to-microstrip adapter at each port. ***Figure 14*** shows plots of S_{31}, the RF to RF + DC transmission, in dB magnitude and phase. The largest difference between the results in both magnitude and phase occurs between 5 and 6 GHz.

The measured versus simulated (without microstrip-to-coaxial adapters) results for S_{21} (the RF to DC transmission) are shown in ***Figure 15***. The magnitude of S_{21} should be low at all frequencies. A very good agreement is obtained between the measured and simulated data in both magnitude and phase. Measured and simulated results for S_{32} (DC to RF + DC transmission) are shown in ***Figure 16***. The magnitude of this transmission is expected to be low except at low frequencies. The magnitude match is excellent between measured and simulated results over the entire measurement band for both S_{21} and S_{32}.

Figure 17 shows the measured and simulated input reflection coeffi-

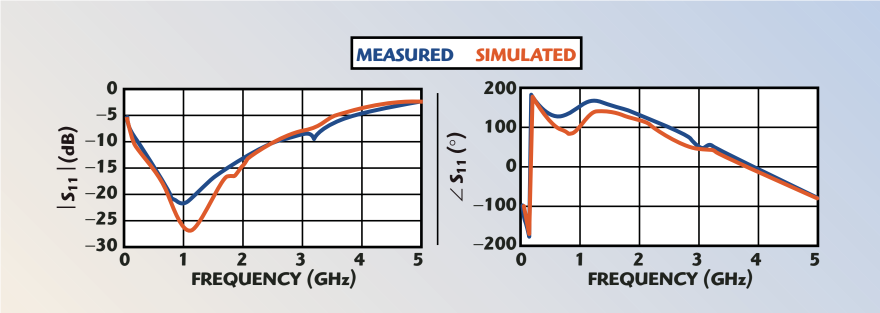

▲ *Fig. 18 Simulated and measured S_{11} parameters.*

cient results for all three ports. The simulation and measured reflection parameters match well at lower frequencies; however, some differences exist at higher frequencies. The simulated parameters have larger magnitude in each case at the higher frequencies, especially S_{33}. This may be due to the difficulty of obtaining a good reflection calibration using a 59-mil FR4 substrate with SMA-to-microstrip adapters at higher frequencies. ***Figures 18, 19*** and ***20*** display the reflection parameters as magnitude and phase versus frequency.

In general, the S-parameter results show good agreement from 40 MHz to 5 GHz. This data seems to indicate that the models have accurately predicted the performance of the design on the first pass.

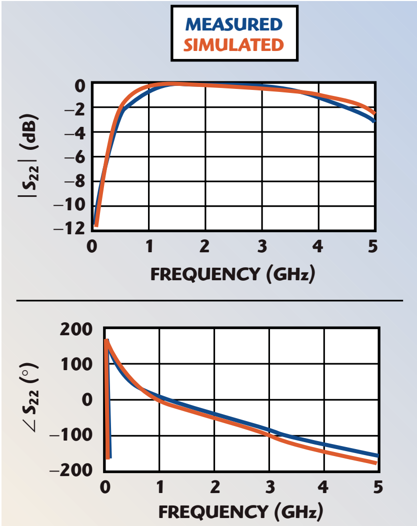

▲ *Fig. 19 Simulated and measured S_{22} parameters.*

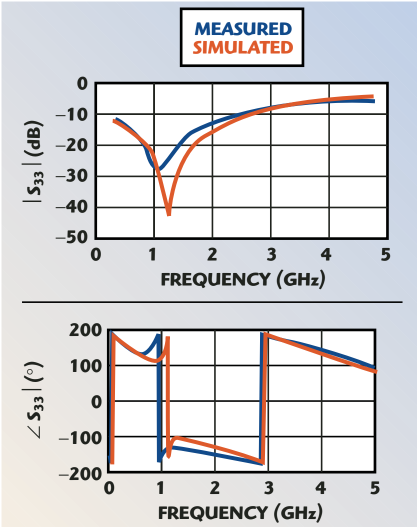

▲ *Fig. 20 Simulated and measured S_{33} parameters.*

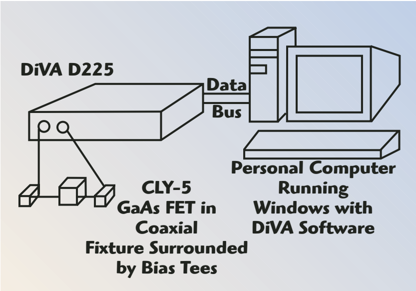

▲ *Fig. 21 Measurement set-up.*

PULSED IV MEASUREMENT THROUGH BIAS TEES

In addition to testing the RF performance of the bias tee, it is also important to ensure that the circuit allows a pulsed bias to be correctly applied to a device under test. A good test method for this is to attempt to perform pulsed IV measurements through the bias tees as attempted previously;[1] if the bias tees do not distort the IV curves, they are adequate for applying a pulsed bias to an RF measurement system. In this experiment, pulsed IV measurements with pulse lengths varying from 0.1 to 1000 µs were performed on a GaAs MESFET, using an Accent Optical Technologies Dynamic i(V) Analyzer (DiVA) model D225. The measurements were performed for three setups: (1) no bias tees; (2) a set of commercially available bias tees; and (3) a set of USF custom bias tees. In the bias tee setups, the DiVA was connected to the DC ports of the bias tees and the RF ports of the bias tees were terminated in 50 Ω loads. The measurement setup is shown in ***Figure 21***. For the commercially available bias tees, the measurements were performed for pulse lengths varying from 1000 to 5 µs. When attempting to measure at 2 µs, the instrument reported that it could not complete the measurement due to the large amount of gate current. Measurements were performed for the custom USF bias tees from 1000 to 0.1 µs. From simulation and initial transient measurement results, it was expected that the bias tee would function very well for pulse lengths as low as 0.1 µs. In addition, it is desired to perform pulsed IV measurements within the pulsed S-parameter system, so it is critical that the IV characteristics be accurately measurable through the bias tees. ***Figure 22*** shows pulsed IV curves taken with different pulse lengths for the commercially available bias tees and the custom USF designed bias tees. In each plot, the dashed sets of curves are the measurements without bias tees. At 1000 µs, there is a "jog" in the knee region characteristic of the curves without bias tees. For measurements made with the commercial bias tees, this jog is not measured; however, the USF bias tees correctly depict this shift in the curves. The physical phenomenon behind this shift may be due to trapping effects. The commercial bias tees may lengthen the resetting time between pulses, so this effect is likely not due to the pulse length, but the pulse separation, as shown in Reference [3] for this device. If the pulse separation were lengthened, this result would likely to improve. However, even in this situation, it is interesting to note that the custom bias tees more closely represent the measurement environment where no bias tees are used.

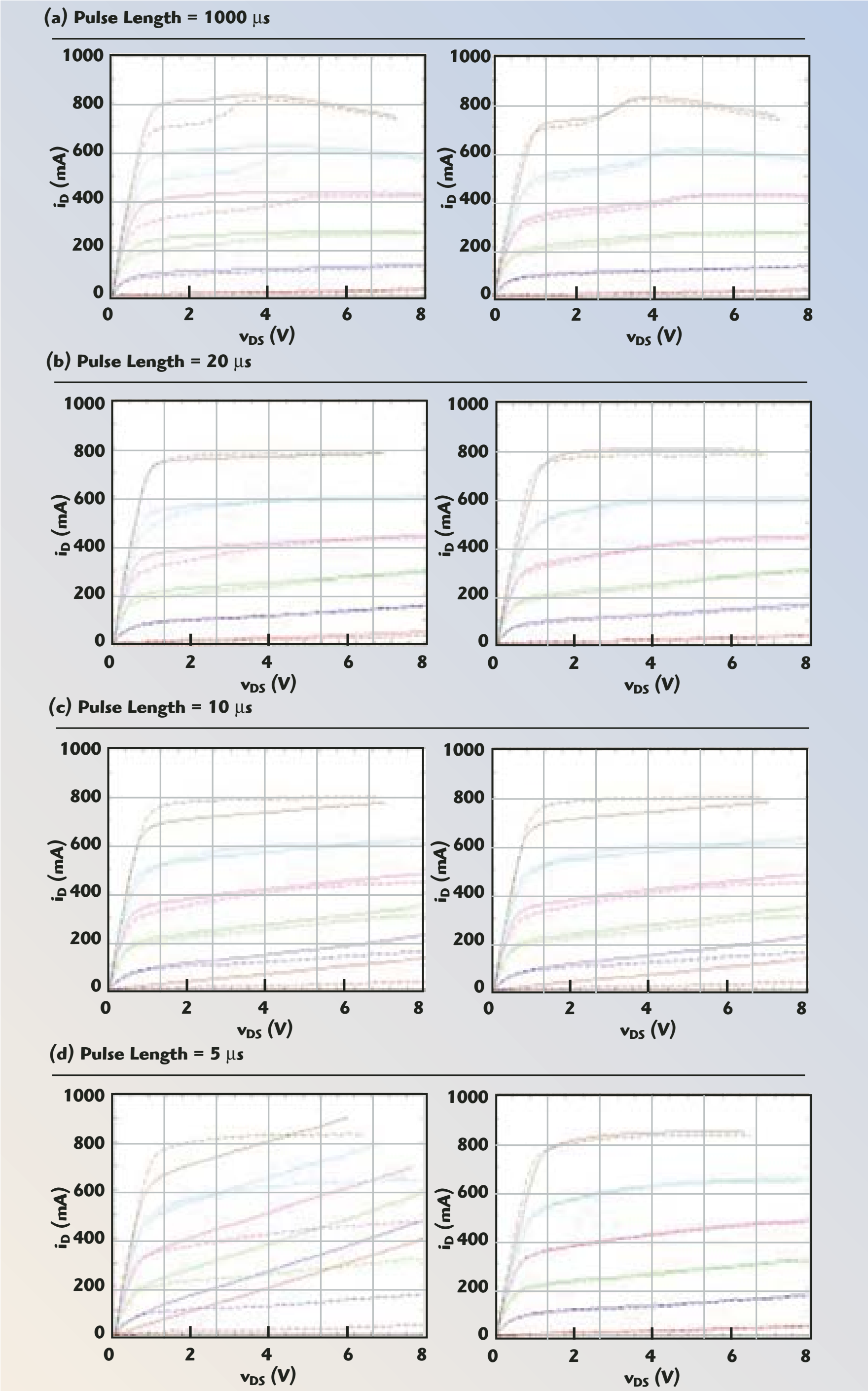

▲ *Fig. 22 Pulsed IV curves measured with no bias tees, commercially available bias tees and custom USF bias tees at different pulse lengths.*

The figure also shows that the commercially available bias tees cannot allow accurate pulsed IV measurement for pulse lengths below about 20 µs. Both bias tees allow accurate measurement of the 20 µs curves. At 10 µs, the IV curves measured through the commercial bias tees are too greatly sloped (g_{ds} is too large), while the custom bias tees allow accurate measurement of the curves. For a pulse length of 5 µs, the commercial bias tees are very clearly in error. The 0.1 µs pulse length measurement through the custom bias tees is compared to a 0.1 µs pulse length measurement without bias tees in ***Figure 23***.

In the custom bias tee measurements, the knee appears to occur at a slightly larger value of V_{DS} than for the measurements without bias tees. This is likely due to the fact that both the inductor and the coaxial-to-microstrip adapters, the FR4 substrate microstrip transmission lines, the solder joints and the inductors themselves add resistance to the drain side of the device, causing a lower voltage to be applied to the device than in the case where no bias tees are used. This DC resistive effect can be easily corrected using a Mathcad sheet if the resistance is measured. In addition, the figure shows that the curves measured through the bias tees are slightly higher than the curves measured without bias tees.

PULSED S-PARAMETERS MEASUREMENT RESULTS

The pulsed bias tee has been used successfully in the design of a pulsed-RF, pulsed-bias S-parameter measurement system, as documented by a recent conference paper.[4] ***Figure 24*** shows the S_{21} measurement results for a 5 W Si laterally diffused MOSFET (LDMOSFET) under both pulsed- and continuous-bias measurement conditions. The RF signal is pulsed in both situations; however, the bias signal is pulsed in one case and is held continuous in the other case. As documented by Parker, et al., the difference in $|S_{21}|$ can be attributed to self-heating in the device.[5] This can be predicted from the IV curves of the device, which are shown in ***Figure 25***. The bias point A is the "pulse-from" bias, while the bias point B is the "pulse-to" bias, the bias at which the measurement is performed. For the gate-voltage, drain-voltage combination given by

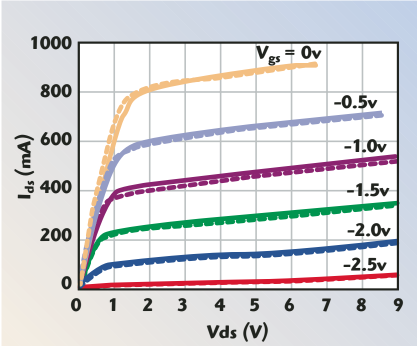

▲ *Fig. 23 Pulsed IV measurements with pulse length = 0.1 µs and without bias tee (dashed lines) or with custom USF bias tees (solid lines).*

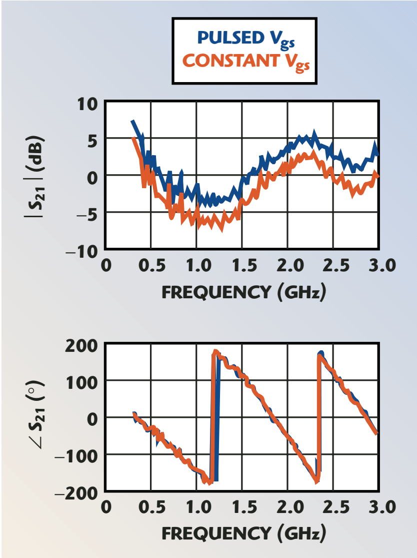

▲ *Fig. 24 S_{21} parameters of a SW Si LDMOSFET for pulsed V_{gs} (from 3.2 to 7 V) and V_{ds} = 10 V constant and continuous bias (Vgs = 7 V, V_{ds} = 10 V).*

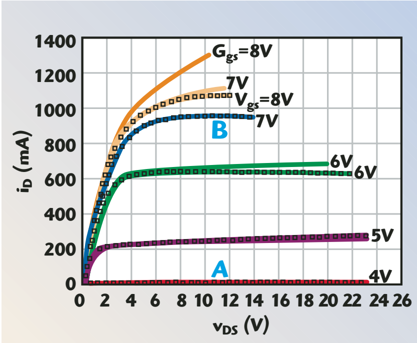

▲ *Fig. 25 Static and pulsed IV for the 5 W Si LDMOSFET; quiescent bias: V_{gs} = 3.5 V, V_{bs} = 0 V; pulsed bias: start A; end B.*

the bias point B, the difference between the current values is substantial. Notice also that the spacing between the surrounding curves is vastly different, which indicates a significant difference in the small-signal value for g_m at this bias point between the pulsed- and continuous-bias cases. This manifests itself in a lower gain for the continuous-bias case, because the value of gm is lower. This is exactly what is observed in the previous figure.

CONCLUSION

A custom bias tee design has been obtained with the assistance of accurate passive component models to accommodate pulsed-bias, pulsed-RF S-parameters measurements with pulse lengths on the order of 1 µs and lower. The simulation results for the time and frequency domains are found to compare remarkably well with the use of the models. An incremental design procedure for this circuit has been demonstrated, followed by the results of measuring pulsed IV characteristics through the bias tees. The pulsed IV results for the custom bias tees are far more accurate than those performed through commercially available bias tees, which are not normally designed to allow pulses to pass through the bias path. Finally, initial pulsed-bias, pulsed-RF S-parameter measurement results are shown and found to correlate with expectations. The design of custom bias tees for pulsed applications using accurate component models has provided first-pass success with the construction of this pulsed measurement system. ■

References

1. C. Baylis and L. Dunleavy, "Understanding Pulsed IV Measurement Waveforms," *2003 IEEE International Symposium on Electron Devices for Microwave and Optoelectronic Applications Digest*, Orlando, FL.
2. C. Baylis, "Improved Current-voltage Methods for RF Transistor Characterization," Master's Thesis, University of South Florida, 2004.
3. C. Baylis, L. Dunleavy and A.D. Snider, "The Normalized Difference Unit as a Metric for Comparing IV Curves," *64th Automatic RF Techniques Group Conference*, Orlando, FL, December 2004.
4. C. Baylis, L. Dunleavy and J. Martens, "Constructing and Benchmarking a Pulsed-RF, Pulsed-bias S-parameter System," *66th Automatic RF Techniques Group Conference*, Washington, DC, December 2005.
5. A. Parker, J. Scott, J. Rathmell and M. Sayed, "Determining Timing for Isothermal Pulsed-bias S-parameter Measurements," *1996 IEEE MTT-S International Microwave Symposium Digest*, Vol. III, pp. 1707–1710.

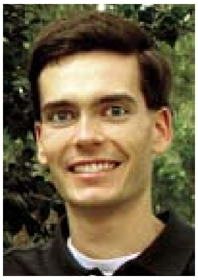

Charles Baylis *received his BS degree in electrical engineering and a minor in mathematics, summa cum laude, from the University of South Florida in 2002 and his MS degree in electrical engineering in 2004. He is now pursuing his PhD degree in the Center for Wireless and Microwave Information Systems at the University of South Florida. He serves as an adjunct instructor and a research assistant under the guidance of Lawrence Dunleavy, where he is focusing on the development and applications of pulsed measurement and electrothermal transistor characterization methods.*

Lawrence P. Dunleavy *received his BSEE degree from the Michigan Technological Institute in 1982 and his MSEE and PhD degrees from the University of Michigan in 1984 and 1988, respectively. He has worked in industry for E-Systems (1982–1983) and Hughes Aircraft Co. (1984–1990), and was a Howard Hughes doctoral fellow (1984–1988). In 1990, he joined the electrical engineering department at the University of South Florida, where he is now a professor and co-founder of the University's Center for Wireless and Microwave Information Systems. In 2001, he co-founded Modelithics Inc. to provide practical commercial modeling solutions and microwave measurement services for RF and microwave designers.*

William Clausen *received his BSEE and MSEE degrees from the University of South Florida in 2003. He has been a member of the technical staff at Modelithics Inc. since 2002. His current interests include microwave measurements, active and passive component modeling, and amplifier design.*

CHECK OUT OUR WEB SITE AT
www.mwjournal.com

A PRACTICAL DESIGN OF A LOW PHASE NOISE AIRBORNE X-BAND FREQUENCY SYNTHESIZER

Frequency synthesizers have been well studied, but difficult problems sometimes arise in their practical implementations. The major concern of synthesizer designers is the phase noise. It is critically important in Doppler radar, frequency-agile radar and various communications systems. In such applications, a synthesizer's phase noise may set the system's limits for dynamic range and reception sensitivity. The choice of an optimal architecture for minimum phase noise, rejection of spurs from different sources, and achieving high efficiency and small volume are the key steps in an airborne synthesizer design. This article describes the design of a frequency synthesizer with the following performance:

- The frequency varies from 8.9 to 9.3 GHz in steps of 20 MHz.
- The phase noise is –80 dBc/Hz at 100 Hz and –97 dBc/Hz at 10 to 600 kHz frequency offset.
- The synthesizer must use a 100 MHz reference with a phase noise of –115 dBc/Hz at 100 Hz.
- The switching time is 20 μs to reach the frequency with an error less than 1 ppm.
- The level of spurs is less than –64 dBc in the bandwidth from 10 MHz to the second harmonic of the output signal.
- The level of the second harmonic is –48 dBc and the level of the third harmonic is –55 dBc.
- The output power is +13 dBm and the power consumption is 2.3 W with a 12 V power supply.
- The volume is 250 cm^3 and the weight 470 grams.

VOLTAGE-CONTROLLED OSCILLATOR (VCO) PHASE NOISE ANALYSIS: CHOICE OF THE VCO BAND

A synthesizer consists of a voltage-controlled oscillator (VCO), a phase-locked loop (PLL) circuit and a reference signal

VSEVOLOD TANYGIN
Orion Science Research Institute
Kiev, Ukraine

source. The upper limit of a PLL IC frequency band is lower than the desired output frequency band, covering only half of it. There are two different ways to design a synthesizer—use a VCO at half the output frequency to produce the input signal to the PLL and then double it or use a VCO at the output frequency and then divide by 2 to produce the input signal to the PLL. The phase noise performance of the VCO is the main criterion to choose the best approach. The VCO phase noise is described by the Leeson equation

$$L(f_{OS})(\mathrm{dBc/Hz}) = 10\log\left\{\left(\frac{1+f_0^2}{(2f_{OS}Q_L)^2}\right)\left(\frac{1+f_C}{f_{OS}}\right)\left(\frac{FkT}{P_S}\right) + \frac{2kTRK_0^2}{f_{OS}{}^2}\right\} \qquad (1)$$

where

f_{OS} = frequency offset (Hz)
F_0 = oscillation frequency (Hz)
Q_L = loaded Q of the resonator circuit with an equivalent noise resistance R
f_C = flicker corner frequency of the active device used as the amplifying element (Hz)
F = noise figure of the active device
k = Boltzmann's constant, 1.38 10^{-21} (J/K)
T = temperature (Kelvin)
P_S = average power of the signal at the input of active device (W)
K_0 = oscillator voltage tuning gain (Hz/V)

The $2kTRK_0^2/f_{OS}^2$ term describes the noise from the resistance R. It is usually significantly lower than the others and may be neglected.
Then

$$L(f_{OS})(\mathrm{dBc/Hz}) = NF + 10\log\left(1+\left(\frac{f_{-3}}{f_{OS}}\right)^2\right) + 10\log\left(1+\frac{f_C}{f_{OS}}\right) \qquad (2)$$

$$NF_{dBc/Hz} = 10\log\left(\frac{FkT}{P_S}\right) = -173.8_{dBm/Hz} + F_{dB} - Pout_{dBm} + G_{dB} \qquad (3)$$

where the noise floor NF describes the wide-band thermal noise in each side band, Pout is the oscillator output power in dBm, G is the gain of the active device in dB, $f_{-3} = f_0/(2Q_L)$ is the oscillator –3 dBm half-bandwidth.

Typical values of $L(f_{OS})$ can be calculated for a published 4.3 GHz VCO[1]. This VCO has a 4 percent tuning bandwidth whose design is close to the one wanted for a synthesizer. The VCO consists of a series resonant circuit and a positive-feedback common-emitter amplifier using an AT-42086 silicon bipolar transistor from Agilent. The transistor noise figure is F = 8.5 dB. There is a significant degradation of the noise figure, because the input termination is far from optimal for minimum noise. The output power of the VCO is 10.5 dBm and the transistor gain is 8 dB. Then the NF = –167.8 dBc/Hz.

The total active resistance of the series resonant circuit is 12.8 Ω. The capacitive reactance of the series resonant circuit is 206 Ω and the loaded Q is 16.1, then f_{-3} = 130 MHz. An empirical value of 4 kHz for the flicker corner frequency has been determined for silicon bipolar transistors. For f_{OS} = 100 kHz then, the calculated VCO phase noise is –105.5 dBc/Hz, while the measured phase noise is –104.4 dBc/Hz.

Typical values of $L(f_{OS})$ can be predicted for a 9.1 GHz VCO based on the Leeson equation and compared with $L(f_{OS})$ for a 4.55 GHz VCO (half of output frequency) with the same relative tuning bandwidth of 4.4 percent needed for the synthesizer. It is assumed that bipolar transistors are used in both VCOs, because they have a 10 to 15 dB lower phase noise than FETs.

The first degradation factor in a 9.1 GHz VCO is the increase of the output frequency. If f_0 in the Leeson equation is multiplied to 2, then $L(f_{OS})$ is increased by 6 dB in the $f_{OS} < f_{-3}$ region. Of course, this degradation is compensated by the frequency doubling of a 4.55 GHz VCO to produce the synthesizer output frequency.

The second degradation factor is that the transistor f_{MAX} is higher for devices with smaller areas, and conversely, larger-area devices yield higher output power at lower frequencies. Therefore, P_s in Leeson's equation for a 9.1 GHz VCO is typically 3 to 6 dB lower than that for a 4.55 GHz VCO. If the transistor noise figure remains constant for both VCOs, the noise floor of a 9.1 GHz VCO is typically 3 to 6 dB higher.

The third degradation factor is the decrease of Q_L, because the resonator's capacitive reactance is divided by 2 when the frequency is doubled. Of course, the designer may use a smaller capacitance varactor to keep the capacitive reactance constant, but he may also use this varactor in a lower frequency VCO.

For example, a high Q microwave abrupt varactor GC1300 from Microsemi has a C(0V) = 1.2 pF, C(4V) = 0.8 pF. If it is series-connected with a 0.27 pF capacitor, it covers a 4.4 percent synthesizer bandwidth. The resonator capacitive reactance is equal to170 Ω at 4.55 GHz or 85 Ω at 9.1 GHz. If the total active resistance of the series resonant circuit remains constant for both VCOs, the loaded Q of the 9.1 GHz VCO is half and the phase noise is 6 dB higher than for the 4.55 GHz VCO. Since the phase noise of the 9.1 GHz VCO is 9 to 12 dB higher than for a 4.55 GHz VCO plus frequency doubler, a 4.55 GHz VCO is used in the synthesizer.

It is far more practical to consider VCOs or integrated oscillator subsystems as components and to purchase them from one of the specialized manufacturers. The HMC429LP4 integrated VCO from Hittite Microwave Corp. is the best choice for a 4.55 GHz VCO, because it has a 100 kHz offset SSB phase noise of –105 dBc/Hz and 4.4 to 4.7 GHz tuning bandwidth.

PLL PHASE NOISE ANALYSIS: CHOICE OF OPTIMAL ARCHITECTURE

The phase noise performance of a PLL is the main criteria to choose the best PLL architecture. The PLL noise model is shown in ***Figure 1***. In this model, θ_{ref} represents the reference phase and $\Delta\theta_{ref}$ (s) represents the noise of the reference phase. The terms θ_{in} (s) and θ_{out} (s) represent the input and output phases of the PLL. 1/M and 1/N are the reference and main divider ratios. K_{pd}, F(s) and K_{vco}/s are the transfer functions of the phase detector, the low pass filter and the VCO. The term $\Delta\theta_{pd}$ (s) represents the PLL chip noise, including

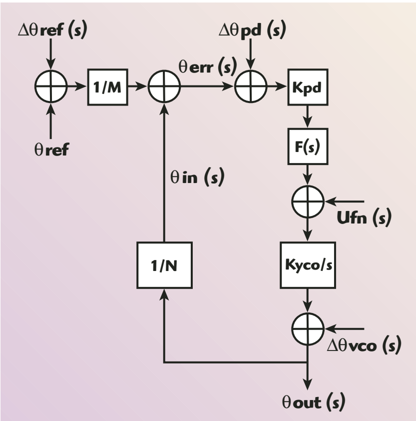

Fig. 1 Noise model of the PLL.

the noise of the dividers and phase detector. The RMS noise voltage of the filter (Ufn) is represented by the additional term U_{fn} (s). The noise of the VCO is represented by the term $\Delta\theta_{vco}$ (s). The open loop gain is given by

$$G(s)=\frac{\theta_{in}(s)}{\theta_{err}(s)}=\frac{K_{pd}F(s)K_{vco}}{(N\ s)}$$

$$s = j\omega = j2\pi f_{os} \tag{4}$$

The transfer functions from the noise inputs to the PLL output are defined by

$$H_{ref}(s)=\frac{\theta_{out}(s)}{\Delta\theta_{ref}(s)}=\frac{N}{M}\frac{1}{\left(1+\frac{1}{G(s)}\right)} \tag{5}$$

$$H_{pd}(s)=\frac{\theta_{out}(s)}{\Delta\theta_{pd}(s)}=N\frac{1}{\left(1+\frac{1}{G(s)}\right)} \tag{6}$$

$$\frac{N}{\left(K_{pd}F(s)\right)}\frac{1}{\left(1+\frac{1}{G(s)}\right)} \tag{7}$$

$$H_{vco}(s)=\frac{\theta_{out}(s)}{\Delta\theta_{vco}(s)}=\frac{1}{\left(1+G(s)\right)} \tag{8}$$

Usually, manufacturers give the phase noise data of the VCO, the reference source and the PLL chip as SSB phase noise $L_{vco}(f_{os})$, $L_{ref}(f_{os})$ and $L_{pd}(f_{os})$. The phase noise at the PLL output is given by

$$L_{out}(f_{os})(dBc/Hz)= 10\log\left\{\text{antilog}\left(\frac{N_{vco}(f_{os})}{10}\right)+\text{antilog}\left(\frac{N_{ref}(f_{os})}{10}\right)+\text{antilog}\left(\frac{N_{fn}(f_{os})}{10}\right)+\text{antilog}\left(\frac{N_{pd}(f_{os})}{10}\right)\right\} \tag{9}$$

where

$$N_{vco}(f_{os})=L_{vco}(f_{os})+20\log\left(\left|\frac{1}{(1+G(s))}\right|\right)\ (dBc/Hz) \tag{10}$$

is the output phase noise from the VCO only,

$$N_{ref}(f_{os})= L_{ref}(f_{os})+20\log\left(\left|\frac{1}{\left(1+\frac{1}{G(s)}\right)}\right|\right) +20\log(N/M)\ (dBc/Hz) \tag{11}$$

is the output phase noise from the reference only,

$$N_{pd}(f_{os})= L_{pd}(f_{os})+20\log\left(\left|\frac{1}{\left(1+\frac{1}{G(s)}\right)}\right|\right) +20\log(N)\ (dBc/Hz) \tag{12}$$

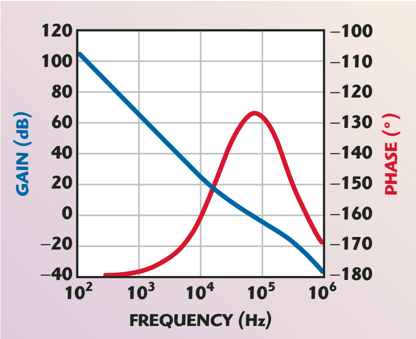

▲ *Fig. 2 Open loop gain and phase.*

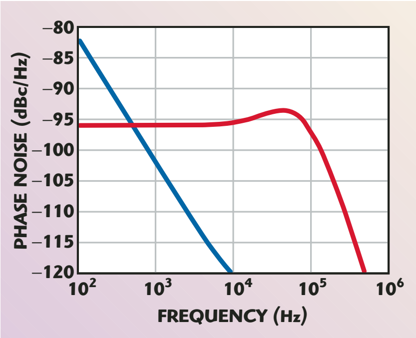

▲ *Fig. 3 Phase noise from the reference only (blue) and from the chip only (red).*

is the output phase noise from the chip only,

$$N_{fn}\left(f_{os}\right) = 20\log\left\{\frac{N}{\left(\sqrt{2}K_{pd}\left|F(s)\right|\bullet\left|1+\frac{1}{G(s)}\right|\right)}\right\} + 20\log\left(U_{fn}\left(f_{os}\right)\right)\ \left(dBc/Hz\right) \quad (13)$$

is the phase noise from the filter only.

INTEGER-N PLL

The simplest PLL architecture is the integer-N PLL. In this case the output frequency is

$$f_{out} = 2\,F_{PD}\,N$$

where F_{PD} = 10 MHz is the frequency of the phase detector (half of the output step) and N = 445…465 is the main division ratio. An ADF4107 PLL chip from Analog Devices is used for the PLL, because it has a high input bandwidth (up to 7 GHz), a high phase detector frequency (up to 104 MHz) and low divider and phase detector phase noise (L_{pd} = –149 dBc/Hz at F_{PD} = 10 MHz). A reference source MV87-1-100 MHz oven-controlled crystal oscillator

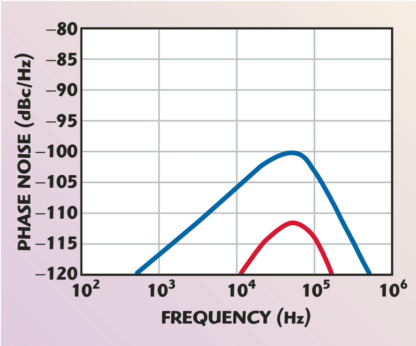

▲ *Fig. 4 Phase noise from the VCO only (blue) and from the loop filter only (red).*

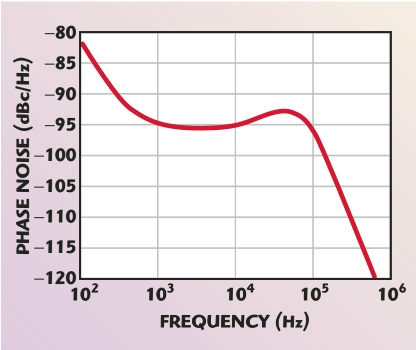

▲ *Fig. 5 Overall PLL output phase noise.*

(OCXO) from Morion Inc. is used for the PLL, because it has a low phase noise, –115 dBc/Hz at 100 Hz offset. A second-order passive charge pump filter[2] is used for the PLL. The filter transfer function is its impedance. The frequency ω_P of phase inflection point of G(s) is equal to the PLL bandwidth. At ω_P, the phase term of G(s) has a maximum: $\phi(\omega_P) = -180° + \phi_P$. A common rule of thumb is to begin the PLL design with ϕ_P = 45°. However, it is recommended to slowly increase ϕ_P up to 53° with only a 1 dB overshoot at ω_P in the Equations 5 to 8 transfer functions.

To achieve minimum phase noise at all offsets, the PLL bandwidth ω_P must be set close to the point where the free-running VCO phase noise is equal to the overall PLL phase noise from other noise sources. If ω_P is less, the PLL cannot improve the VCO phase noise at high frequency offsets. If ω_P is more, the PLL begins to degrade the VCO phase noise at frequency offsets beyond ω_P. From Equations 11 and 12, with ϕ_P = 53°, $\omega = \omega_P$, N = 455, M = 10, N_{ref} = –125.8 dBc/Hz and N_{pd} = –94.8 dBc/Hz.

Assuming $\omega = \omega_P$, the loop filter noise is much lower than N_{pd}, and then N_{pd} dominates over the other noise sources. From the VCO phase noise plot, f_{os} = 75 kHz, at which L_{vco} is equal to –101 dBc/Hz. With ω_P = 2π 75 kHz and calculating from Equation 9, L_{out} = –93.7 dBc/Hz. If ϕ_P and ω_P are defined, the filter elements can be found: C_1 = 1.66 nF, C_2 = 13.1 nF, R_1 = 483 Ω. To obtain the RMS noise voltage at the filter output, a practical resistor R_1 can be substituted by an ideal resistor and an in-series connected equivalent noise source with a RMS voltage

$$En = 2\sqrt{\left(kTR_1\right)} = \frac{2.82nV}{\sqrt{Hz}} \quad (14)$$

The output phase noise from the filter only can be found from Equations 12 and 14,

$$N_{fn}\left(f_{os}\right)\left(dBc/Hz\right) = 20\log\left\{\frac{N_sC_2}{\left(\sqrt{2}K_{pd}\left|1+sR_1C_2\right|\bullet\left|1+\frac{1}{G(s)}\right|\right)}\right\} + 20\log\left(E_n\right) \quad (15)$$

Calculations for f_o = 75 kHz give N_{fn} = –112 dBc/Hz. To confirm the assumptions, the ADI SimPLL™ software from Analog Devices is used to simulate the PLL performance with the previously defined parameters. The open loop gain and phase plots are calculated with Equation 4 and shown in ***Figure 2***. The output phase noise from the reference N_{ref} (f_{os}) only and the output phase noise from the chip $N_{pd}(f_{os})$ only are calculated from the manufacturer's data with Equations 11 and 12 and shown in ***Figure 3***. The output phase noise from the VCO $N_{vco}(f_{os})$ only and the output phase noise from the loop filter $N_{fn}(f_{os})$ only are calculated from the manufacturer's data with Equations 10 and 15 and shown in ***Figure 4***. The overall PLL output phase noise is calculated with Equation 9 and shown in ***Figure 5***.

There are two regions in the PLL bandwidth. In the first region (f_{os} < 500 Hz), the reference phase noise is the greatest of all noise sources. The synthesizer output phase noise (SPN) in the first region at f_{os} = 100 Hz is given by

$$SPN_1 \approx L_{ref}(f_{os}) + 20\log\left(\frac{N}{M}\right) + 6\ dB = -75.8\ dBc/Hz \quad (16)$$

In the second region (1 kHz < f_{os} < 50 kHz), the chip phase noise is the greatest of all noise sources. The chip phase noise dependence on the phase detector frequency is given by

$$L_{pd} = L_{PN\ Floor} + 10\log(F_{PD}) \quad (17)$$

where $L_{PN\ Floor}$ = –219 dBc/Hz is the ADF4107 phase detector phase noise floor if F_{PD} = 1 Hz. Therefore, in the second region, the synthesizer output phase noise is given by

$$SPN_2 \approx L_{PN\ Floor} + 10\log(F_{PD}) + 20\log(N) + 6\ dB = -89.8\ dBc/Hz \quad (18)$$

FRACTIONAL-N PLL

From Equations 16 and 18, it can be seen that to decrease SPN_1 and SPN_2, F_{PD} must be increased and N must be decreased. However, N becomes fractional in this case. To operate with a fractional-N, a fractional-N PLL chip must be used. An ADF4193 chip from Analog Devices and a V630ME09 VCO from Z-Communications were used to simulate the performance of the fractional-N PLL. Because the maximum input frequency of the PLL chip is only 3.5 GHz, a multiplier by four is used to produce the synthesizer output signal. In this case, the output frequency is given by

$$f_{out} = 4F_{PD}N = 4F_{PD}\left(INT + \frac{FRAC}{MOD}\right) \quad (19)$$

where INT is an integer part of N and FRAC/MOD is a fractional part of N. Because the maximum phase detector frequency of the ADF4193 is 26 MHz, F_{PD} is set to 25 MHz (M = 4) and MOD = 25. Then, INT = 89…92, FRAC = 0…24 and a set of output frequencies with spacing of 4 F_{PD}/MOD = 4 MHz is obtained. Only every fifth frequency of this set are used. The PLL phase noise versus frequency-offset plot is shown in ***Figure 6***. The synthesizer output phase noise in the first region at f_{os} = 100 Hz is given by

$$SPN_1 \approx L_{ref}(f_{os}) + 20\log\left(\frac{N}{M}\right) + 12\ dB = -75.8\ dBc/Hz \quad (20)$$

It is equal to the SPN_1 at 100 Hz offset of the integer-N PLL, because the overall multipliers of the reference frequency in these synthesizers are equal. The synthesizer output phase noise in the second region is given by

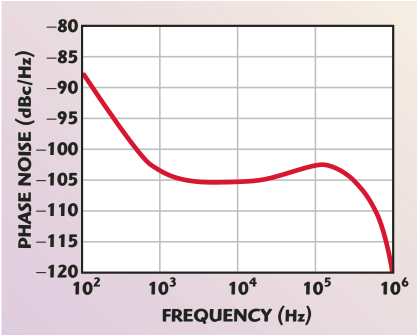

▲ *Fig. 6 Phase noise simulation for a fractional-N PLL.*

$$SPN_2 \approx L_{PN\ Floor} + 10\log(F_{PD}) + 20\log(N) + 12\ dB = -93.6\ dBc/Hz \quad (21)$$

There is a 4 dB improvement with respect to the integer-N PLL, because the F_{PD} in a fractional-N PLL is also greater by 4 dB.

HYBRID SYNTHESIZER

Another way to operate with fractional N is to use the hybrid synthesizer architecture with frequency translation,[3] as shown in ***Figure 7***. This architecture contains the first fixed integer-N PLL with maximum available F_{PD} and the second tunable integer-N PLL. The signals of these sources are combined in the mixer, filtered and doubled. The output frequency is given by

$$f_{out} = 2(f_1 + f_2) = 2(F_{PD1}N_1 + F_{PD2}N_2) = 2\ F_{PD1}\left(INT + \frac{FRAC}{MOD}\right) \quad (22)$$

where the terms f_1 and f_2 are the frequencies of the first and second PLL. The phase detector frequency of the fixed PLL F_{PD1} is 100 MHz to operate with the maximum available F_{PD}. The phase detector frequency of the tunable PLL F_{PD2} is half the output step or 10 MHz.

Equation 22 represents the "virtual" fractional-N PLL with FPD = 100 MHz. The coefficients in Equation 22 are

$$MOD = \frac{F_{PD1}}{F_{PD2}} = 10 \quad (23)$$

$$INT = N_1 + int\left(F_{PD2} \bullet \frac{N_2}{F_{PD1}}\right) = N_1 + int\left(\frac{N_2}{10}\right) \quad (24)$$

$$\frac{FRAC}{MOD} = \frac{N_2}{10} - int\left(\frac{N_2}{10}\right) \quad (25)$$

where $int(x)$ is the operation of taking only the integer part of the variable x.

The chip phase noises of the first and second PLLs are independent, because they are generated by two independent chips. Therefore, if they are equal, their combination has a minimum

$$L_{PN\ Floor\ 1} + 10\log(F_{PD1}) + 20\log(N_1) = L_{PN\ Floor\ 2} + 10\log(F_{PD2}) + 20\log(N_2) \quad (26)$$

An ADF4107 is used in both PLL, because it has a minimum PN floor. Therefore

$$10\log(F_{PD1}/F_{PD2}) = 20\log(N_2/N_1)$$

then $N2/N_1 = 3.16$

In order to produce f_{out} and to keep the minimum input frequency of the ADF4107 (1.0 GHz), $N_1 = 34$, $N_2 = 105\ldots125$ can be obtained. Then, from Equations 24 and 25,

$$INT = 34 + 10\ldots12 = 44\ldots46,$$
$$FRAC = 0\ldots9$$

Therefore, the values of the PLL frequencies are $f_1 = 3400$ MHz, and $f_2 = 1050\ldots1250$ MHz.

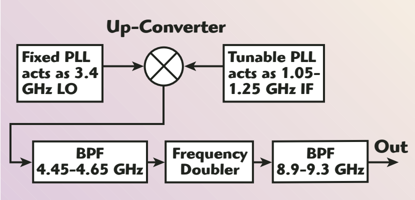

▲ *Fig. 7 A hybrid synthesizer architecture with frequency translation.*

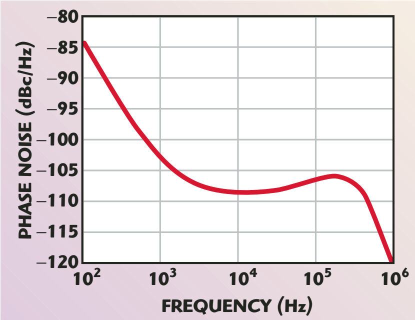

▲ *Fig. 8 Simulated phase noise of the fixed PLL .*

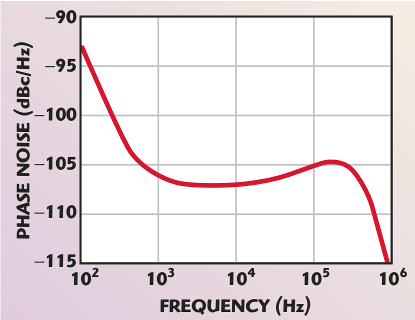

▲ *Fig. 9 Simulated phase noise for the tunable PLL .*

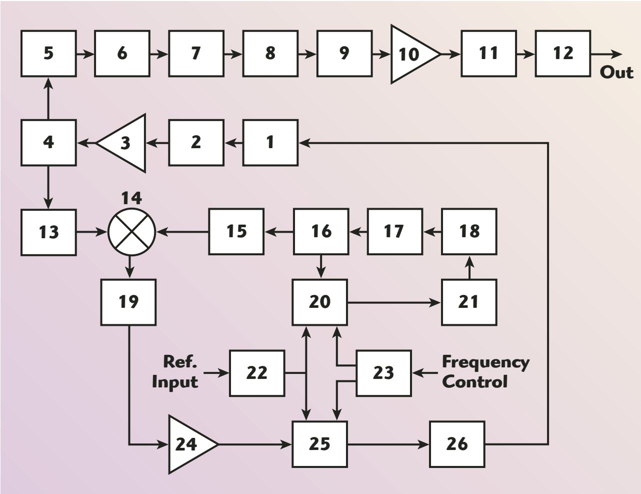

Fig. 10 A practical frequency translation architecture.

The HMC389LP4 VCO from Hittite Microwave Corp. is used to simulate the performance of the fixed PLL. The phase noise versus frequency offset plots for the first and second PLLs are given in ***Figures 8*** and ***9***.

The levels of the chip's phase noise are approximately equal to –107 dBc/Hz. Their combination at 4.45 to 4.65 GHz has a phase noise 3 dB greater, because they are independent: –104 dBc/Hz. SPN_2 is equal to –104 + 6 = –98 dBc/Hz. There is an 8 dB improvement with respect to the integer-N PLL, because FPD in the hybrid synthesizer is greater than 10 dB, but the degradation from the combination is only 3 dB. At a 100 Hz offset, the phase noise of both PLLs and the combined phase noise are calculated from

$$L_1 \approx L_{ref} + 20\log(N_1/M_1) = -115 + 30.6 = -84.4 \text{ dBc/Hz},$$

$$L_2 \approx L_{ref} + 20\log(N_2/M_2) = -115 + 21.2 = -93.8 \text{ dBc/Hz}$$

$$L_\Sigma = 20\log(\text{antilog}(L_1/20) + \text{antilog}(L_2/20)) = -81.9 \text{ dBc/Hz}$$

SPN_1 is equal to –81.9 + 6 = –75.9 dBc/Hz. It is equal to the SPN_1 of the integer-N PLL, because the overall multipliers of the reference frequency in these synthesizers are equal. It can be seen that any architecture cannot improve the reference phase noise, but a hybrid architecture improves the chip phase noise by up to 8 dB.

PRACTICAL FREQUENCY TRANSLATION ARCHITECTURE

There are two disadvantages in the frequency translation architecture—the low level of the mixer output and the high relative level of mixer spurs. A modified practical architecture is shown in ***Figure 10***. The HMC429LP4 VCO (1) generates a 4.45 to 4.65 GHz signal. After an isolator (2) and an FET amplifier (3) the signal, with a +14 dBm power level, is divided by a power divider (4) into two parts. The first part goes to the FET frequency doubler (6) through an isolator (5). The second part goes to the HMC213MS8 double-balanced mixer (14) from Hittite Microwave through an isolator (13) and acts as the LO.

The fixed 3.4 GHz PLL contains an HMC389LP4 VCO (18), an isolator (17), a power divider (16), an ADF4107 PLL chip (20) and a passive three-pole loop filter (21). The 3.4 GHz signal from the power divider (16) goes through a harmonic filter (15) to the RF input of the mixer (14) with a power level of –10 dBm. The mixer (14) translates the 4.45 to 4.65 GHz LO frequency to the 1.05 to 1.25 GHz IF frequency. Then the IF signal goes through a low pass filter (19) and an MMIC amplifier (24) to the ADF4107 PLL chip (25) with a power level of +2 dBm. The tuned 1.05 to1.25 GHz PLL contains a chip (25), an active three poles loop filter (26) and becomes a "virtual VCO" with sensitivity and phase noise similar to the HMC429LP4 VCO. After the frequency doubler (6), the signal goes through the isolator (7) to the bandpass filter (BPF) (8). The signal then goes through the isolator (9) to the two-stage FET amplifier (10). After amplification, the +16 dBm signal goes through an isolator (11) and a harmonic filter (12) to the output, where it emerges with a +13 dBm level. The reference signal from the external 100

MHz OCXO is amplified by the amplifier (22) and goes to the PLL chips (20, 25). The frequency control TTL signals go to the ADuC814 MicroConverter (23) from Analog Devices. It writes the control bits into the PLL chips.

There are two differences between this architecture and the previous one. First, the 4.45 to 4.65 GHz signal is generated by the VCO at a higher power level and acts as the LO of the mixer. Second, the mixer acts as a down-converter and operates at lower power levels for both 3.4 and 1.05 to 1.25 GHz signals. As a result, a higher power level for the desired signal and a lower level for unwanted signals are achieved at the doubler's input. This is very important, because the frequency doubler can produce high order spurs, which can arise within the bandwidth of the BPF (8). The output spectrum of the synthesizer, measured with a HP8592A spectrum analyzer with a resolution bandwidth of 3 kHz, is shown in ***Figure 11***. A 6 dB attenuator is connected to the synthesizer output. The measured average noise level at 20 to 100 kHz offset frequencies is approximately – 63 dBc. Then, the average noise level in dBc/Hz is given by

$$L_{out}\,(\text{dBc/Hz}) = L_{measured}\,(\text{dBc}) - 10\log(3000) = -97\ \text{dBc/Hz}$$

which agrees well with the theoretical result of –98 dBc/Hz.

REJECTION OF SPURS IN PRACTICAL ARCHITECTURE

There are three sources of spurs in the practical architecture - the mixer, the frequency doubler and the PLL charge pumps. The mixer (14) has a –33 dBm, 3.4 GHz, RF leakage at the LO input. The isolator (13) attenuates this signal down to –50 dBm. The frequency doubler produces high order spurs over a wide bandwidth, but the spur at the unwanted 3.4 GHz has a very low power level. The desired signal at the doubler output is the second harmonic and all other harmonics are unwanted and must be rejected by the BPF (8). The synthesizer's output level for the 4.5 GHz spur is –64 dBc. The BPF (8) has a rejection level for the third harmonic of approximately 48 dB, with an extra rejection of 20 dB provided by the filter (12). The PLL charge pump spurs are the result of the charge pump unbalance and the DC current at its output. The total leakage current IL on the charge pump output can be assumed to combine all sources of leakage. The charge pump current waveform I(t) is a periodic series of short pulses with an I_{cp} amplitude and an FPD repetition frequency. The relative level of the first spurs can be found from the Fourier transform of this signal and FM theory as

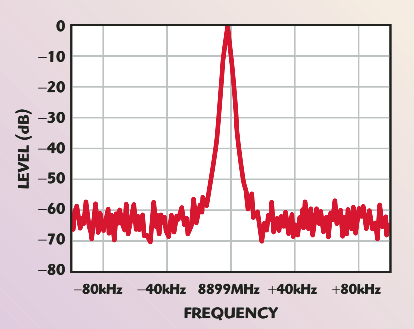

▲ *Fig. 11 Measured output spectrum of the synthesizer.*

$$L_1(\text{dBc}) = 20\log\left(\frac{I_L Z_1 K_{vco}}{(2\pi n\ F_{PD})}\right) \quad (27)$$

where Z_1 is the loop filter impedance[2] at the frequency F_{PD}.

First, the maximum spur level is calculated for a fixed 3.4 GHz PLL. The PLL parameters are: F_{PD} = 100 MHz, $K_{vco} = 2\pi \cdot 50$ MHz/V, K_{pd} = 5 mA/(2π rad), N = 34, $\phi_P = 53°$, $\omega_P = 2\pi$ 300 kHz. The loop filter elements are: C_1 = 692 pF, C_2 = 5.49 nF, R_1 = 289 Ω. The loop filter impedance is Z_1 = 2.3 Ω. The leakage current at the tuning port of the VCO (18) is 10 μA maximum. Equation 27 gives the value of the maximum spur level: L_1 = –99 dBc. It is an acceptable value, but an extra RC LPF with a 3.0 MHz pole frequency is added to reject a 100 MHz EMI from the reference

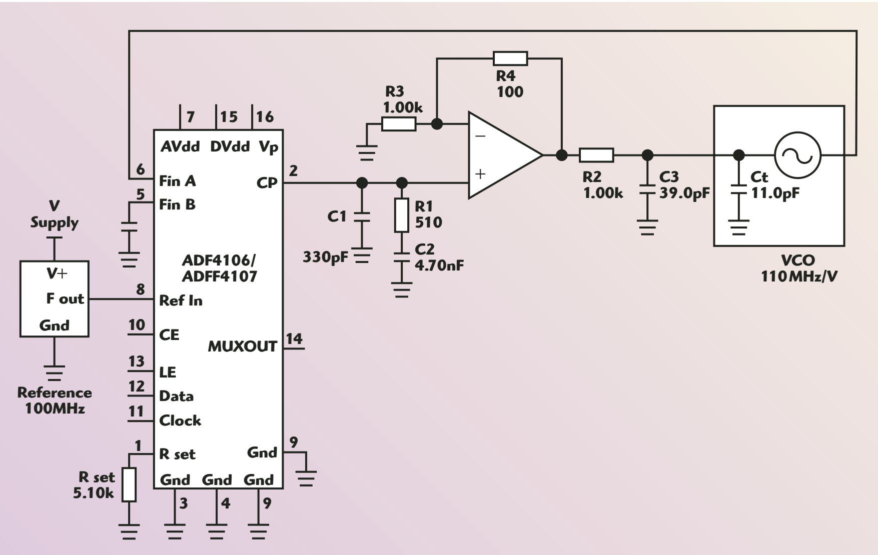

▲ *Fig. 12 Schematic of the active third-order 350 kHz loop filter.*

source. This additional RC circuit forms a third-order passive loop filter, which is placed as closely as possible to the tuning pin of the VCO (18). It produces an additional 30 dB attenuation of the reference frequency. The synthesizer's output first spur level is –123 dBc and cannot be measured.

In the tunable 1.05 to 1.25 GHz PLL, the leakage current at the tuning port of the VCO (1) is 10 µA also, but the phase detector frequency is 10 MHz. The same loop filter as filter (21) rejects this spurs only to –51 dBc (first output spur). An active third-order 350 kHz loop filter with a 3.2 MHz last pole is used to reject the charge pump spurs. Its schematic is shown in ***Figure 12***. The operational amplifier (op-amp) is a low noise OP184FS from Analog Devices. The main advantage of the active filter is the reducing of the leakage current down to 0.6 µA. It decreases the level of the first output spurs to –72 dBc. Their measured level is –70 dBc.

REJECTION OF SPURS FROM THE POWER SUPPLY UNIT

Achieving high efficiency is very important for airborne equipment. All the components of the synthesizer require a power supply voltage of +3.0 or +5.0 V, but the power supply voltage available is +12 V. A DC-to-DC step-down converter solves this problem, but it becomes the fourth source of spurs and extra phase noise in a common small-volume housing of 190 cm^3. High grade rejection of electrical and magnetic noises from the DC-to-DC converter is needed.[4,5] There are two paths through which these noises propagate—conductive and through the magnetic field of the converters inductors. This last path is rejected by using self-shielding inductor cores with small air gaps. The conductive path has two modes of propagation—common-mode and differential-mode. The common-mode is rejected by suspending the converters PCBs in the housing (decreasing the parasitic capacitance to ground) and using common-mode chokes at the input and output of the converters. The differential-mode ripple and noise are rejected by LC-LPF and voltage regulators ADP3301 from Analog Devices. The PLL does not work at the 260 kHz converter's switching frequency and the VCO (1) is approximately in a free-running condition. One finds 260 kHz spurs from the ripple of the power supply. The level of sinusoidal FM spurs at the output of the VCO is given by[4,5]

$$L_{VCO(1)}(\mathrm{dBc}) = 20\log\left(\frac{K_p U_m}{(2 \bullet 2\pi F_{mod})}\right) \mathrm{dBc} \qquad (28)$$

where

U_m = peak modulation voltage
F_{mod} = 260 kHz
K_p = $2\pi 14$ MHz/V is the pushing sensitivity

The DC-to-DC converter has 20 mV peak output ripples, the LC-LPF ripple rejection is 34 dB and the ADP3301 ripple rejection is 35 dB.

Then, $U_m = 7\ \mu V$, $L_{VCO(1)} = -74$ dBc and the synthesizer's output spurs are 6 dB higher: –68 dBc.

The ripples go to the tuning port of VCO through the charge pump supply line. The charge pump has a power supply rejection ratio (PSRR) probably greater than 20 dB, but the tuning sensitivity $K_{vco} = 2\pi 110$ MHz/V is 18 dB greater than the pushing. Therefore, the output level of the 260 kHz spurs from ripple on the tuning port is less than –70 dBc. Another path to the tuning port of the VCO (1) is the supply line of the operational amplifier (26). However, the PSRR of the OP184 is approximately 30 dB in the 100 to 300 kHz band. Therefore, the output spur level from this path is –80 dBc. Combining these spurs results in output spur levels of –63 dBc. The measured level of the converter spurs at the synthesizer's output is approximately –65 dBc.

WIDEBAND NOISE IN THE PRACTICAL ARCHITECTURE

To design an optimal PLL, its bandwidth must be set closely to the point where the free-running VCO phase noise is equal to the chip phase noise. However, in practice, the noise of the power supply and of the loop filter elements must be taken into account. The phase noise at 200 kHz offset frequency must be found from the voltage noise on the supply line of VCO (1) under free-running conditions. The phase noise level at the output of the VCO is given by[4,5]

$$\text{PN supply}\left(\text{dBc/Hz}\right) = 20\log\left(\frac{K_p U_{NS}}{\left(\sqrt{2}\ 2\pi f_{os}\right)}\right) \qquad (29)$$

The ADP3301 voltage regulator has an output noise voltage density $U_{NS} = 40\ \text{nV}/\sqrt{\text{Hz}}$ at $f_{os} = 200$ kHz. Then, the supply PN is equal to –114 dBc/Hz. The total noise voltage density at 200 kHz, U_{fn}, at the tuning port of the VCO (1), must be found. There are seven independent sources of this noise—the noises of resistances R_1 to R_4 and the op-amp equivalent input noise voltage and current. The seventh is the noise of the voltage regulator, which goes through the charge pump with a minimum of 20 dB attenuation and through the op-amp with a 30 dB attenuation.

After RMS combining, the total noise voltage density at 200 kHz at the tuning port of the VCO (1) can be found: $U_{fn} = 7.8\ \text{nV}/\sqrt{\text{Hz}}$. The VCO output phase noise can obtained from Equation 29

$$\text{PN tune} = 20\log(K_{vco}U_{fn}/(\sqrt{2}\ 2\pi f_{os})) = -110.3\ \text{dBc/Hz}$$

The VCO (1), with a "clean" power supply and a "clean" tuning voltage, has an $L_{vco} = -111$ dBc/Hz at 200 kHz offset. Therefore, the total phase noise of VCO (1) at 200 kHz offset, in a practical architecture, is

$$L_{vco}(1) = 10\log(\text{antilog}(L_{vco}/10) + \text{antilog}(\text{PN supply}/10) + \text{antilog}(\text{PN tune}/10)) = -106.7\ \text{dBc/Hz}$$

The chip phase noise is equal to –107 dBc/Hz. If the PLL bandwidth is set at 200 kHz, then a 3 dB overshoot is generated at the 200 kHz offset frequency. Thus, the PLL bandwidth is set at 350 kHz and ϕ_P at 60°.

The measured output spectrum of the synthesizer, measured with a 10 kHz resolution bandwidth over a 2 MHz span, is shown in ***Figure 13***. There is extra phase noise in the 300 to 1000 kHz offset frequency range, compared with simulation results. From Equation 1, it can be seen that the phase noise response must have a slope of –20 dB/decade above 350 kHz. However, the figure shows a constant level in the 300 to 600 kHz range. The source of this effect is a decrease of the op-amp and charge pump PSRRs in the 300 to 600 kHz band.

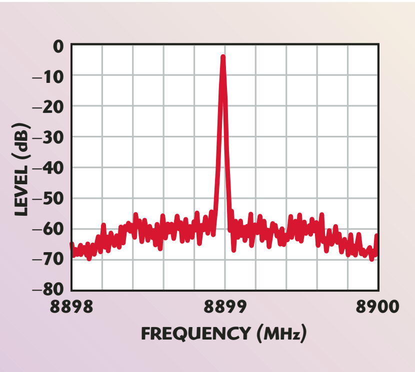

▲ *Fig. 13 Measured output spectrum of the synthesizer.*

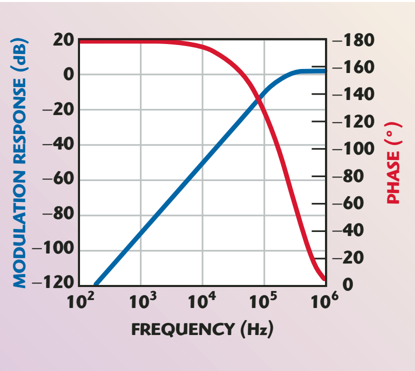

▲ *Fig. 14 Simulation of the FM response of the fixed PLL.*

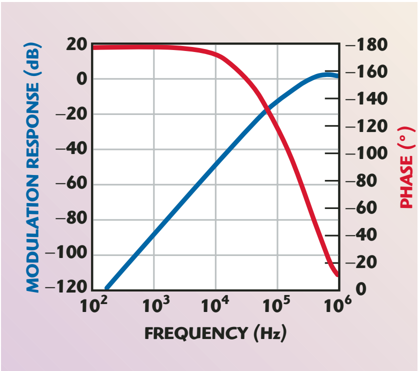

▲ *Fig. 15 Simulation of the FM response of the tunable PLL.*

HARMONIC REJECTION

The next problem is achieving a high efficiency with low harmonic levels. The output amplifier efficiency is maximum when saturated and therefore high harmonics are generated. The harmonic filter (12) contains microstrip lines with open stubs. Their lengths are a quarter-wave at frequencies of 1.5, 2 and 3 F_{OUT}, with separations equal to a quarter-wavelength at F_{OUT}. This line is placed on the wide side of a waveguide with a 12.5 GHz cut-off frequency. The waveguide has an absorber on its narrow side, upon which all the stubs ends. The high harmonic signals radiated by the stubs are immediately absorbed. The insertion loss is 3 dB at F_{OUT}, 36 dB at 2 F_{OUT} and 40 dB at 3 F_{OUT}. The measured level of the second harmonic is –48 dBc and the third harmonic level is less than –55 dBc. The output power is +13 dBm and the total power consumption is 2.3 W.

SUPPRESSION OF THE MICROPHONE EFFECT

Suppression of the microphonic effect is very important in airborne equipment. The ceramic chip capacitors have a piezoelectric effect. If they are used in high impedance circuits, such as the tuning port of a VCO, they become the sources of microphonic FM. A piezoelectric voltage of only 0.13 µV on the tuning port of the free-running VCO (1), due to vibrations at 100 Hz, produces an output spur level of –30 dBc. The ferrite microwave isolators also have a microphonic effect. They are the sources of microphonic FM because they are the loads of the VCOs.

The PLL suppression of low frequency modulations of the VCO from the tuning port, the power supply port and modulation of the load reflection coefficient must be tested. The measurement of the tuning port FM is very practical for both PLLs—fixed and tuned. First, the PLL is disabled by setting the charge pump in three-state. A small sinusoidal signal is injected at the tuning port of the VCO through a high resistor. The relative level of spurs under free-running condition is measured. It is given by

$$L_{F-R}\left(\mathrm{dBc}\right) = 20\log\left(\frac{K_{vco}U_m}{2\ 2\pi F_{mod}}\right) \quad (30)$$

where U_m and F_{mod} are the amplitude and frequency of the modulation signal at the tuning port. Second, the PLL is enabled. The relative level of spurs under this condition is measured. It is given by

$$L_{PLL}\left(\mathrm{dBc}\right) = 20\log\left(\frac{K_{vco}U_m}{\left(2\ 2\pi\ F_{mod}\left|1+G(s)\right|\right)}\right) = L_{F-R} - 20\log\left(\left|1+G(s)\right|\right) \quad (31)$$

where $s = j2\pi F_{mod}$. The term $20 \bullet \log(|1 + G(s)|)$ is the PLL FM suppression. It has been calculated for the fixed and tunable PLLs. The phase term of $(1 + G(s))$ is also calculated. The results are shown in ***Figures 14*** and ***15***. There is approximately a 100 dB FM suppression at 500 Hz. Measurements of this level are difficult, then practical measurements were made for F_{mod} = 20 kHz. The measured FM suppression was 37 to 39 dB for both PLLs. These are approximately equal to the simulation results.

CONCLUSION

A practical airborne frequency synthesizer design is presented. A hybrid synthesizer architecture improves the chip phase noise by 8 dB. The optimal practical synthesizer architecture rejects all spurs from different sources to levels less than –64 dBc. Their levels are calculated and ways to reject spurs are discussed. An optimal power supply unit architecture permits the design to achieve high efficiency, low additional spurs and small volume, but there is a low additional phase noise from the power supply in the 300 to 600 kHz offset frequency range. The PLL FM suppression was simulated and measured. ■

References

1. M. Seo, J.Y. Lee and K.K. Lee, "A Varactor-tuned Oscillator with Linear Tuning Characteristic," *Microwave Journal*, Vol. 45, No. 2, February 2002, pp. 100–114.
2. W.O. Keese, "An Analysis and Performance Evaluation of a Passive Filter Design Technique for Charge Pump Phase-locked Loops," National Semiconductor Application Note 1001, May 1996.
3. D. Crook, "Hybrid Synthesizer Tutorial," *Microwave Journal*, Vol. 46, No. 2, February 2003, pp. 20–38.
4. D. Colin, "Externally Induced VCO Phase Noise," *Microwave Journal*, Vol. 45, No. 2, February 2002, pp. 20–41.
5. W.F. Graves, "Managing Noise and Spurious within Complex Microwave Assemblies," *RF Design*, No. 7, July 2003, pp. 26–36.

Vsevolod Tanygin *graduated from the radio-engineering department of Kiev Polytechnic Institute, Kiev, Ukraine, in 1986. He is currently a senior scientist with Orion Science Research Institute, Kiev, Ukraine.*

MICROWAVE JOURNAL REVIEWED EDITORIAL BOARD

A BROADBAND DOUBLE DIPOLE ANTENNA WITH TRIANGLE AND RHOMBUS SHAPES AND STABLE END-FIRE RADIATION PATTERNS FOR PHASED-ARRAY ANTENNA SYSTEMS

A broadband microstrip-fed printed antenna is presented for phased-array antenna systems. The presented antenna consists of two parallel dipoles of different lengths to obtain two main resonances. The distance between the two dipoles is adjusted to reduce the VSWR between the two main resonances. The regular dipole shape is modified to a triangle and a quasi-rhombus shape to enhance the impedance bandwidth. Using two dipoles helps maintain stable radiation patterns close to their resonance frequencies. The antenna provides end-fire radiation patterns over a wide usable bandwidth of 93 percent for phased-array antenna systems.

Microstrip antennas have recently gained wide popularity, because they exhibit a low profile, small size, lightweight, low manufacturing cost, high efficiency, and an easy method of fabrication and installation. Furthermore, they are generally economical to produce since they are readily adaptable to hybrid and monolithic integrated circuit fabrication techniques at RF and microwave frequencies.[1] Phased arrays and spatial power combiners[2,3] are among the present areas that extensively explore the use of microstrip antennas. In these applications, there is a particular interest to obtain a larger operational bandwidth of the array, which implicitly means the need for wideband antenna elements.

In order for an antenna element to be considered for wideband phased arrays and power combiners, it has to have stable radiation characteristics over the entire operating band. The antenna should provide end-fire radiation with a high front-to-back ratio, polarization purity and a wide 3 dB beam width to allow for wide scanning capabilities. A low coupling between array elements is also required in phased-array

ABDELNASSER A. ELDEK
Jackson State University
Jackson, MS

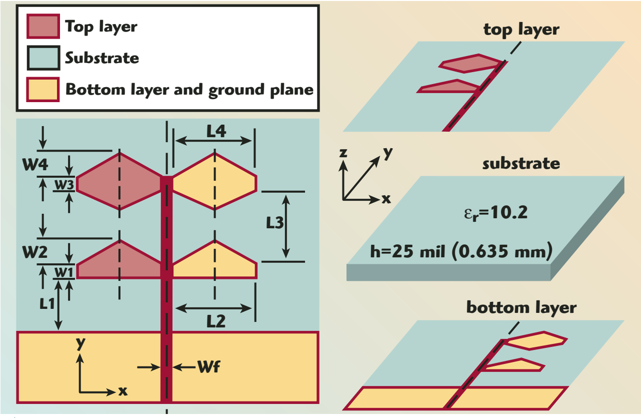

▲ *Fig. 1 Geometry and parameters of the proposed antenna.*

systems in order to avoid scan blindness and anomalies within the desired bandwidth and scan volume. Among the most widely used printed antennas in phased-array systems are quasi-Yagi, dipole, printed Lotus and bow-tie antennas.

The microstrip-fed quasi-Yagi antenna consists of a half-wavelength dipole and an approximately quarter wavelength rectangular director to increase the gain and improve the front-to-back ratio. A wide operational bandwidth of 48 percent was demonstrated at X-band.[4,5] By replacing the dipole and the director of the quasi-Yagi antenna with a bow-tie, the bandwidth was improved to 60 percent, and the antenna size was reduced by 20 percent.[6] Further research resulted in a novel microstrip-fed printed antenna, called a printed Lotus antenna, with a modified balun.[7] The printed Lotus provides 60 percent bandwidth with a fairly low return loss. However, the balun is based on a half-wavelength delay line, designed at the center frequency. This narrow band delay line limits the bandwidth of the antenna. In addition, the radiation patterns are deteriorated at the higher frequencies, which decrease the antenna usable bandwidth.

An alternative method of feeding such antennas has been reported.[8–14] One half of the antenna dipole or bow-tie is printed on the top substrate layer and connected to the microstrip feed line, while the second half is printed on the bottom substrate layer and connected to the ground plane. This avoids using the half-wavelength balun and simplifies the antenna geometry. In addition, one can also obtain end-fire radiation patterns with good front-to-back ratio.[12–14] Wide impedance bandwidths of 68 percent[13] and 91 percent[14] have been obtained by this method. The wide bandwidth is mainly obtained by modifying the antenna shape and its matching circuit, and by increasing the substrate height. However, using an antenna with one resonator results in a distorted pattern at high frequencies, where the antenna size is much bigger than a half wavelength. Additionally, if the substrate height is large relative to the free space wavelength at the upper operating frequency, the radiation patterns at the higher frequencies will be distorted. The deterioration of the radiation patterns results in a small usable bandwidth of 60 percent compared to an impedance bandwidth of 91 percent.

In order to solve this problem, antennas with thin substrate and multiple resonators are proposed. This article presents a new broadband antenna design with an enhanced pattern stability and usable bandwidth. This design offers advantages over existing antennas used in phased arrays and power combiners. The antenna exhibits low cross polarization, high gain and wide 3 dB beam width over the entire operating band. A numerical analysis for its parameters is presented for the physical understanding of the antenna operation. The VSWR and far-field radiation characteristics of the antenna final design are presented. Results for a modified two-element array configuration are also presented. The simulations and analyses for the antennas are performed using a commercial computer software package, Ansoft HFSS, which is based on the finite element method. Verifications for the computed VSWR, coupling and far-field radiation patterns are performed using measurements on a prototype antenna.

ANTENNA GEOMETRY AND OPERATION

The schematic and parameters of the proposed antenna are illustrated in detail in ***Figure 1***. The antenna consists of two modified dipoles with different lengths. The short dipole has a rhombus shape, while the long one consists of a rectangular dipole and triangle. The left halves of the two dipoles are on the top of the substrate, while the right halves are on the bottom. The upper and lower halves are then connected to a microstrip feed line with a truncated ground plane through two printed microstrip lines on the top and bottom layers. The truncated ground plane acts as a reflector to produce the end-fire patterns. The proposed antenna is printed on a Rogers RT/Duroid 6010/6010 LM substrate with a dielectric constant of 10.2, a dielectric loss (tanδ) of 0.0023 and a thickness of 25 mil (0.635 mm).

The operation of this antenna depends mainly on its high dielectric constant substrate material and its shape. Due to the high dielectric constant substrate material, most of the electromagnetic field is concentrated in the dielectric between the conductive strip and the ground plane, and travels on the surface in the transverse directions (y and x), supported by the electric currents in the two halves of the dipoles, and the fringing fields at the far edges of the dipoles, respectively. However, the fringing field is much weaker. The truncated ground plane reflects the radiated fields in the y direction, which results in end-fire radiation. On the other hand, the antenna shape is playing the main role in the antenna operating bandwidth, because it acts as a matching circuit connected to the open circuited terminal of the microstrip feed line. The lengths of the long and short modified dipoles (L2 and L4) control the lower and upper operating frequencies, respectively. The distance between the two modified dipoles (L3) and the distance between the first modified dipole and the truncated ground plane (L1) control the VSWR level between the two main resonances.

ANTENNA ANALYSIS

To begin with, the dimensions of this antenna were selected so that the lengths of the long and short dipoles are $\lambda_g/2$ at 5 and 14 GHz, respectively, to cover the same frequency band as the antenna reported previously.[14] The dimensions were then optimized based on the numerical results until initial values were obtained for the design to cover the required frequency range. The initial dimensions are shown in ***Table 1***. Next, a parametric study was performed to understand the effect of each antenna and to further improve on the antenna results. One parameter is changed at a time, while all other parameters are kept as given in the table. ***Figures 2*** to ***9*** show the effect of the antenna para-

TABLE I

ANTENNA INITIAL DIMENSIONS (mm)

Parameter	Wf	W1	W2	W3	W4
Value	0.6	1.0	0.6	0.75	1.0
Parameter	L1	L2	L3	L4	
Value	5.2	5.7	4.15	2.7	

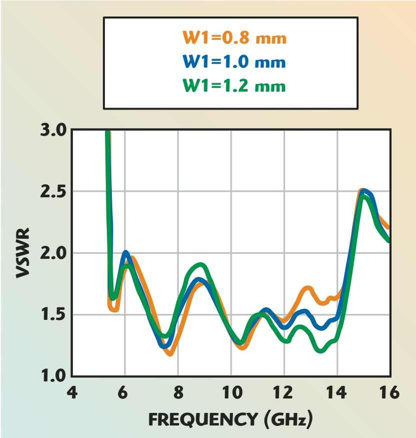

▲ *Fig. 2 Effect of W1 variations.*

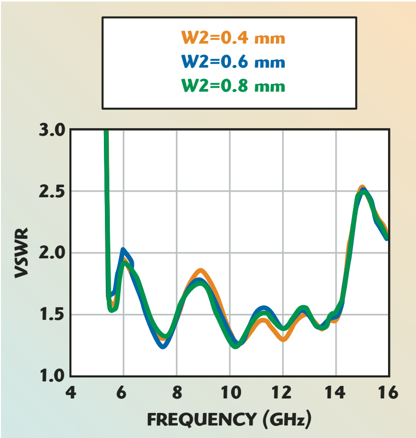

▲ *Fig. 3 Effect of W2 variations.*

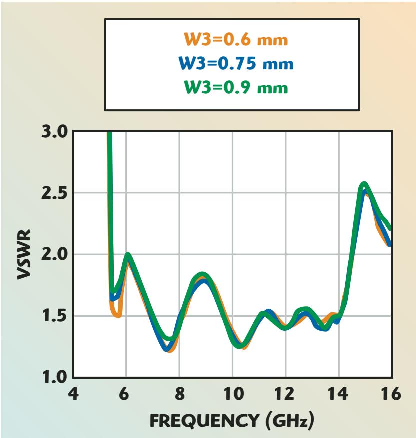

▲ *Fig. 4 Effect of W3 variations.*

meters on the computed VSWR using Ansoft HFSS.

The VSWR level at 6 GHz and between 11 and 14.5 GHz improves by increasing W1, while it increases between 7.3 and 9.2 GHz. Increasing W2 decreases the VSWR level around 9 GHz and increases it at 6 GHz and between 11 and 13 GHz. Increasing W3 decreases the VSWR level between 5.5 and 6.5 GHz. Increasing W4 decreases the VSWR level between 5.5 and 6.5 GHz and between 10.5 and 14 GHz. Generally, all the "W" parameters do not have a noticeable effect on the bandwidth.

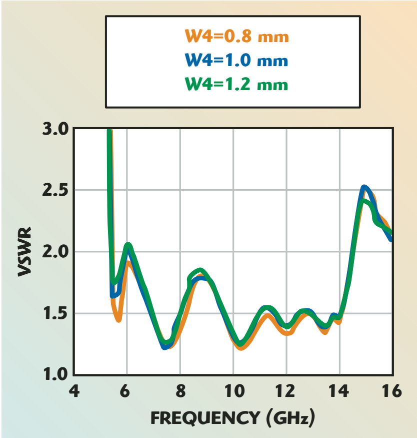

▲ *Fig. 5 Effect of W4 variations.*

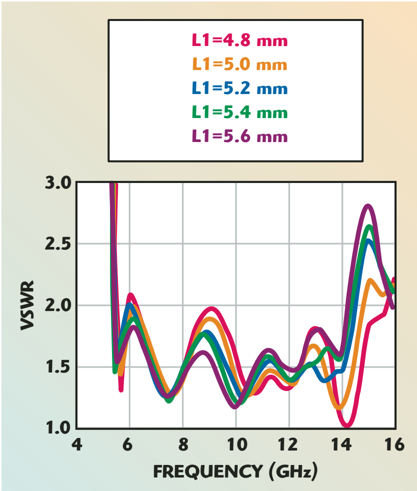

▲ *Fig. 6 Effect of L1 variations.*

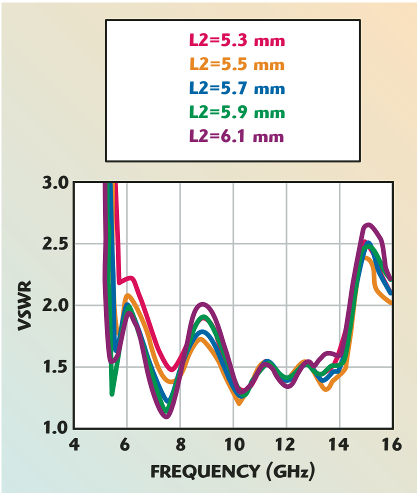

▲ *Fig. 7 Effect of L2 variations.*

L1 has an obvious effect at higher frequencies between 8 and 16 GHz.

As L1 increases, the bandwidth decreases and the VSWR level decreases at 6 GHz, between 8 and 10.5 GHz, and around 13 GHz, and increases around 11 GHz and between 13.5 and 16 GHz. In contrast, the effect of L2 is more at lower frequencies before 11 GHz. As L2 increases, the VSWR level improves before 8 GHz causing the lower operating frequency to shift to lower frequencies because the length of the long dipole increases. Increasing L3 improves the VSWR between 11 and 14 GHz, and increases it at 6 GHz and around 8.7 GHz, which is opposite to the effect of L1. Finally, as L4 increases, the VSWR level increases around between 5.5 and 8.5 GHz, and between 14 and 16 GHz, while it decreases between 8.5 and 14 GHz.

From this parametric study, it is clear that the "L" parameters have more effect on the antenna performance. L2 and L4 are generally controlling the lower and upper operating frequencies. L1 and L3 together with L2 and L4 compose two tap monopoles on both top and bottom substrate layers, which add new resonances to the antenna. Since L1 affects the length of both monopoles, it has more effect than L3. In addition, L1 and L3 control the couplings between the ground plane and the long dipole, and between the long and short dipoles. The "W" parameters have some effect on these couplings, too. In addition, W3 and W4 play an important role in matching the dipoles to the feed line by introducing a tapered transition rather than a sharp one.

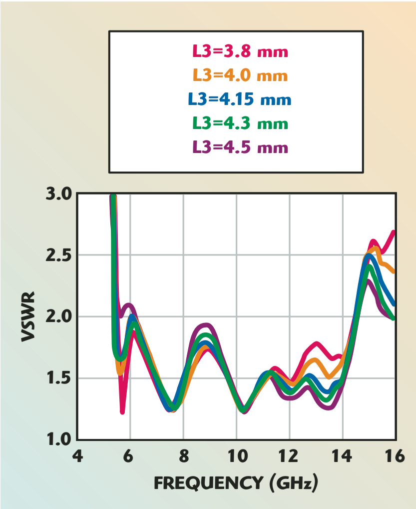

▲ *Fig. 8 Effect of L3 variations.*

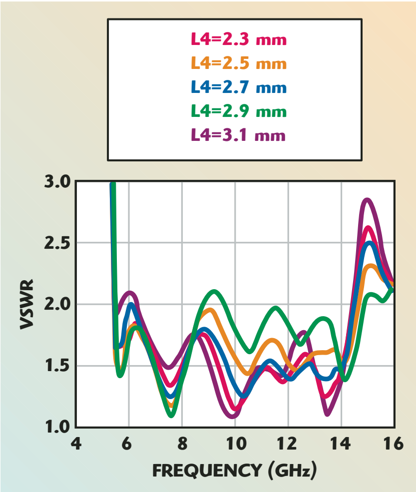

▲ *Fig. 9 Effect of L4 variations.*

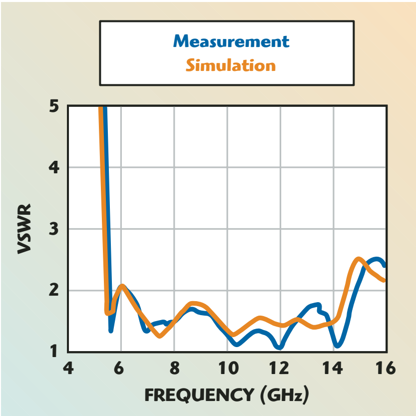

▲ *Fig. 10 VSWR versus frequency.*

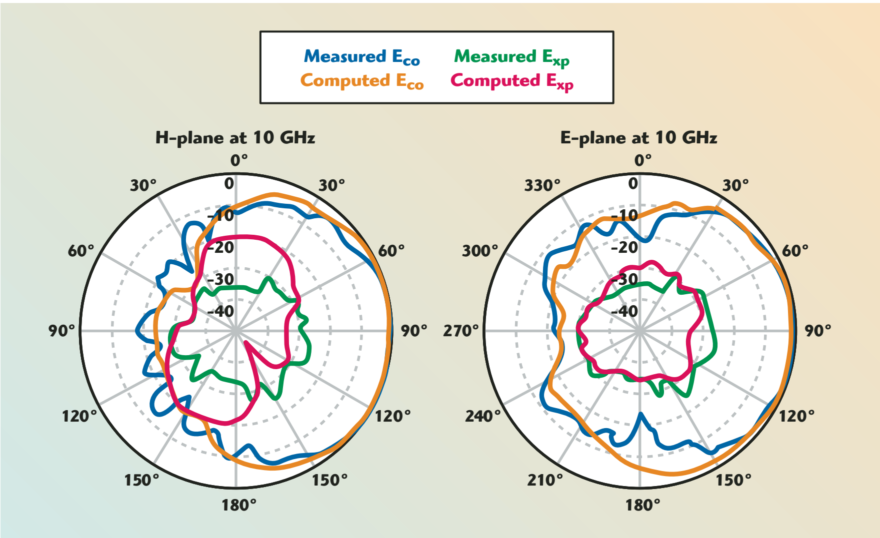

▲ *Fig. 11 The measured and computed radiation patterns at 10 GHz.*

MEASURED AND COMPUTED RESULTS FOR ONE ELEMENT

A prototype of this antenna was built with the dimensions shown in Table 1. The VSWR was computed using Ansoft HFSS and measured using a HP 8510 vector network analyzer. The measured and simulated VSWR of this antenna are shown in ***Figure 10*** and show good agreement. The small discrepancies between the computed and measured results may occur because of the effect of the SMA connector and fabrication imperfections. The antenna operates from 5.4 to 14.8 GHz with a wide impedance bandwidth of 93 percent. For this operating frequency band, the size of the antenna is approximately 0.22 and 0.59 free space wavelengths at the lower and upper operating frequencies, respectively. This length allows this antenna to fit into phased arrays with only minor grating lobes at higher frequencies. The measured and simulated radiation patterns at 10 GHz in the H- and E-planes are shown in ***Figure 11***. A good agreement is noticed, which further verifies the simulation results using Ansoft HFSS.

The radiation patterns are then computed at selective frequencies that cover the entire operating band and are shown in ***Figures 12*** and ***13*** in the H- and E-planes, respectively. The radiation patterns at the lower operating frequencies are more stable; therefore, they are presented at 6, 8 and 10 GHz only. In the higher operating frequency range, the radiation patterns are less stable and for that reason are presented at 11, 12, 13, 13.5 and 14 GHz. In the H-plane (y-z), the antenna provides end-fire radiation patterns up to 14 GHz, with

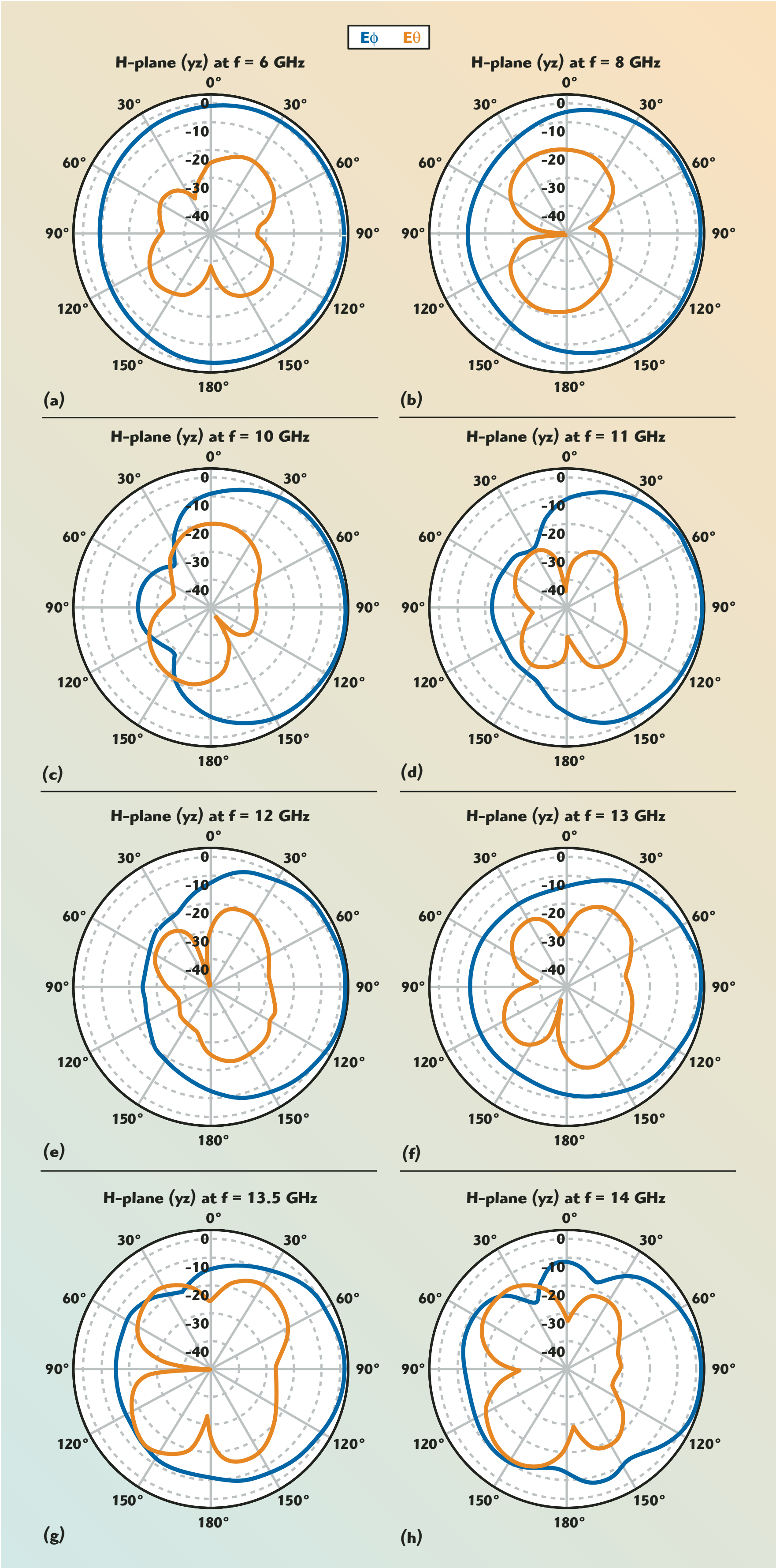

▲ *Fig. 12 The radiation patterns for the proposed antenna in the H-plane.*

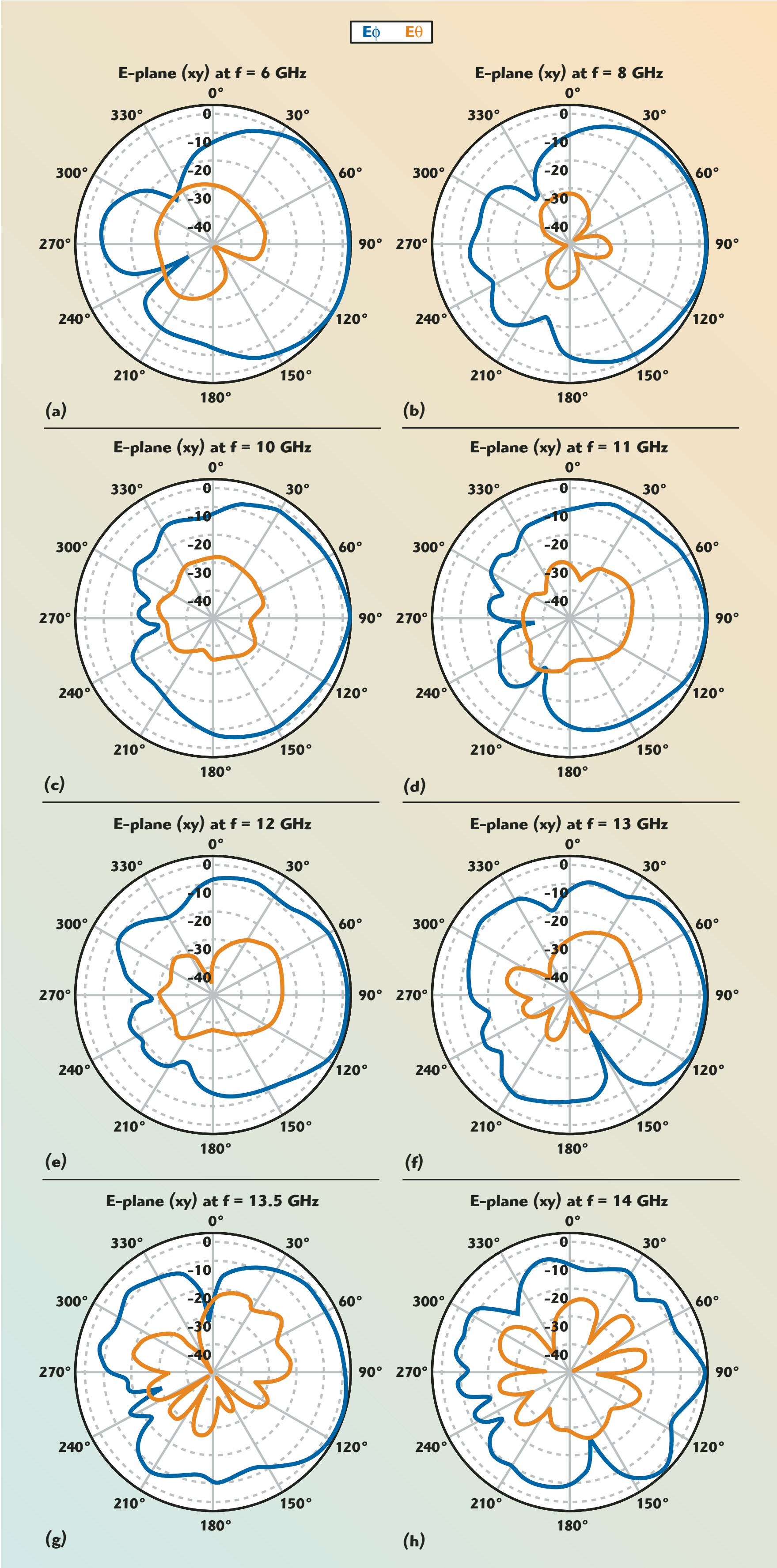

▲ *Fig. 13 The radiation patterns for the proposed antenna in the E-plane.*

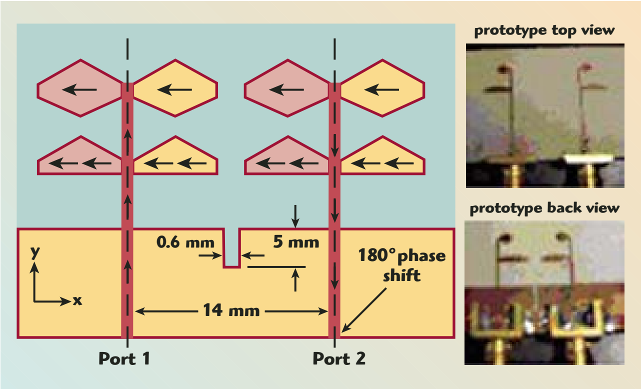

▲ *Fig. 14 Configuration and photographs of a two-element modified dipole antenna array.*

high front-to-back ratios between 9 and 25 dB. The maximum cross-polarization level is around –11 dB considering only the 3 dB beamwidth range. The first dotted circle in the polar plots represents the –3 dB level. The 3 dB beamwidth is generally wide and spans from 110° to 180°. In the E-plane (x-y), the antenna is also providing end-fire radiation patterns up to 14 GHz, but they are distorted at 14 GHz. The 3 dB beamwidth spans from 75° to 130° between 6 and 13.5 GHz, and 20° at 14 GHz.

These results show that the usable bandwidth of this antenna is approximately 86 percent. Consequently, it provides a significant improvement over all previously published antennas in terms of usable bandwidth. Compared with the one described previously by the author,[14] this antenna shows a 26 percent improvement in usable bandwidth.

RESULTS OF MODIFIED TWO-ELEMENT ARRAYS

A modified two-element array configuration is used to test the antenna performance in an array environment. The proposed two-element array configuration and its prototype are shown in ***Figure 14***. The second element is mirrored along the y-axis, and consequently a 180° phase shift is introduced at Port 2 to have the same current direction in both elements. The current direction is roughly illustrated in the figure. This modification is required, especially at high frequencies where the effect of the substrate height is significant, in order to provide balanced patterns. This modification also reduces the cross-polarization level, because the electric fields between the upper and lower layers in the z-direction and the electric currents in the y-direction in one antenna are opposite to those of the other antenna. A slit is introduced in the ground plane to decrease the coupling by disturbing the path of the transverse surface waves traveling in the substrate. The distance between elements should be as small as possible to reduce the grating lobes at high frequencies; therefore, it is chosen to be 14 mm.

Figures 15 and ***16*** show the radiation patterns in the H- and E-planes, respectively, for the two-element array

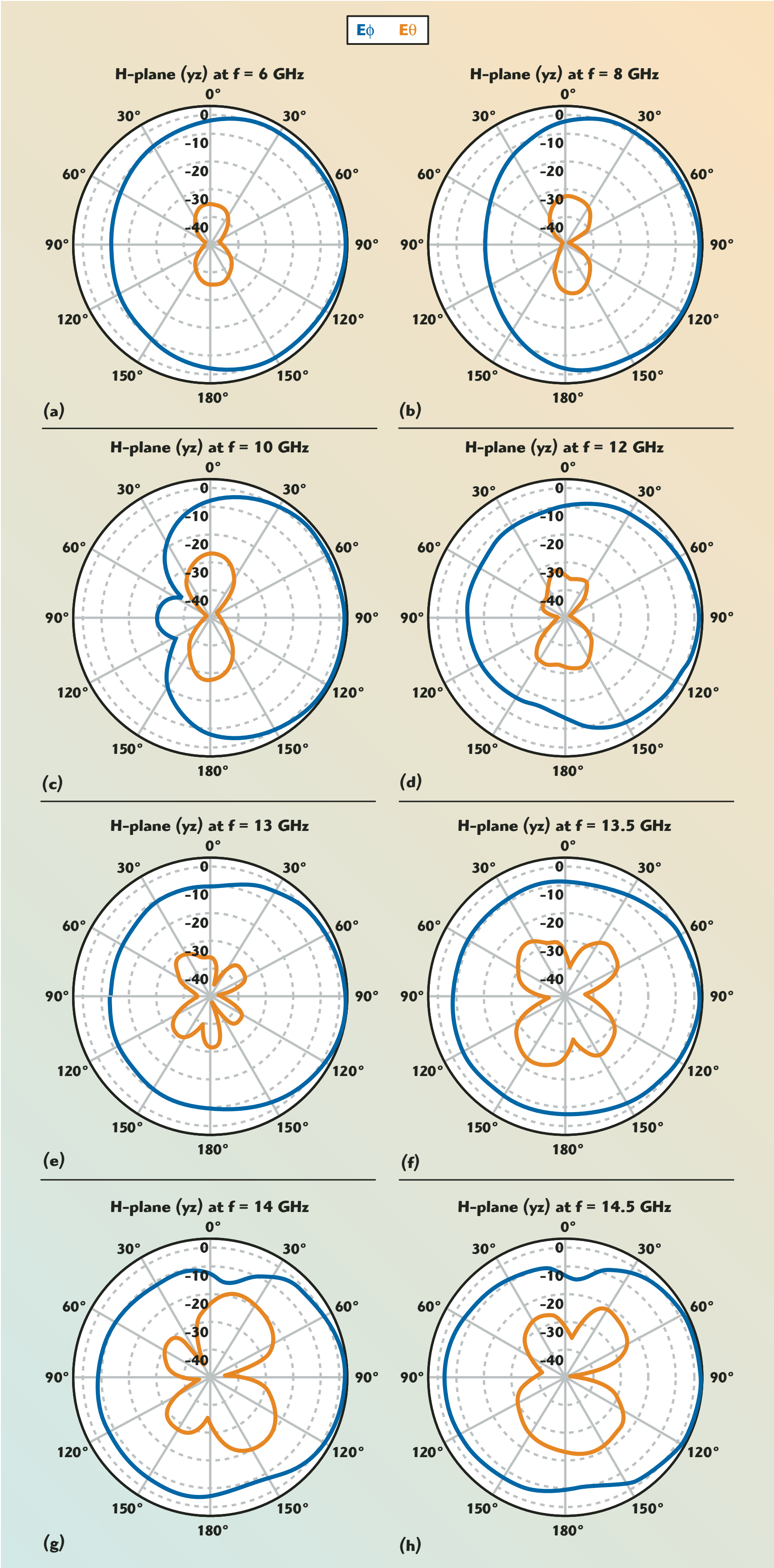

▲ *Fig. 15 Radiation patterns in the H-plane for the two-element array shown in Fig. 14.*

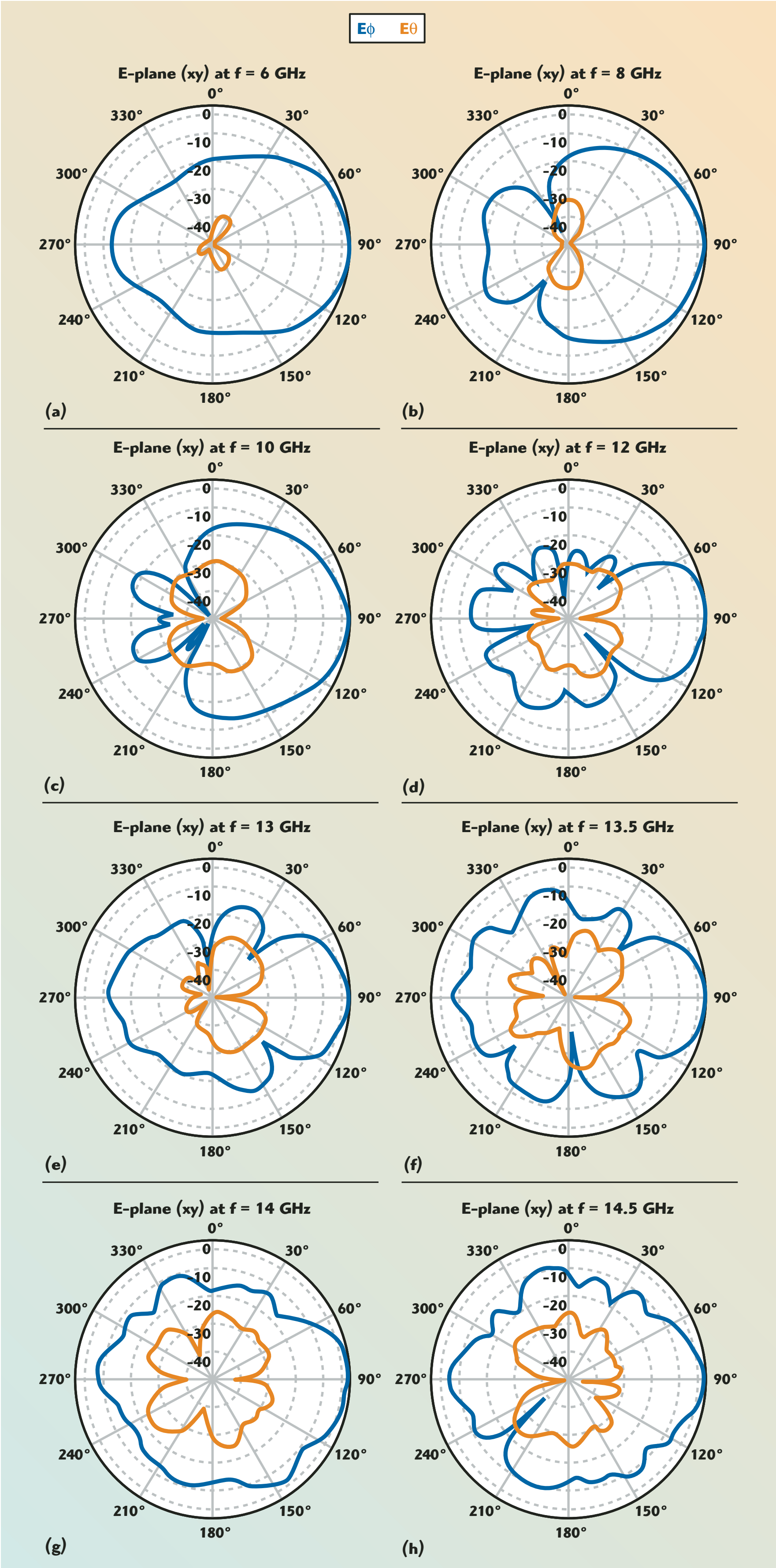

▲ *Fig. 16 Radiation patterns in the E-plane for the two-element array shown in Fig. 14.*

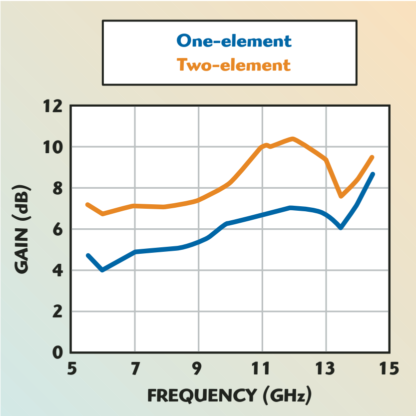

▲ *Fig. 17 Gain for the one- and two-element antennas.*

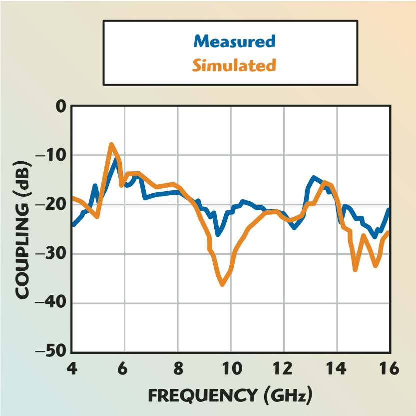

▲ *Fig. 18 Measured and simulated coupling between elements of the two-element array.*

at 6, 8, 10, 12, 13, 13.5, 14 and 14.5 GHz. If the H-plane radiation patterns of the two-element array are compared to those of a single element, it is noticed that in the two-element antenna array the cross-polarization level is reduced significantly and is completely eliminated in the direction of maximum gain, due to the array symmetry. In the E-plane, the cross-polarization level is also reduced, and the radiation patterns are stable up to 14.5 GHz. Therefore, by using this configuration, the usable bandwidth is equal to the impedance bandwidth, that is 93 percent. The gains for a one-element and two-element array are depicted in ***Figure 17***. The average gain for one element is approximately 6 dB, while for the two-element array the average is approximately 8.4 dB. Finally, the measured and computed couplings are shown in ***Figure 18***. A good agreement is noticed, which further verifies the simulation results. The average coupling between elements is approximately –20 dB, with a minimum value of –25 dB and a maximum value of –11 dB.

CONCLUSION

A new antenna is presented that achieves a wide usable bandwidth of 86 percent. The pattern stability is obtained by using two resonators built on both sides of a thin substrate. A modified array configuration is used to enhance the radiation characteristics and stability, and results in a 93 percent usable bandwidth. This antenna is a very good candidate for wideband wireless communications, phased-array antenna systems and power combiners. ■

ACKNOWLEDGMENT

The author would like to thank Guiping Zheng from the department of electrical engineering, University of Mississippi, for building and measuring the antennas presented in this article.

References

1. L.G. Maloratsky, "Reviewing the Basics of Microstrip Lines," *Microwave & RF*, March 2000, pp. 79–88.
2. R.J. Mailloux, *Phased Array Handbook*, Artech House Inc., Norwood, MA, 1994.
3. J.A. Navarro and K. Chang, Eds., *Integrated Active Antennas and Spatial Power Combining*, John Wiley & Sons Inc., New York, NY, 1996.
4. W. Deal, N. Kaneda, J. Sor, Y. Qian and T. Itoh, "A New Quasi-yagi Antenna for Planar Active Antenna Arrays," *IEEE Transactions on Microwave Theory and Techniques*, Vol. 48, No. 6, June 2000, pp. 910–918.
5. N. Kaneda, W. Deal, Y. Qian, R. Waterhouse and T. Itoh, "A Broadband Planar Quasi-yagi Antenna," *IEEE Transactions on Antennas and Propagation*, Vol. 50, No. 8, August 2002, pp. 1158–1160.
6. A.A. Eldek, A.Z. Elsherbeni and C.E. Smith, "Characteristics of a Microstrip-fed Printed Bow-tie Antenna," *Microwave and Optical Technology Letters*, Vol. 43, No. 2, October 2004, pp. 123–126.
7. A.Z. Elsherbeni, A.A. Eldek and C.E. Smith, "Wideband Slot and Printed Antennas," book chapter in *Encyclopedia of RF and Microwave Engineering*, K. Change, Ed., John Wiley & Sons Inc., New York, NY, March 2005.
8. S. Dey, C.K. Aanandan, P. Mohanan and K.G. Nair, "Analysis of Cavity Backed Printed Dipoles," *Electronics Letters*, Vol. 30, No. 30, 1994, pp. 173–174.
9. G.A. Evtioushkine, J.W. Kim and K.S. Han, "Very Wideband Printed Dipole Antenna Array," *Electronics Letters*, Vol. 34, No. 24, 1998, pp. 2292–2293.
10. Y.D Lin and S.N Tsai, "Analysis and Design of Broadband Coupled Stripline-fed Bow-tie Antennas," *IEEE Transactions on Antennas and Propagation*, Vol. 46, No. 3, March 1998, pp. 459–560.
11. G.Y Chen and J.S Sun, "A Printed Dipole Antenna with Microstrip Tapered Balun," *Microwave and Optical Technology Letters*, Vol. 40, No. 4, February 2004, pp. 344–346.
12. F. Tefiku and C.A. Grimes, "Design of Broadband and Dual-band Antennas Comprised of Series-fed Printed-strip Dipole Pairs," *IEEE Transactions on Antennas and Propagation*, Vol. 48, No. 6, June 2000, pp. 895–900.
13. G. Zheng, A.A. Kishk, A.W. Glisson and A.B. Yakovlev, "A Broadband Printed Bow-tie Antenna with a Simplified Balanced Feed," *Microwave and Optical Technology Letters*, Vol. 47, No. 6, December 2005, pp. 534–536.
14. A.A. Eldek, A.Z. Elsherbeni and C.E. Smith, "Wideband Modified Printed Bow-tie Antenna with Single and Dual Polarization for C- and X-band Applications," *IEEE Transaction on Antennas and Propagation*, Vol. 53, No. 9, September 2005, pp. 3067–3072.

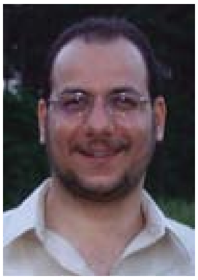

Abdelnasser A. Eldek *received his BSc degree (with honors) in electronics and communications engineering from Zagazig University, Egypt, in 1993, his MS degree in electrical engineering from the Eindhoven University of Technology, The Netherlands, in 1999, and his PhD degree in electrical engineering from the University of Mississippi in 2004. He was a research assistant in the department of microwaves at the Electronic Research Institute, Cairo, Egypt, from 1995 to 1996. From January 2001 to December 2004, he was a research and teacher assistant in the department of electrical engineering at the University of Mississippi. He is currently an assistant professor in the department of computer engineering, Jackson State University, Jackson, MS. His current research interests include electromagnetic theory, antennas, phased arrays and numerical methods.*

MEASURING THE CAPACITANCE COEFFICIENTS OF COAXIAL OPEN-CIRCUITS WITH TRACEABILITY TO NATIONAL STANDARDS

Coaxial open-circuits are often used as measurement reference standards and can be found in most commercially available vector network analyzer (VNA) calibration kits. The capacitance characteristics of these devices are usually summarized in terms of the coefficients of a polynomial used to describe their frequency dependence. This article describes a method of measuring these capacitance coefficients and presents a detailed analysis of the uncertainty of the measurement, which includes using the Monte Carlo method in conjunction with a least-squares fitting process. The resulting measurement method enables these standards to be 'calibrated' with known uncertainty and with traceability to national measurement standards.

Coaxial open-circuit standards are found in many of today's commercially available vector network analyzer (VNA) calibration kits.[1,2] They are most commonly used as standards in calibration schemes such as short-open-load-through (SOLT). In this capacity, they are assumed to have known characteristics, that is, they are assumed to provide a known value of reflection when connected to a VNA test port reference plane. In this respect, it is common practice to consider the open-circuit as a frequency-dependent shunt capacitance, C(f), and to determine the reflection coefficient, Γ, at a given frequency, f, using

$$\Gamma = \frac{Y_0 - Y}{Y_0 + Y} \qquad (1)$$

where

Y_0 = characteristic admittance of the coaxial line (such as 0.02 S)
Y = admittance of the terminating load, G+jB
G = shunt conductance
B = shunt susceptance

For a coaxial capacitor, the loss can be assumed to be zero (G=0) and the susceptance is given by 2πfC. After some manipulation, Equation 1 becomes

MARTIN J. SALTER AND
NICK M. RIDLER
National Physical Laboratory
Teddington, Middlesex, UK

$$\phi(f) = -2\tan^{-1}\left(\frac{2\pi f C(f)}{Y_0}\right) \quad (2)$$

where

$\phi(f)$ = phase, in degrees, of the reflection coefficient as a function of frequency

This means that if the capacitance of the open-circuit is known, then its reflection coefficient is also known. In particular, at any given frequency, the phase of the reflection coefficient can be determined from the capacitance. In practice, there is often an offset (such as a length of coaxial line) between the connector of the open-circuit and the shunt capacitance. In this article, it will be assumed that a correction has been applied to the phase of the reflection coefficient of the open-circuit to remove the effect of any offset that may be present.

The frequency dependence of the capacitor, C(f), is usually modeled using the following expression, involving a third-order (cubic) polynomial[3]

$$C(f) = C_0 + C_1 f + C_2 f^2 + C_3 f^3 \quad (3)$$

where C_0, C_1, C_2 and C_3 are the coefficients of the polynomial.

Most manufacturers of coaxial open-circuits provide generic values for these polynomial coefficients, which are expected to be applicable for all open-circuits of a given type (that is for a given line size and connector type). In practice, however, each manufactured open-circuit will have a unique set of coefficients based on its own construction and constituent parts. Therefore, in order to use a particular open-circuit as a standard to achieve the utmost accuracy, it is important to know (such as through measurements) the coefficients for the individual open-circuit. There is also a quality assurance consideration here, in that quality standards[4,5] require that assumed known values of standards are periodically re-assessed to demonstrate whether their known values remain valid or require adjusting, due to extensive use and/or other time-varying effects, for instance.

Based on the above considerations, a research program was undertaken at the UK's National Physical Laboratory (NPL) to provide a measurement service, traceable to national standards, for determining the capacitance polynomial coefficients for coaxial open-circuits based on precision measurements. This article describes the method adopted and presents some typical results obtained for open-circuits found in commercially available VNA calibration kits.

OBTAINING CAPACITANCE COEFFICIENTS FROM REFLECTION DATA

The method adopted can be summarized by the following five-step process, as described previously.[6]

Step 1: Specify the Measurement Model

Measurement, with uncertainty, the reflection coefficient, Γ, of the open-circuit at n frequencies, $(f_1 \ldots f_n)$ using a high precision measurement system.[7] The measurement model is given by

$$\left(C_0, C_1, C_2, C_3\right) = g\left(\phi\left(f\right), f\right) \quad (4)$$

where g describes the functional relationship between input and output quantities and is derived from Equations 2 and 3. Using the n pairs of values of $\phi(f)$ and f, the outputs quantities are obtained by solving Equation 4, as a least-squares problem, for C_0, C_1, C_2 and C_3.

Step 2: Assign a Distribution to the Input Quantities

The next step is to assign a distribution to the input quantities, that is the n values of the phase of the reflection coefficient, $\phi(f)$. Therefore, an n-dimensional normal distribution with mean vector

$$\left(\phi_1 \ldots \phi_n\right)^T \quad (5)$$

and a diagonal co-variance (or uncertainty) matrix

$$\begin{bmatrix} u_1^2 & \cdots & 0 \\ \vdots & \ddots & \vdots \\ 0 & \cdots & u_n^2 \end{bmatrix} \quad (6)$$

are assigned to the measured phase values. It is assumed that the phase values measured at different frequencies are uncorrelated and so all off-diagonal elements in the uncertainty matrix are zero. It is further assumed that the uncertainty in frequency is negligible.

Step 3: Generate a Large Random Sample from the Distribution of Input Quantities

A large random sample of size m (where m is typically 50,000) is generated from the n-dimensional normal distribution assigned to the measured phase values, above. (This is an implementation of the Monte Carlo method, which involves performing statistical sampling experiments using a computer.) For example, this can be achieved using the procedure described in Reference 8. The sample is represented by the following (m×n) matrix in which each row represents an n-dimensional point corresponding to the phase measured at the n frequencies, $f_1 \ldots f_n$.

$$\begin{bmatrix} \phi_1\left(f_1\right) & \cdots & \phi_1\left(f_n\right) \\ \vdots & & \vdots \\ \phi_m\left(f_1\right) & \cdots & \phi_m\left(f_n\right) \end{bmatrix} \quad (7)$$

Step 4: Apply the Measurement Model to Obtain a Corresponding Large Sample from the Distribution of the Output Quantities

Applying the measurement model to each row in Equation 5 gives m sets of capacitance coefficients (C_0, C_1, C_2, C_3), which can be represented by the following matrix

$$\begin{bmatrix} C_0\left(1\right) & \cdots & C_3\left(1\right) \\ \vdots & & \vdots \\ C_0\left(m\right) & \cdots & C_3\left(m\right) \end{bmatrix} \quad (8)$$

Step 5: Obtain Estimates for the Measurands

The required information—mean value and uncertainty information—for each capacitance coefficient is extracted from the columns in Equation 6. Since this process determines four polynomial coefficients simultaneously, the associated uncertainty information is represented by a (4×4) uncertainty matrix. The diagonal elements of this matrix represent the squares of the standard uncertainties (that is variances) in each polynomial coefficient and the off-diagonal elements represent the co-variances of these polynomial coefficients.

An expanded uncertainty (at a specified level of confidence) for each capacitance coefficient can be obtained by arranging the data in each column of Equation 6 in order of size and establishing an interval that encompasses the desired proportion of values (such as 95 percent). The co-variances can be used to determine the amount of correlation (in terms of correlation coefficients) between the capacitance polynomial coefficients. A correlation coefficient describes the degree to which variations in two components are interrelated. For example, if a variation in some physical process (such as connector misalignment) causes both components to increase, then these components are said to be positively correlated (indicated by a correlation coefficient with a positive value). If, on the other hand, a variation in the physical process causes one component to increase while the other component decreases, then this is termed negative correlation (indicated by a correlation coefficient with a negative value). Values of correlation coefficient can range from –1 to +1. This information, along with the mean measured values for each polynomial coefficient, is included on the certificate of calibration that is issued by the NPL measurement service for the open-circuit.

TABLE I
CAPACITANCE COEFFICIENTS FOR A PRECISION 7 MM OPEN-CIRCUIT

	$C_0/10^{-15}$ (F)	$C_1/10^{-25}$ (F/Hz)	$C_2/10^{-35}$ (F/Hz^2)	$C_3/10^{-45}$ (F/Hz^3)
Measured capacitance coefficients	91.23	6.927	–5.3398	6.1253
Expanded uncertainty (95% level of confidence)	±1.7	±5.6	±5.7	±1.8
Manufacturer's specified values	90.48	7.636	–6.3818	6.4337

EXAMPLE 1: PRECISION 7 MM OPEN-CIRCUIT

To illustrate the above technique, the reflection coefficient of a precision 7 mm open-circuit (from an Agilent 85050C VNA calibration kit)[1] was measured from 1 to 18 GHz using an NPL's primary standard VNA measurement system,[7] which provides an assessment of the overall uncertainty of the measurements. The resulting capacitance coefficients are shown in ***Table 1***. The achieved uncertainty of measurement is dependent on the number of measured values used to determine the capacitance coefficients (that is the number of frequencies at which reflection measurements were made). In general, the more values used, the more accurate the determinations. Here, 35 values were generated from reflection measurements made every 0.5 GHz.

An additional benefit in using this method is that it is possible to view the distribution of values for each determined capacitance coefficient. The overall shape of the distribution can quickly reveal any unusual behavior that may be present in a given measurement quantity (such as if the distribution is skewed or departs significantly from the characteristic 'bell' shape of the usually assumed normal distribution). For example, ***Figure 1*** shows the distributions, presented as histograms, obtained during the determination of the capacitance coefficients in Table 1. Strictly speaking, these are marginal (uni-variate) distributions of the underlying four-dimensional (multi-variate) distribution for C_0, C_1, C_2 and C_3. It is clear that these distributions look reasonably 'normal' and therefore one would not expect any unusual behavior in the presented results.

For completeness, ***Table 2*** shows the correlation coefficients between the four capacitance terms determined during the measurements. This

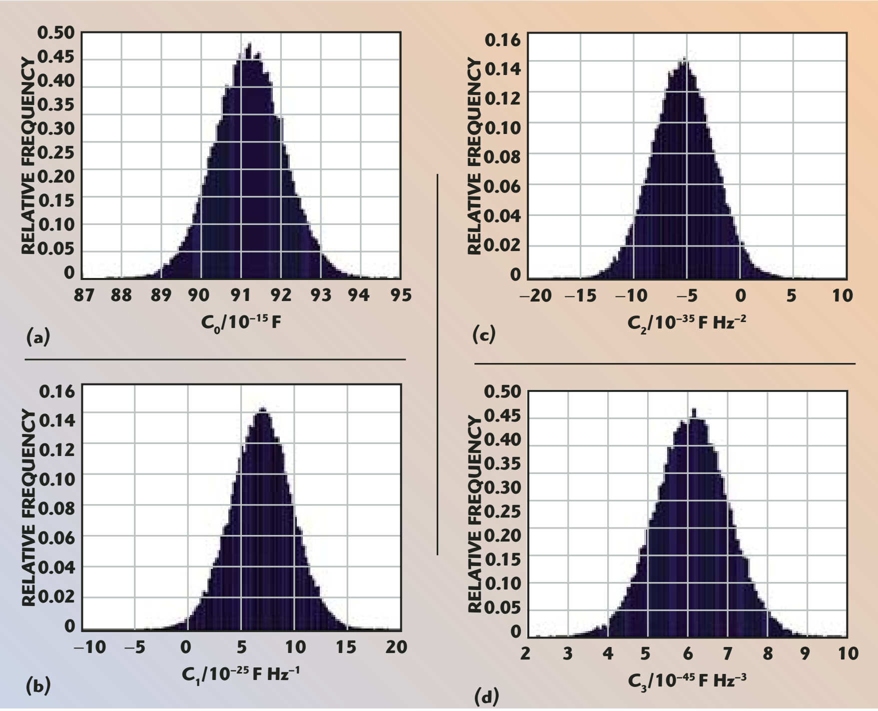

▲ *Fig. 1 Histograms of the distributions of C_0, C_1, C_2 and C_3 (normalized to have unit area).*

TABLE II
EXPERIMENTALLY DETERMINED CORRELATION COEFFICIENTS FOR THE CAPACITANCE COEFFICIENT VALUES GIVEN IN TABLE I

	C_0	C_1	C_2	C_3
C_0	1.00	–0.97	0.92	–0.86
C_1	–	1.00	–0.99	0.95
C_2	–	–	1.00	–0.99
C_3	–	–	–	1.00

table shows that pairs of capacitance coefficients are either strongly positively correlated (that is correlation coefficient close to +1) or strongly negatively correlated (correlation coefficient close to –1). For example, there is strong positive correlation between the determinations of C_0 and C_2 and between the determinations of C_1 and C_3. There is strong negative correlation between the remaining pairs of capacitance coefficients. In principle, this correlation information should be taken into account, depending on where the values of these capacitance coefficients are used (when propagating uncertainties to other measurement quantities, for example).[9] This is why this information is included on the certificate of calibration for each measured open-circuit.

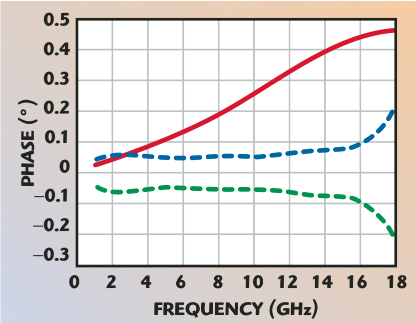

▲ *Fig. 2 Phase of the open-circuit predicted using the manufacturer's capacitance coefficients normalized to the phase predicted from capacitance coefficient measurements.*

DERIVING PHASE VALUES FROM CAPACITANCE COEFFICIENT VALUES

Table 1 also shows the manufacturer's specified generic values for this type of open-circuit. These are often stored on the calibration coefficients disk supplied with the calibration kit containing the open-circuit standard. It can be seen from this table that all the manufacturer's values for these coefficients fall inside the 95 percent confidence intervals for the corresponding measured values, that is the two sets of capacitance coefficients appear to show good agreement. Equations 2 and 3 can be used to generate phase values in a range of frequencies, using either the measured or the manufacturer's capacitance coefficients. In the case of the measured values, this can be done for each set of capacitance coefficients in Equation 6, that is for each row of Equation 6, generating a vector of m phase values

$$\begin{bmatrix} \phi_1(f) \\ \vdots \\ \phi_m(f) \end{bmatrix} \tag{9}$$

This vector contains information about the distribution of $\phi(f)$ and can therefore be used to establish a 95 percent prediction interval for $\phi(f)$. For example, this can be achieved by sorting the components of Equation 7 into ascending order and then obtaining the 0.025 and 0.975 percentiles. Extra care is needed if the components of Equation 7 fall on either side of the "cut" in the phase scale at ±180°. This prediction interval takes into account the uncertainties in the measured capacitance coefficients and also any correlation between them.

Figure 2 shows the 95 percent prediction interval (dashed curves) for the phase predicted from the measured capacitance coefficients, normalized so that the predicted phase is set to zero. The phase predicted using the manufacturer's capacitance coefficients (solid curve), similarly normalized, is also shown. The two predictions clearly disagree since the manufacturer's prediction curve lies outside the 95 percent prediction interval derived from the measured capacitance coefficients over most of the frequency range. Thus, although the measured capacitance coefficients appear to show good agreement with the manufacturer's capacitance coefficients, the phase curves derived from the two sets of coefficients clearly disagree. In other words, a small change in the capacitance coefficient (such as that between the measured and manufacturer's values) can result in a relatively large change in the predicted phase curve. Presumably, this is a result of the strong correlation between the capacitance coefficients. For this reason, when making use of the capacitance coefficients, care needs to be taken to retain a sufficient number of significant figures in order to not unduly affect the predicted phase curve. The maximum difference between the two-phase predictions approaches 0.5° at 18 GHz. Since the wavelength at 18 GHz is approximately 17 mm, this phase error equates to an equivalent 'length' error of approximately 25 μm. Under normal circumstances, for measurements in precision coaxial lines at these frequencies, one would expect the S-parameter measurement accuracy of a VNA, when expressed in these 'length' terms, to be of the order of only a few microns (that is a VNA should make a reasonably good 'electrical micrometer'). Therefore, in light of the above, an error of 25 μm is excessive and unnecessarily detrimental to the overall achievable accuracy for a VNA.

To investigate this error further, a phase error, $u(\phi)$, can be converted to an equivalent error in linear magnitude, $u(|\Gamma|)$, using the following formula[10]

$$u(\phi) = \sin^{-1}\left(\frac{u(|\Gamma|)}{|\Gamma|}\right) \tag{10}$$

This assumes that the error in the reflection coefficient is represented by a circle of radius $u(|\Gamma|)$ in the complex plane. This is a simplified representation of a more general view that has been discussed previously.[11] However, applying this simplified representation is sufficient to illustrate the point.

With $u(f)$ = 0.5° at 18 GHz and choosing $|\Gamma|$ = 1, this gives

$$u(|\Gamma|) = \sin(u(\phi)) = 0.01 \tag{11}$$

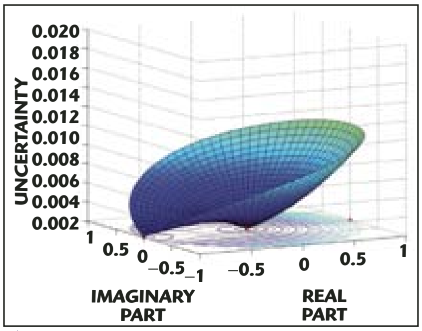

▲ *Fig. 3 Uncertainty profile for an SOL calibration scheme.*

TABLE III

CAPACITANCE COEFFICIENTS FOR THE LA TECHNIQUES PRECISION 2.92 MM MALE OPEN-CIRCUIT STANDARD

	$C_0/10^{-15}$ (F)	$C_1/10^{-23}$ (F/Hz)	$C_2/10^{-32}$ (F/Hz^2)	$C_3/10^{-42}$ (F/Hz^3)
Measured capacitance coefficients	+47.8	–3.27	+1.60	–2.43
Expanded uncertainty (95% level of confidence)	±18.1	±3.35	±1.94	±3.50

This error in reflection coefficient magnitude is large, compared with other similar published values for the achieved accuracy of VNAs.[12]

Figure 3 shows the impact of this uncertainty in the open-circuit standard, on subsequent reflection measurement, by plotting an uncertainty profile[13] for a short-open-load (SOL) calibration scheme with the uncertainty in the open-circuit standard taken to be $u(|\Gamma|) = 0.01$. Here, the uncertainties of the matched load and short-circuit standards are taken to be zero. Of course, in practice, the uncertainties in the matched load and short-circuit will also be non-zero. This surface indicates the uncertainty that may be present in an SOL calibration scheme if one relies only on the manufacturer's specified capacitance coefficients. By using the measured capacitance coefficients instead of the manufacturer's values, these uncertainties should be substantially reduced. From Figure 2, the maximum phased prediction error, based on the measured capacitance coefficients, is approximately 0.2° at 18 GHz. This equates to a worst-case error of approximately $u(|\Gamma|) = 0.003$.

EXAMPLE 2: LA TECHNIQUES PRECISION 2.92 MM OPEN-CIRCUIT

As a second example, an open-circuit manufactured by LA Techniques[2] for use in the frequency range 3 MHz to 3 GHz was measured. This (male) open-circuit is effectively a coaxial end cap that attaches to a female precision 2.92 mm connector (used to form the VNA's test port). The values obtained for the capacitance coefficients, using the method previously described, are listed in ***Table 3***, together with the expanded uncertainties (at a level of confidence of 95%). As before, the achieved uncertainty of measurement is dependent on the number of measured values used to determine the capacitance coefficients. Here, 99 values were generated from reflection measurements made approximately every

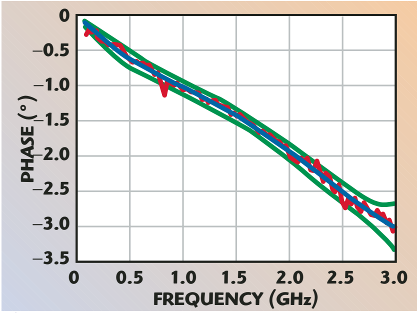

▲ *Fig. 4 Measured reflection coefficient phase of the LA Techniques 2.92 mm male open-circuit.*

30 MHz to 3 GHz, this being the maximum operating frequency of the LA Techniques VNA that uses this open-circuit during calibration. It should be noted that these capacitance coefficient values are only considered to be applicable within the bandwidth of the reflection coefficient measurements used to obtain them. Here, the frequencies of the reflection coefficient measurements were chosen to approximate the bandwidth of use for the open-circuit (3 MHz to 3 GHz). However, if the open-circuit is used at frequencies outside this bandwidth, then these capacitance coefficients should be re-evaluated using reflection coefficient measurements obtained at frequencies chosen to represent the modified bandwidth.

For the results shown, it was again found that the (marginal) distributions associated with the capacitance coefficients were fairly 'normal' and that pairs of capacitance coefficients are strongly correlated (either positively or negatively). ***Figure 4*** shows the phase of the reflection coefficient (red) as measured by the NPL's primary standard VNA measurement system,[7] the phase predicted from the extracted capacitance coefficients (blue) and the 95 percent prediction interval for phase (green), based on the capacitance coefficients. The manufacturer (LA Techniques) is planning to use the capacitance coefficient values of Table 3 as generic values for this design of open-circuit when used in the frequency range 3 MHz to 3 GHz.

CONCLUSION

A method has been presented for obtaining traceable values for the capacitance coefficients of coaxial open-circuits, derived from reflection coefficient measurements. Some sample results for a precision 7 mm open-circuit have been given. It has been shown that even when the values for the capacitance coefficients agree with those supplied by the manufacturer within the measurement uncertainties, relatively large errors in the predicted reflection coefficient for the open-circuit can still result due to the strong correlation between the capacitance coefficients. This can lead to a substantial component of uncertainty for subsequent VNA measurements when the open-circuit, used as a standard, has not been individually characterized (such as by using the method described in this article). Results have also been given for a male open-circuit in the 2.92 mm line size, which the manufacturer will use as generic values for all open-circuits of this design for the frequency range 3 MHz to 3 GHz. Where possible, the actual capacitance for a given open-circuit should be established through traceable measurements, and the capacitance coefficients so determined should be used for specifying the open-circuit during a VNA calibration process. ■

ACKNOWLEDGMENT

The authors would like to thank Nils Nazoa of LA Techniques for loaning the 2.92 mm open-circuit standard. The work described in this article was funded by the UK Government and, specifically, by the Electromagnetic and Measurement for Innovators Programs of the National Measurement System

Directorate, Department of Trade and Industry. ©Crown Copyright 2006. Reproduced by permission of the Controller of HMSO.

References

1. *Agilent Technologies 85050C 7 mm Precision Calibration Kit – User's and Service Guide*, Agilent Part Number 85050-90051, June 2002.
2. *LA Techniques 2.92 mm Connector Calibration Kits*, http://www.latechniques.com/.
3. *Network Analysis: Specifying Calibration Standards for the HP 8510 Network Analyzer*, HP Product Note 8510-5A, February 1988.
4. *Measurement Management Systems—Requirements for Measurement Processes and Measuring Equipment*, ISO/IEC 10012: 2003, International Organization for Standardization, Geneva, Switzerland.
5. *General Requirements for the Competence of Testing and Calibration Laboratories*, ISO/IEC 17025:2005, International Organization for Standardization, Geneva, Switzerland.
6. N.M. Ridler and M.J. Salter, "A Generalized Approach to the Propagation of Uncertainty in Complex S-parameter Measurements," *64th ARFTG Conference Digest*, December 2–3, 2004, Orlando, FL, pp. 1–14.
7. N.M. Ridler, "A Review of Existing National Measurement Standards for RF and Microwave Impedance Parameters in the UK," *IEE Colloquium Digest*, No. 99/008, February 1999, pp. 6/1–6/6.
8. M.J. Salter, N.M. Ridler and M.G. Cox, "Distribution of Correlation Coefficient for Samples Taken from a Bi-variate Normal Distribution," NPL Report CETM 22, September 2000.
9. N.M. Ridler and M.J. Salter, "Propagating S-parameter Uncertainties to Other Measurement Quantities," *58th ARFTG Conference Digest*, San Diego, CA, November 29–30, 2001.
10. J.P. Ide, "NPL's Expression of Uncertainty for Scattering Coefficient Measurements," ANAlyse Technical Note, No. 17, May 1996 (available from www.npl.co.uk/anamet).
11. N.M. Ridler and M.J. Salter, "Evaluating and Expressing Uncertainty in Complex S-parameter Measurements," *56th ARFTG Conference Digest*, Boulder, CO, November 30 and December 1, 2000, pp. 63–75.
12. N.M. Ridler and C. Graham, "Some Typical Values for the Residual Error Terms of a Calibrated Vector Automatic Network Analyzer (ANA)," *BEMC 99 – 9th International Conference on Electromagnetic Measurement*, Brighton Metropole Hotel, UK, November 2–4, 1999, pp. 45/1–45/4.
13. P.R. Young, "Propagation of Uncertainty in One-port ANA Measurements," ANAMET Report 017, August 1998 (available from www.npl.co.uk/anamet).

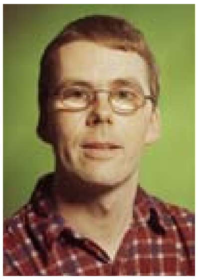

Martin J. Salter *received his BSc degree from the University of Manchester, UK, and his MSc degree from the University of London, UK, in 1986 and 1992, respectively. Since 1986, he has been with the UK's National Physical Laboratory (NPL), where is has been involved with UHF and VHF antenna measurements and more recently with the development of RF and microwave impedance standards and with the treatment of measurement uncertainty for vector-valued quantities.*

Nick M. Ridler *received his BSc degree from the University of London, UK, in 1981. He has since spent almost 25 years working in both industrial and government scientific research laboratories. He is currently lead scientist and principal research scientist at the UK's National Physical Laboratory (NPL). His current research interests include millimeter-wave, on-wafer measurements, uncertainties for vector measurements and providing instrument traceability remotely using the Internet.*

ELIMINATING FFT ARTIFACTS IN VECTOR SIGNAL ANALYZER SPECTRA

This article presents a method to minimize the spectral leakage in measurements of periodic signals made with a vector signal analyzer (VSA) by taking into account the periodic nature of the Fast Fourier Transform (FFT). This method negates the need for filtering the time-domain signal, enabling distortion-free, repeatable measurements of signal components throughout the acquisition band. The method is demonstrated on a simple multisine signal. However, this method can also be used on more complex periodic signals that emulate digital signals, such as those generated by 802.11-/802.16-based communications devices.

The vector signal analyzer (VSA) has several measurement advantages over a spectrum analyzer in the acquisition of bandpass RF signals, including its time-domain capture, which enables measurement of both magnitude and phase information, and its ability to display data in the time and frequency domains.[1,2] The highly sampled, down-converted waveform gives a good amount of spectral detail around the carrier frequency. However, the resolution of the frequency spectrum may be affected by the relation between the length of the time capture and the bandpass signal envelope period for periodic signals such as multisines.[3–5]

A procedure for optimizing VSA measurements of periodic signals to minimize spectral leakage is presented. The underlying principle of this method has been known for years,[5] but it finds new application with the recent emphasis on the use of periodic well-behaved signals to characterize complicated wireless devices, systems and channels. In these situations, multisine test signals, consisting of a collection of sine waves at frequencies that are slightly offset from each other to emulate digital test signals, are often used. In these test environments, complete knowledge of the stimulus is obtained and it becomes practical to use this type of measurement method. This procedure determines the proper settings such that the VSA will obtain an integer multiple of the envelope period of the measured

MICHAEL D. MCKINLEY AND KATE A. REMLEY
National Inst. of Standards and Technology Boulder, CO
MACIEJ MYSLINSKI
Katholieke Universiteit Leuven, Belgium
J. STEVENSON KENNEY
Georgia Institute of Technology Atlanta, GA

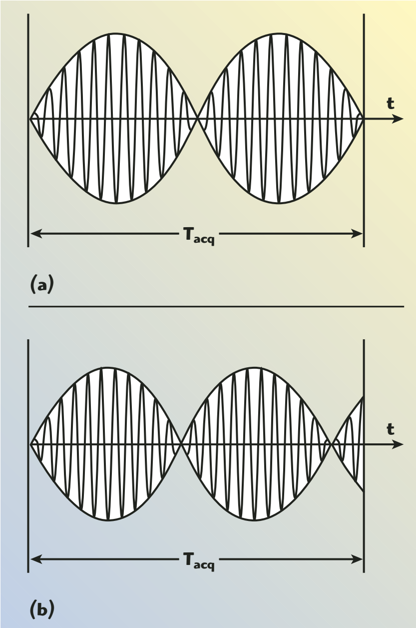

▲ *Fig. 1 A two-tone multisine signal in the time domain; (a) an integer multiple of acquired envelopes and (b) a non-integer multiple of acquired envelopes.*

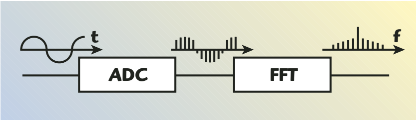

▲ *Fig. 2 Sine wave incident on the ADC and FFT of a VSA.*

signal, as illustrated in ***Figure 1***. Specifying an integer multiple of periods preserves an undistorted time-domain signal. Thus, the FFT used by the VSA will portray the frequency-domain characteristics of the signal with minimal distortion as well. This method also negates the need for time-domain filtering (windowing) for periodic signals, which is one method for improving the spectrum when a fraction of an envelope period is present at the input.[6] Eliminating filtering removes one more potential source of distortion in the measurement and is useful when looking for a weak adjacent tone or distortion product.

VECTOR SIGNAL ANALYZER SETTINGS THAT AFFECT SPECTRAL LEAKAGE

FFT Considerations

The beauty of this procedure is in its simplicity. Although the VSA has many advanced features, such as filters, which ensure amplitude accuracy and help reduce side lobes on the acquired signals, as well as modulation/demodulation functions to interpret digital signals, this procedure uses only the RF signal and, after it is digitized, the FFT function of the VSA. The FFT is integral to the VSA for transforming the acquired time record to the frequency domain. It is an efficient algorithm for calculating the discrete Fourier transform (DFT) by significantly decreasing the quantity of calculations, from $2N^2$ to $2N \log_2(N)$, for N points in a sequence.[7] The FFT algorithm essentially replicates the captured section of the time-domain signal applied to its input such that it is periodic for all time. For modulated RF signals, if the FFT input does not have an integer number of time-domain envelope cycles, there will be a discontinuity on the input to the FFT, which results in finite amounts of power being spread over multiple frequency bins in the spectrum, as shown in ***Figure 2***. This spreading decays around a given spectral peak as $1/f^n$, where the degree n is related to the smoothness of the function in the time domain (that is n is higher for a smoother function than for one with sharp discontinuities). Superimposed on this decaying function is a sinc function, due to discretization and is called "spectral leakage."[4–6]

VSA Settings

Four VSA parameters are considered to ensure the periodicity of the time-domain input to the FFT (called "self windowing"):[6] the number of acquired frequency bins, the frequency span, the resolution bandwidth (RBW) and the acquired time window. Some VSAs use noise bandwidth (NBW) instead of RBW. RBW is defined by the hardware; NBW is defined mathematically. Otherwise, they perform the same function. Each parameter is described and then a method is developed for setting them to minimize the spectral leakage. This method may be applied directly or with minor modifications to many currently available commercial VSAs. The effect of these four parameters on the FFT in a VSA is demonstrated using a five-component multisine $m(t)$, as shown mathematically in Equation 1. Although here these principles are applied to VSAs, they are true for any FFT calculations.

$$m(t) = \sum_{i=1}^{NS} A_i \cos(\omega_i t + \phi) \qquad (1)$$

The first parameter considered is the number of frequency bins to use in the VSA measurement. The VSA takes a time-based measurement and then performs an FFT to produce the data necessary to find the signal spectrum. The FFT runs fastest if the actual number of recorded frequency bins is a power of two (such as, 64, 128…131,072).[3,8,9]

The number of frequency bins displayed on the analyzer usually does not equal the number of bins acquired. For the calculations shown here, one must use the actual number of bins acquired. The second parameter considered is the frequency span. The frequency span, the RBW and the time window are all interrelated and, for this method, a change in one parameter will force a change in one of the other parameters. First, an approximate value for the frequency span is chosen to ensure that the frequency band of interest will be captured in the measurement. However, the time window capture length and the RBW must still be taken into account before settling on the final frequency span that minimizes spectral leakage. The third parameter, the RBW, sets the spacing between frequency bins when no windowing is applied.[10] In this case, RBW is the inverse of the time window, and is proportional to the span and inversely proportional to the number of frequency bins the VSA is set to calculate. The fourth parameter is the time window. This sets the time capture length, so the VSA obtains either an integer or fractional number of envelope periods for each acquired signal. Thus, the time window determines whether the signal acquired by the FFT is smoothly periodic or has discontinuities.

Five-component Multisine

The test set-up is shown in ***Figure 3***. First, a simple multisine is considered since it clearly shows the effects

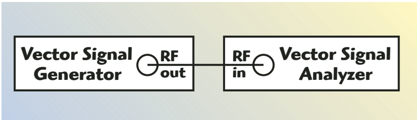

▲ *Fig. 3 Basic diagram of the test set-up.*

of the VSA parameter settings on the spectral leakage. A vector signal generator is used to create a five-component multisine, where the components have equal amplitudes and zero-degree relative phases. For the measurement examples shown here, the output power of the signal generator was –10 dBm; the frequency spacing between the tones (Δf) was 1 MHz and the center frequency was 1 GHz. A measurement of the signal generator output taken with non-optimized VSA settings is shown in ***Figure 4***. The skirts around each tone demonstrate the spectral leakage referred to earlier. This spectral smearing can cause amplitude and phase error in the measurement, particularly for weak signal components. To make accurate measurements without windowing, it is essential that these five sine waves fall directly on five of the measurement window frequency bins after the FFT is performed. ***Figure 5*** shows the result of this not happening for two of its five sine components. To eliminate spectral leakage and obtain a clean spectrum, the four key parameters mentioned above, frequency bins, fre-

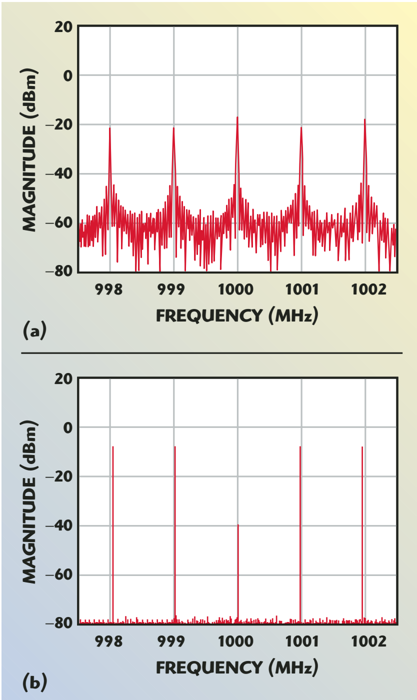

▲ *Fig. 4 VSA spectral plot of a five-component multisine signal (a) showing spectral leakage and (b) with spectral leakage minimized.*

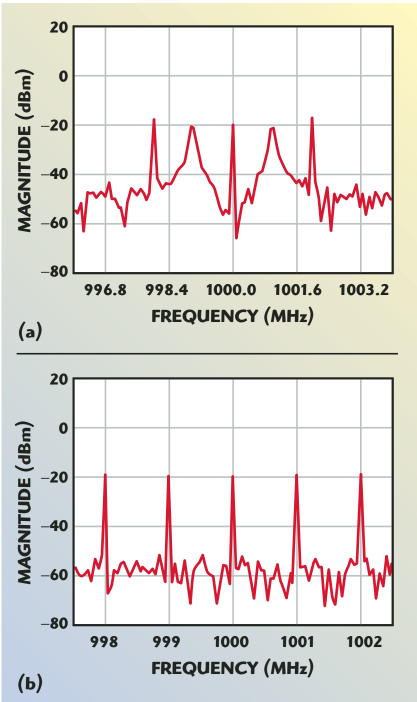

▲ *Fig. 5 VSA spectral plot of a five-component multisine with the number of FFT points calculated equal to 128.*

quency span, RBW and time window, must all interrelate properly. Since this procedure requires having maximum flexibility in setting these parameters, some adjustments must be made to the VSA's default settings. First, the RBW coupling must be set such that the RBW can be changed independently from the span. Second, to have maximum flexibility in setting the RBW, the VSA must be able to allow a user-defined RBW to be specified (not all VSAs have this option). Third, all windowing filters must be disabled. For some VSAs, this corresponds to a brick wall filter. This allows the direct FFT result to be clearly seen. Fourth, the number of frequency bins is set. For the example shown, the maximum of 131,072 frequency bins was used, the highest setting for N to lower the spectral floor and show the most detail. For some VSAs, the setting one enters for frequency bins is $2^N/1.28$. The results shown used only 128 points.

The next step is to choose an approximate frequency span ($Span_{approx}$) that will display the spectrum of interest. For this example, 5 MHz is chosen. Using $Span_{approx}$ and the number of frequency bins (N), the time window (TW_{approx}) is calculated to be 26.2144 ms using the relation

$$TW_{approx} = \frac{N}{Span_{approx}} \qquad (2)$$

The time window must be equal to an integer number of the signal-envelope periods to avoid truncation errors caused by the periodic nature of the FFT. As a result, TW_{approx} needs to be refined. For multisines with equally spaced frequency components, the envelope period can be easily found by taking the inverse of the frequency spacing between adjacent sine waves (Δf) within the multisine that are being measured. This inverse is then multiplied by the largest value of M that will satisfy the equation

$$TW_{opt} = M\left(\frac{1}{\Delta f}\right) \le TW_{approx} \qquad (2a)$$

where

$$TW_{opt} \approx TW_{approx} \qquad (2b)$$

A high M ensures that an integer number of periods are acquired without the need for phase locking or triggering. Using $\Delta f = 1$ MHz, the integer M = 20,000 was found to give an optimized value of 6.5536 MHz for the span used:

$$Span_{opt} = \frac{N}{TW_{opt}} \qquad (3)$$

This acquired span is equivalent to the displayed span of 5.12 MHz (or 6.5536/1.28) on the VSA used for the measurement shown previously. If the inverse of the optimum time window is taken, the RBW is obtained, and the VSA can now be set to these optimized Span/RBW/TW settings. It is important to specify as many digits as possible. The results are optimal when rounding is minimized for each setting. From the spectrums shown, note how the skirts around each sine wave have vanished. This clean spectrum indicates that the FFT has obtained a periodic input with no discontinuities. This corresponds to an integer number of envelope cycles in this case. Of the parameters discussed in eliminating spectral leakage, it is found that the span had the greatest impact on minimizing amplitude and phase errors for the multisine spectrum. It is, however, important to optimize all four parameters because measurements of small signals surrounding each sine wave could be distorted or obscured by spectral leakage.

CONCLUSION

A method has been described for reducing the spectral leakage when performing a spectrum measurement on a VSA. This method, based on acquiring an integer number of envelope periods of a bandpass signal, is general enough to be applied to most commercially available VSAs. Since the VSA takes a time-based measurement, it is important that the number of frequency bins, span, time window and resolution bandwidth are set such that the FFT calculation can be optimized. This provides a clean spectrum and may improve the measurement of the signal's magnitude and phase and the resolution of small signals. ■

ACKNOWLEDGMENTS

The authors wish to thank the following reviewers from industry, NIST and academia: Ken Voelker, product manager, Agilent Technologies; Abhay Samant, RF software group manager, National Instruments; Bill Byrom, application engineer, Tektronix; Kevin Thomason, application engineer, Rohde and Schwarz; Eric Hakanson, design engineer, Anritsu Co.; Andrew Dienstfrey, mathematician, NIST; and Dominique Schreurs, professor, Katholieke Universiteit in Leuven.

Note: Certain commercial equipment, instruments, or materials are identified in this article in order to adequately specify the experimental procedure. Such identification does not imply recommendation or endorsement by the National Institute of Standards and Technology, nor does it imply that the materials or equipment identified are necessarily the best available for the purpose.

References

1. "Modulation Analysis for Transient RF Signals," Tektronix Technical Brief.
2. "Perform More Effective RF Measurements Using Vector Analysis," National Instruments Application Note.
3. "The Fundamentals of Signal Analysis," Agilent Application Note, AN 243.
4. E.O. Brigham, *The Fast Fourier Transform and Its Applications*, Prentice Hall, Englewood Cliffs, NJ, 1988.
5. R.G. Lyons, *Understanding Digital Signal Processing*, Second Edition, Prentice Hall, Upper Saddle River, NJ, 2004.
6. "Vector Signal Analysis Basics," Agilent Application Note, AN 150-15.
7. http://mathworld.wolfram.com/FastFourierTransform.html.
8. J. Archambault and S. Surineni, "IEEE 802.11 Spectral Measurements Using Vector Signal Analyzers," *RF Design*, June 2004, pp. 38–49.
9. "Time-Capture Capabilities of the Agilent 89400 Series Vector Signal Analyzers," Agilent Product Note, PN 89400-10.
10. "Understanding Time and Frequency Domain Interactions in the Agilent 89400 Series Vector Signal Analyzers," Agilent Product Note, PN 89400-12.

FREQUENCY CONVERTERS: UNDERSTANDING THE BENEFITS OF SIMPLE AND COMPLEX ARCHITECTURES

Frequency converters are rapidly becoming the only analog building block in a variety of RF and microwave systems. This trend is obvious in wireless consumer products, instrumentation, radar and radar-warning systems, telemetry and secure communications. The advent of synthetic instruments puts frequency converters at center stage within the RF architecture of test systems. A synthetic instrument is a concatenation of hardware and software modules used in combination to emulate a traditional piece of electronic instrumentation, such as a spectrum analyzer or a signal generator. This definition is derived from meeting notes of the Synthetic Instruments Working Group, a joint participation between the Department of Defense, Defense Prime Contractors and Suppliers. Performance parameters relating to frequency converters are quite numerous and can only be fully optimized with complex, multi-stage architectures. The purpose of this article is to provide understanding for the trade-offs in performance involved in using simpler, less costly architectural approaches. This will help select and devise frequency conversion solutions that are optimized for specific classes of applications. For example, a downconverter aimed at surveillance of the airwaves and identifying specific signals in the presence of a multitude of others has different requirements from a test and measurement application where signals are few and known. The introduction of high frequency quadrature demodulators, such as the LTC 5515, direct quadrature demodulator from Linear Technology, raises the opportunity to simplify downconverter block diagrams. Similarly, quadrature modulators, such as the HMC495LP3, direct quadrature modulator from Hittite Microwave make it equally possible to reduce the complexity of upconverters. This article is intended to shed light on some of the key performance parameters and to help system designers and integrators identify appropriately priced solutions to meet their needs. Some performance parameters related to frequency converters are directly tied to the complexity of the block diagram. It will also be seen that a great many of the most significant parameters are independent of the approach taken. It is therefore possible to obtain low phase noise, accurate conversion gain and good modulation quality from a single-stage, lower cost converter.

This article is intended to shed light on some of the key performance parameters and to help system designers and integrators identify appropriately priced solutions to meet their needs.

ROLAND HASSUN
Roland Hassun Consulting

TABLE I

KEY FREQUENCY CONVERTER PARAMETERS

Deterministic		Random		
Linear	*Nonlinear*	*Multiplicative*		*Additive*
Amplitude response	AM to AM conversion	phase noise	amplitude noise	noise floor or noise figure
Phase response (group delay variation)	(intermodulation)			
Spurious signals and responses	AM to PM (critical in high order digital modulation formats)			

CATEGORIZING CONVERTER TRANSMISSION AND SIGNAL QUALITY PARAMETERS

Table 1 shows parameters that define the transmission quality of a converter categorized in a logical manner. How only spurious signals and responses are affected by the architecture will be discussed. All other parameters can be just as easily optimized in a simple architecture. One could even argue that a configuration with shorter and fewer signal paths is better suited for optimizing transmission parameters such as amplitude and phase response.

Performance Factors Dictated by the Architecture

The following parameters are definitely favored in a multi-stage design:

- Spurious responses (downconverters)
- Spurious sidebands (upconverters)
- Frequency range
- Port isolation

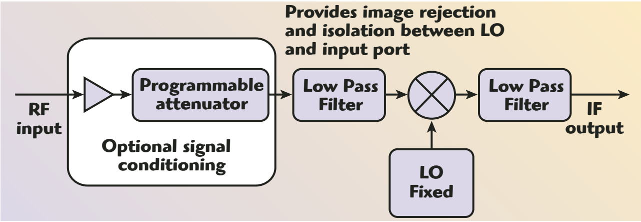

▲ *Fig. 1 Single-stage block downconverter LO>RF>IF.*

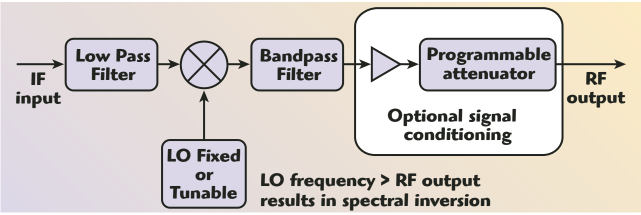

▲ *Fig. 2 Single-stage block upconverter LO>RF>IF.*

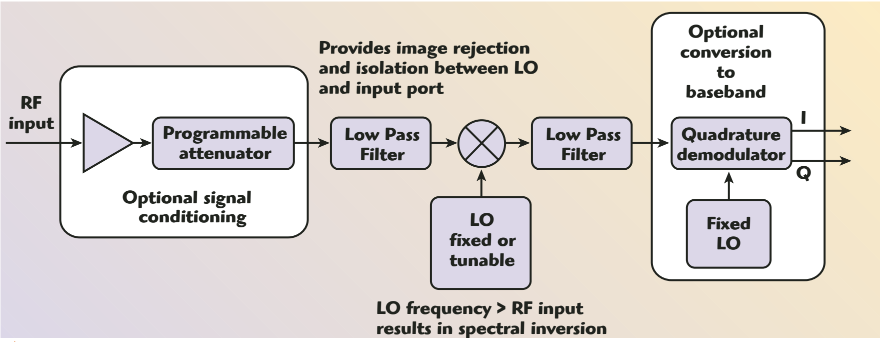

▲ *Fig. 3 Single-stage downconverter with quadrature demodulator.*

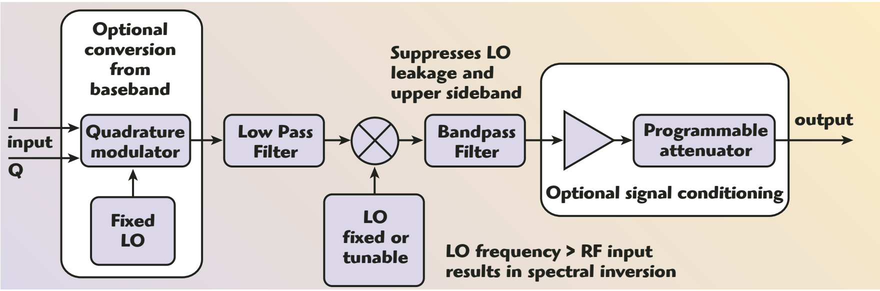

▲ *Fig. 4 Single-stage upconverter with quadrature modulator.*

Performance Factors that Can Be Enhanced by Calibration and Signal Processing

- Conversion gain accuracy
- Conversion gain uniformity with respect to input or output frequency
- Signal level accuracy
- Linear modulation parameters such as amplitude and phase response over the bandwidth occupied by the signal

Performance Factors that Can Be Enhanced by Technology Regardless of Architecture

- Noise floor, through the use of low noise amplifiers
- Enhanced image frequency suppression, through the use of YIG-tuned input filters
- Phase noise

SINGLE-STAGE BLOCK CONVERTER DESIGN EXAMPLE

A block converter takes a frequency band and converts it to another one and preserves the extent of the band. For example, an input band ranging from 4.9 to 6.0 GHz may be downconverted to 1.1 to 2.2 GHz, as shown in ***Figure 1***, or the reverse upconversion process can take place, as depicted in ***Figure 2***. In the case of the block downconverter, one relies heavily on the selectivity of the low pass filter for isolating the LO from the input port as well as suppressing the image frequency. In the case of the upconverter, the low pass filter (LPF) at the input is more straightforward, since the LO frequency is farther removed from the IF input. The bandpass filter, on the other hand, ensures isolation between the LO and the output RF port as well as the selection of the desired lower sideband.

SINGLE-STAGE TUNABLE CONVERTER

Consider the configurations in ***Figures 3*** and ***4***, which represent a straightforward single-stage up or downconverter. The selection of IF and LO frequencies has a direct influence on the spurious response (downconverter) and spurious side-

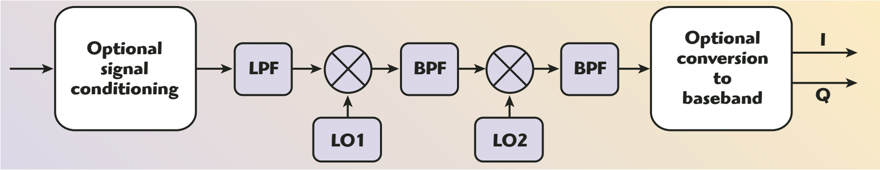

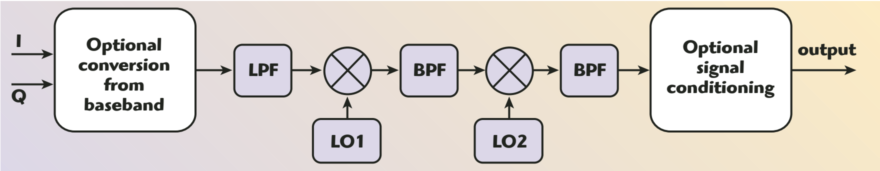

Figs. 5 (top) & 6 (bottom) Multi-stage downconverter improves spurious responses; multi-stage upconverter improves spurious sidebands.

bands (upconverter). The higher the IF frequency, the easier it is to filter unwanted sidebands (upconverter) and prevent signals at LO + IF from getting into the mixer. The latter is known as image frequency suppression and becomes practically impossible when the IF frequency is too low. Also shown are optional stages of IQ (or quadrature) demodulation and modulation for converting directly from baseband to IF, if needed. Direct conversion is used extensively in consumer products because it is economical in parts count, size and power consumption. In this case, it offers the added benefit of coping with the spectral inversion issue. This is done by interchanging the I and Q signal ports.

TWO-STAGE DESIGN EXAMPLE

The multi-stage architectures (see ***Figures 5*** and ***6***) offer some benefits:

- Easier filtering to protect against spurious responses in downconverters.
- Easier filtering to suppress unwanted sidebands, such as LO feed through, alternate sideband and other undesired out of band signals.
- Possibility of covering a frequency range with LOs having a more limited range than in the simpler architecture.
- Better isolation between input, output and LO ports.
- When each of the two stages undergoes a spectral inversion, the resulting spectrum at the output is unchanged.

SPECTRAL INVERSION

Spectral inversion in frequency conversion occurs whenever an increase in the frequency of the input signal results in a decrease of the frequency of the output signal. This is usually the case when the output frequency is below that of the LO. The effect of spectral inversion is seen in ***Figures 7*** and ***8***. When the I and Q baseband signals are used on the input for an upconverter or on the output for a downconverter, the spectrum can be redressed simply by interchanging the I and Q ports. It is possible to implement the equivalent

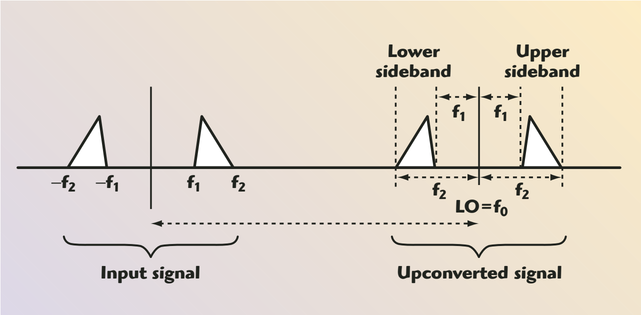

Fig. 7 *Spectral inversion in lower sideband upconversion.*

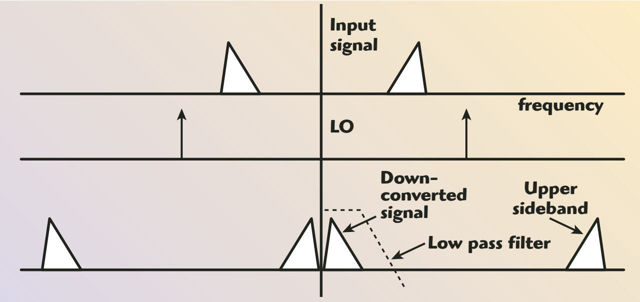

Fig. 8 *Spectral inversion in single-stage downconversion.*

of the interchange of I and Q in software when processing the signal.

IMPACT OF LO ON ARCHITECTURE

This topic requires much more elaboration than the scope of this article allows. Very often, the block diagram configuration is dictated by LO considerations. In particular, one generally tries to use the narrowest possible frequency range for the LO to limit design complexity, cost, size and power consumption.

The narrower range of the LO is circumvented in one of two ways:

- Multiply the LO output to extend the frequency range. This leads to complications in filtering subharmonic sidebands sufficiently to reduce unwanted effects such as spurious sidebands (upconverter) and spurious responses (downconverter).
- Add switched IF paths to extend the frequency range while avoiding the undesired effects mentioned above.

In general, the LO(s) are the main contributors to phase noise and are therefore selected or designed to produce desired levels of phase noise. The trade-offs with respect to block diagram complexity can be quite significant since the phase noise fares better when the frequency range is limited. The LO is a key component in the design of converters and generally drives cost, size and time to market.

COMPARISON BETWEEN ARCHITECTURALLY DETERMINED PERFORMANCE PARAMETERS FOR SINGLE- AND MULTI-STAGE FREQUENCY CONVERTERS

It is clear from **Table 2** that the multi-stage architecture is superior in protecting the output port from signals present on the input port or the LO. All other parameters are independent of the architecture. This is quite significant, since it opens up the possibility of

TABLE II

COMPARISON BETWEEN SINGLE- AND MULTI-STAGE FREQUENCY CONVERTERS

Parameter	Single Stage	Multiple Stages
Cost, size, power consumption, component count	better	
Leakage of signals on the input port to the output port		more isolation (better)
Leakage of LO to input port	same	same
Leakage of LO to output port		more isolation
Spurious responses of downconverter		more suppression
Conversion gain, accuracy, attenuation, amplitude and phase response, input/output VSWR, IIP3, phase noise, amplitude noise, noise figure	same	same

using less expensive units with a smaller footprint and lower power consumption in a variety of applications. One such application is dedicated test systems. In this instance, the number of signals present is limited and known in the great majority of cases. For example, the presence of an LO component far removed from the signal of interest is of little consequence, so long as it does not introduce intermodulation products or interfere with the accuracy of the measurement. It should be noted that everyone is familiar with the signal spike on the far left of the screen of a spectrum analyzer caused by LO leakage into the IF. It has become an indicator of zero frequency. A counter example is a radar system destined to work in hostile environments. Susceptibility to signals on the input leaking to the output raises the possibility of jamming signals rendering the radar ineffective. A multi-stage approach with appropriate protection is better suited for this application. It is important to note that a converter required to cover a frequency range of several octaves is unlikely to be realized effectively by means of a single-stage, single IF path architecture.

CONCLUSION

For applications that tolerate some level of spurious responses (downconverters) or out-of-band spurious sidebands (upconverters), a simple one-stage converter solution may be all that is required. The consequences in time to market, cost, size and power consumption may be very significant. ■

Roland Hassun *is an independent technical consultant specializing in test and measurement, frequency synthesizers and converters. Prior to consulting, he worked for HP/Agilent, where he was involved in pioneering several areas of instrumentation, including low noise RF signal generators, high speed digital waveform generation and direct digital synthesis.*

AN X-BAND PHASED-ARRAY RADAR MMIC CHIP SET

Radio detection and ranging or RADAR has been around since its first implementation in the early 1900s when the use of radio waves was first used to detect the presence of ships in dense fog. The actual acronym was not coined until the early 1940s. X-band radar, in particular, has been around since the outset of World War II and continues to see extensive use. Typical X-band radar applications include air traffic control, detection of precipitation, speeding traffic and military use. Military uses include detecting and tracking aircraft, ships, missiles and other objects with the intention of harming any of our armed forces protecting our country and its interests. Various types of radar include continuous wave (CW), dual-pole, phased array, pulsed, single-pole and synthetic aperture radar (SAR). Many of the advanced X-band radars used today are typically based on active phased arrays requiring the use of many multiple phase array element sections.

Fig. 1 The X-band radar chip set block diagram used in a typical phased-array antenna element application.

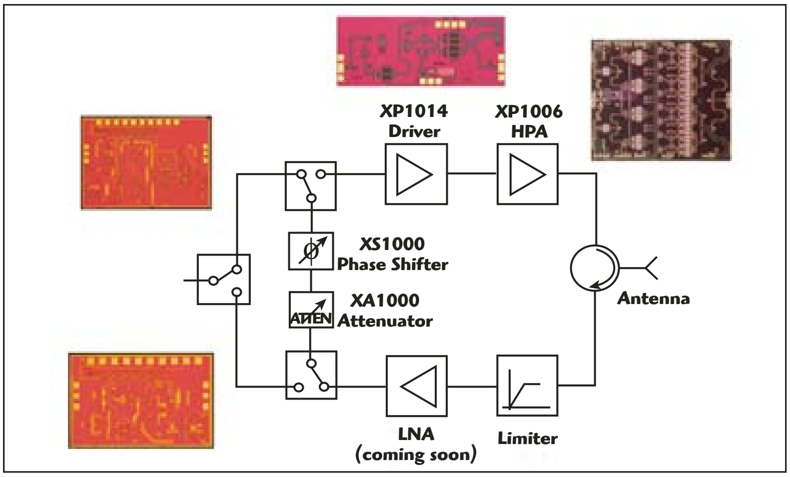

DESIGN AND TECHNOLOGY

Mimix Broadband is pleased to offer a very competitive and high performance X-band radar phased-array element chip set. ***Figure 1*** shows a typical X-band radar phased-array antenna element block diagram. The transmit portion of the phased-array element includes a 10 W output power amplifier stage (XP1006) specifically designed for pulsed radar applications. The output driver stage (XP1014) is a

MIMIX BROADBAND INC.
Houston, TX

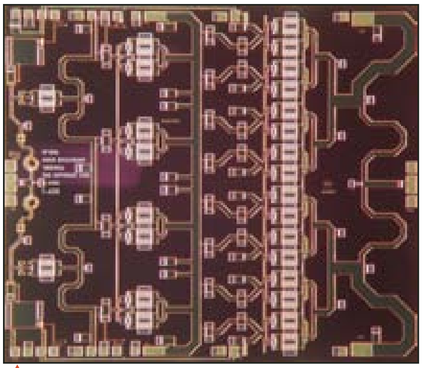

▲ *Fig. 2 XP1006 chip layout.*

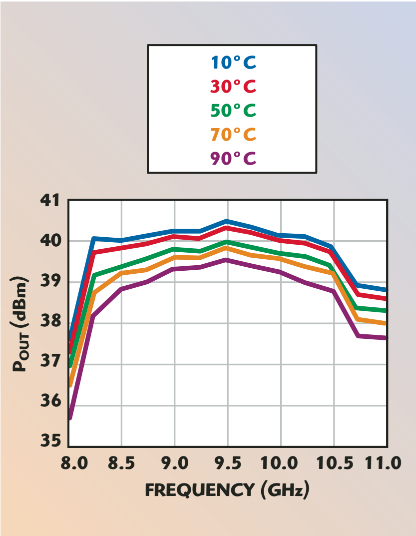

▲ *Fig. 3 XP1006 saturated output power vs. temperature.*

1 W MMIC designed to drive the XP1006 device completing the transmit chain. On the receive side of the phased-array element the company will soon be offering a combined low noise amplifier/limiter MMIC that will provide excellent noise figure and high power limiting capability. Lastly, to complete the phased-array element control chain both a wide band attenuator (XA1000) and phase shifter (XS1000) MMIC device are available.

The X-band MMIC chip set uses Mimix Broadband's six-inch 0.5 µm GaAs PHEMT device model technology and is based on an optical gate lithography to ensure high repeatability and uniformity. Using a 0.5 µm process allows lower cost optical lithography to be used for device deposition and in conjunction with six-inch wafer area provides users with a highly repeatable and lower cost MMIC chip set solution.

All Mimix die products include surface passivation to protect and provide a rugged part with backside vias allowing either a conductive epoxy or eutectic solder die attach process. Most of the company's products are available in both die and packaged versions, with many provided in RoHS compliant surface-mount packages compatible with high volume solder installation. Both the flanged ceramic and surface-mount packaged amplifiers offer excellent RF and thermal properties.

POWER AMPLIFIER

The XP1006 device, shown in ***Figure 2***, is a three-stage 8.5 to 11.0 GHz 10 W power amplifier that has a large-signal gain of 21 dB and provides excellent input/output return loss. Power-added efficiency (PAE) is 30 percent with +40 dBm saturated output power (see ***Figure 3***). This device not only includes on-chip bias circuitry that allows the user to provide a single –5 V bias input but also provides additional gate bias inputs that allow separate gate bias control. All devices are 100 percent wafer probed for RF, DC and output power performance. The power amplifier is offered both in die form and in a soon to be released ceramic flanged package.

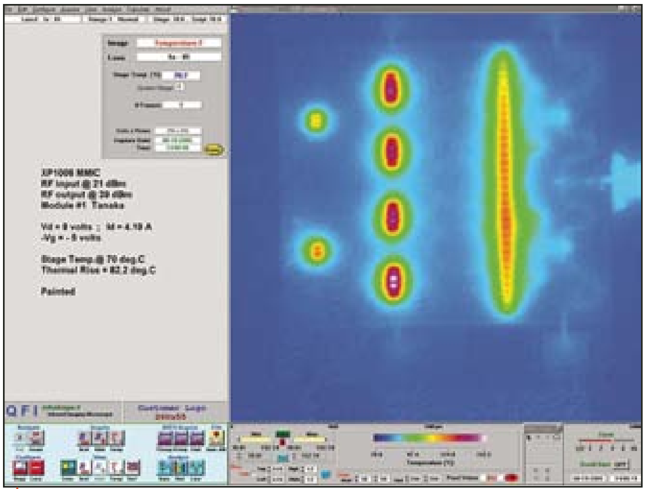

▲ *Fig. 4 XP1006 thermal image.*

Thermal imagery of the XP1006 (see ***Figure 4***) has been taken under various bias conditions using thermal image equipment located at the company's facility in Houston. Unlike thermal analysis using models to predict thermal resistance, this imager allows Mimix to actually measure channel temperatures of all the devices on the MMIC thus allowing a much more accurate thermal resistance to be determined. Once the thermal resistance has been calculated, reliability information such as mean time to failure (MTTF) and failures in time (FIT) can be calculated allowing more accurate optimal base temperatures to be provided for determining safe operation. An application note describing the usage of the XP1006 in more detail can be found on the company's web site.

DRIVER AMPLIFIER

The XP1014 MMIC, shown in ***Figure 5***, is a two-stage 8.5 to 11.0 GHz 1 W power amplifier that has a small-signal gain of 18 dB. Its PAE is 35 percent with +31 dBm saturated output power (see ***Figure 6***). This

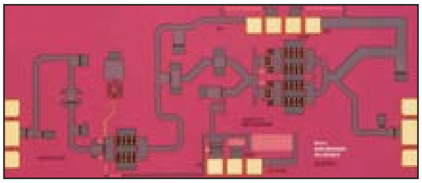

▲ *Fig. 5 XP1014 chip layout.*

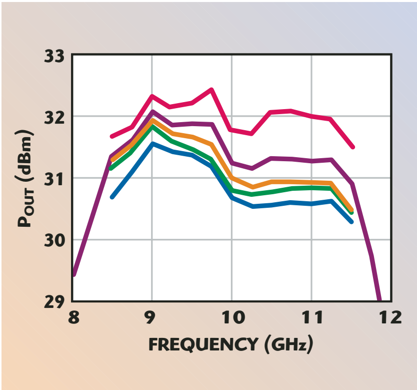

▲ *Fig. 6 XP1014 saturated output power from multiple devices.*

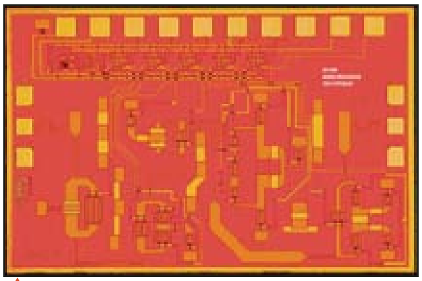

▲ *Fig. 7 XA1000 chip layout.*

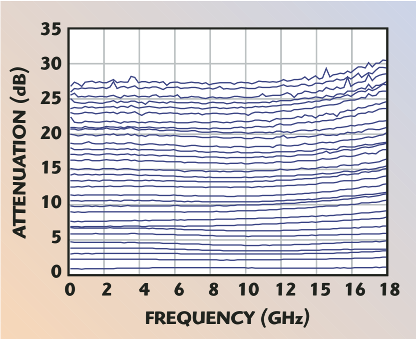

Fig. 8 XA1000 attenuation for all states.

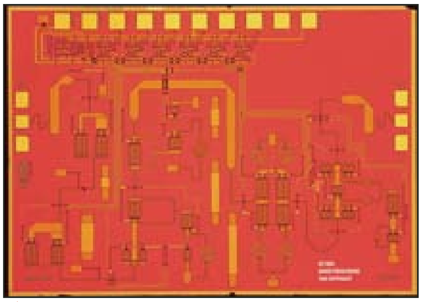

Fig. 10 XS1000 chip layout.

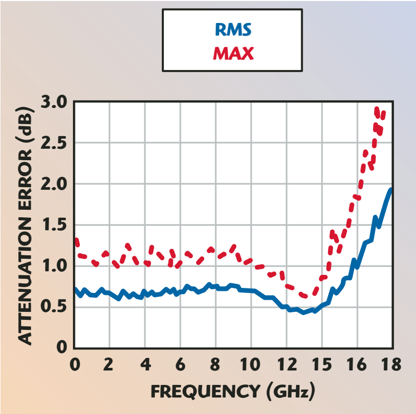

Fig. 9 XA1000 attenuation error.

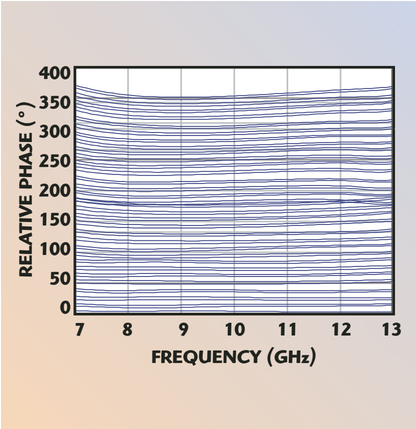

Fig. 11 XS1000 relative phase for all states.

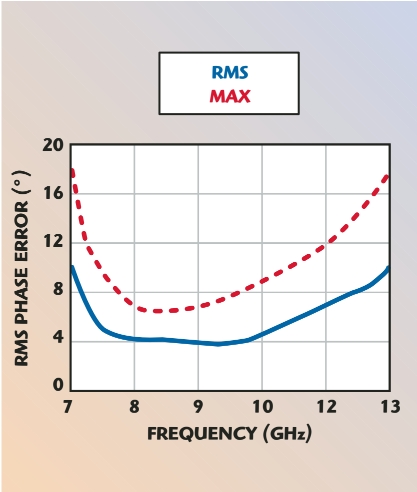

Fig. 12 XS1000 phase error.

device includes on-chip bias circuitry that allows the user to provide a single –5 V bias input. As with the previous power amplifier, these devices are 100 percent wafer probed for RF, DC and output power performance as well. They are offered both in die form and in a soon to be released ceramic flanged package.

ATTENUATOR

The XA1000 device, shown in ***Figure 7***, is a DC to 18 GHz, five-bit digital attenuator. The device has a 27 dB attenuation range (see ***Figure 8***) with 5.5 dB insertion loss. Its input and output return loss is excellent across all states and the input 1 dB compression point (P1dB) is +24 dBm. Its attenuation error, shown in ***Figure 9***, is less than 1 dB with a phase error of less than 20°. The device is operated using a single –7.5 V supply voltage with five digital binary inputs that meet LVCMOS specifications. All devices are 100 percent wafer probed for RF, DC and attenuation performance. The attenuator is currently offered only in die form with packaged device development starting in the near future.

PHASE SHIFTER

The XS1000 MMIC, shown in ***Figure 10***, is a 7 to 13 GHz, six-bit phase shifter. The device has a LSB of 5.625° (see ***Figure 11***) with 6.5 dB insertion loss. Its input and output return loss is excellent across all states and the input P1dB is +25 dBm. Attenuation error is less than 1 dB with a RMS phase error (shown in ***Figure 12***) of less than 3°. The device is operated using a single 7.5 V supply voltage with six control inputs. All devices are 100 percent wafer probed for RF, DC and phase bit performance. The phase shifter is currently offered only in die form with packaged devices available in 2007.

LNA/LIMITER

Lastly are the LNA and limiter functions of the phased-array element. Since radar front ends are susceptible to damage from high input power transmitters, the

LNA needs some sort of protection to keep its lower level input devices from being damaged. While there are a number of options that can been chosen, a low loss limiter is typically the best choice for this application. The limiter provides a low insertion loss solution providing the least amount of degradation to front end noise figure but at the same time enough level of input transmit power protection when it is needed to protect the LNA from damage.

The X-band LNA/limiter is still in development at this time and is expected to be available at the end of CY2006. Additional information and its updated status may be obtained from the company's web site.

CONCLUSION

A high performance X-band radar phased-array element chip set has been presented that includes driver and power amplifier devices for the transmit side, an LNA/limiter for the receive side, and an attenuator and phase shifter for the control side. The new chip set is fabricated using Mimix Broadband's six-inch 0.5 µm GaAs PHEMT device model technology and is based on an optical gate lithography process. The new devices represent a highly repeatable, low cost MMIC chip set solution for a radar phased-array element interface. The individual die are surface passivated with backside vias to allow conductive epoxy or eutectic die attach. In addition, the devices are 100 percent RF and DC tested, guaranteeing their performance and allowing users to increase their yields and lower costs.

Devices are now available in die form or in soon to be released ceramic flanged mount and surface-mount packages. Additional information and individual data sheets may be obtained from the company's web site.

Mimix Broadband Inc.,
Houston, TX (281) 988-4600,
www.mimixbroadband.com.

RS No. 300

METAL-CLAD FIBERS WITH SIGNIFICANT WEIGHT SAVINGS AND EMI PERFORMANCE

Micro-Coax is now offering the ARACON® family of metal-clad fibers that combines the conductivity of metal with the strength, light weight and flexibility of Kevlar® aramid fibers. The ARACON fibers are a superior lightweight alternative to traditional nickel-plated copper wire for EMI shielding. Replacing standard wire with ARACON offers significant weight savings without sacrificing EMI performance, as well as other benefits that copper and alloy wires cannot match.

Critical signal paths in aircraft wiring harnesses and cables require shielding to prevent electromagnetic interference (EMI). Braided EMI shields are traditionally made from standard copper wire. Utilizing ARACON fibers for these braided shields can save substantial weight on an airborne platform. ***Table 1*** shows examples of braid configurations and the overall weight savings ARACON can offer. The density of the Kevlar aramid fibers is only 1.44 g/cc, vastly superior to copper's 8.90 g/cc. When metal coatings of nickel or silver are added to the ARACON fibers, the density becomes 3.0 to 4.0 g/cc, depending on the material choice and thickness required in the application.

TABLE I

APPROXIMATE WEIGHT SAVINGS (POUNDS) REALIZED WHEN REPLACING Ni-PLATED COPPER WIRE WITH AN ARACON BLEND (75%/25%)

Inside Diameter of Over-braid (")	1.00	93	186	465	930
	0.75	48	97	242	483
	0.50	30	61	152	304
	0.25	17	34	85	171
	Total over-braid usage per system(')	1000	2000	5000	10000

ARACON fibers offer equal or better shielding effectiveness when compared to copper wire at frequencies of 50 MHz and above. At higher microwave frequencies, shielding performance is often better than copper due to the improved braid coverage. To protect against signals below 50 MHz, a hybrid blend of 75 percent ARACON and 25 percent copper wire can be used. This hybrid reduces the transfer impedance of the overall braid, which results in better shielding, as shown in ***Figure 1***.

Additionally, the weight savings of the ARACON metal-clad fibers is complemented with higher break strength that is nearly three times

MICRO-COAX
Pottstown, PA

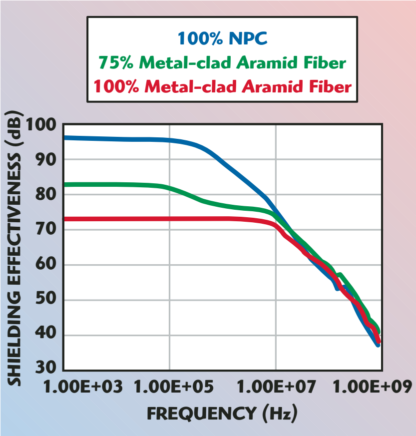

▲ *Fig. 1 Shielding effectiveness comparison. (Tokarsky, Edward W., Case Histories of Aerospace Wire and Cable Uses of Metal Clad Fibers in Harness Overbraids and Shielding, AEISC, 1999)*

that of copper. This eases installations and allows the EMI protection to withstand thousands of flexures during years of high vibration, high stress environments. In fact, ARACON fiber has been tested to more than 10,000 flexes without any degradation in performance. The tensile strength of the aramid core is 350 Kpsi, much stronger than traditional copper cores, which range from 35 to 95 Kpsi. The high strength of the fiber also affords greater termination reliability. The integrity of standard crimp connections is improved. Soldered connections are used in conjunction with optional silver-plated ARACON.

All the benefits of ARACON performance are achieved due to the properties of the conductors, which are comprised of numerous fine fibers twisted together. Made from aromatic polyamides, ARACON fibers are only 16 microns in diameter. The textile-like properties of the fibers contribute to extremely effective, uniform shield coverage.

THREE FIBER TYPES

Micro-Coax currently offers a Nickel-clad fiber, Silver-clad fiber and salt fog resistant fiber. Nickel-clad fiber is the most economical choice for good overall performance. The Silver-clad fiber is designed for applications in which higher conductivity and solderability are desired. Both weigh 60 percent less than copper wire at equal volume. Providing maximum stability against salt fog and thermal exposure, the salt fog resistant fiber weighs 55 percent less than copper alternatives. All three metal-clad fiber types can be braided on the same equipment used for metal wire, and are available on 3000-foot Wardwell spools or 2000-foot Butt braider bobbins.

For other special applications, Micro-Coax can develop custom ARACON yarns to meet specific design requirements. By varying the metal cladding type and thickness, as well as the base fiber size, Micro-Coax can offer yarns with a wide range of properties. For special applications, the electrical resistance of the fiber can be tailored from 100 to more than 500,000 ohms per thousand feet. Additional information may be obtained by e-mailing techinfo @micro-coax. com.

ARACON® is a registered trademark of Micro-Coax and Kevlar® is a registered trademark of DuPont.

Micro-Coax,
Pottstown, PA (800) 223-2629,
www.micro-coax.com.

RS No. 301

DC TO 26.5 GHZ SIZE 8 COAXIAL CONTACTS THAT FIT STANDARD MIL-C-38999 CONNECTORS

Times Microwave Systems has introduced a new series of Size 8 coaxial contact designs that fit all standard MIL-C-38999 connector shells and are capable of operating broadband from DC to 26.5 GHz with exceptional electrical performance. These unique contact designs have also been carefully engineered with a host of other design features that greatly improve maintainability and offer the design engineer an additional degree of design freedom not previously available.

INTEGRATED CONTACT REMOVAL TOOL FEATURE

A novel solution now completely eliminates the age old problems associated with current MIL-C-38999 Size 8 contact designs—the need to use awkward contact removal tools, often in confined spaces inside LRUs/equipment boxes.

To remove these new Times Microwave Size 8 contacts from their MIL-C-38999 shells, the user simply pushes down on the integrated tool built into the rear of the new Size 8 contacts and slides it out—no tools are required, making contact removal extremely easy and simple (see ***Figures 1*** and **2**).

ALL CONTACTS ARE FULLY FIELD REPLACEABLE

In the unlikely event of contact damage, for whatever reason, there is no need to completely change the cable assembly, as is the case today with dedicated Size 8 contact designs. Instead simply remove and replace the Size 8 contacts in seconds and re-install. This new feature saves downtime and the cost of new replacement cable assemblies.

LOW PROFILE 90° CONTACT DESIGNS NOW AVAILABLE

A real limitation of existing Size 8 contact designs has been the lack of any 90°, low pro-

TIMES MICROWAVE SYSTEMS
Wallingford, CT

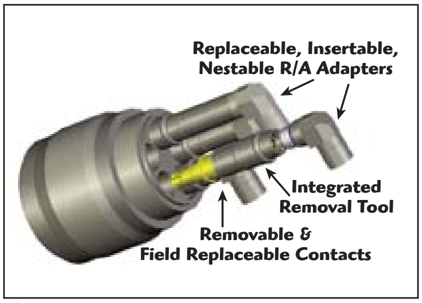

▲ *Fig. 1 Typical application of the new Size 8 coaxial contacts.*

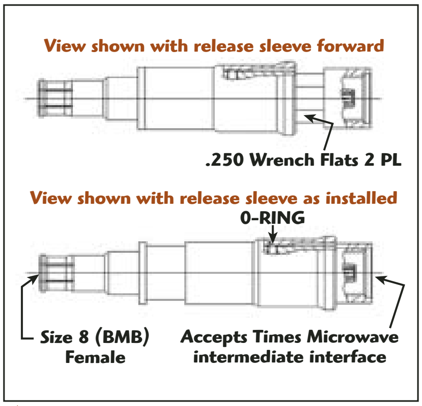

▲ *Fig. 2 Contacts with tool shown in normal and disconnect positions.*

file contacts. A full range of different profiles/nested 90° contact designs are also now available that offer exceptional performance from DC to 26.5 GHz.

CONTACTS HAVE BMB MILITARY SPECIFICATION INTERFACES

Unlike other Size 8 contact designs that are not properly impedance matched and typically operate to a maximum frequency of 3 GHz, the new Times Microwave Size 8 contacts employ the popular BMB Mil Spec interface and correctly internally compensate such that these contacts are fully suitable for use at frequencies up to 26.5 GHz.

The new Times MIL-C-38999 Size 8 microwave contact is already the interface of choice for all modern AESA Radar Systems and many other demanding applications in difficult environments. These contacts are available in both sexes and can therefore be installed on either or both sides of the connector body as needed.

Times Microwave Systems, Wallingford, CT (203) 949-8400, www.timesmicrowave.com.

RS No. 302

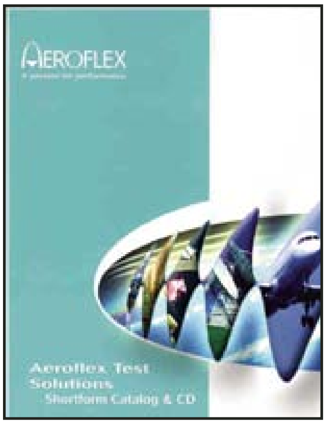

Instrument Portfolio

This short form catalog includes the company's complete spectrum of test and measurement solutions and systems. The catalog carries a range of products for the testing of PMR, cellular mobile, cellular network, cellular interoperability, military communications, avionics, signal sources, manufacturing, R&D and parametric. Further product sections include microwave, counter and power meters, PXI, spectrum and signal analyzers. A CD comprising data sheets for all products is also included.

Aeroflex Test Solutions, Instruments Division, Stevenage, UK +44 (0) 1438 772087, www.aeroflex.com.

RS No. 311

Capabilities Brochure

This new capabilities brochure from Aeroflex Microelectronic Solutions outlines the company's broad offering of standard products, innovative custom-engineered designs and comprehensive resources that enable Aeroflex to support the most demanding high performance, high quality microwave product needs of its customers worldwide.

Aeroflex/Weinschel Inc., Frederick, MD (301) 846-9222, www.aeroflex-weinschel.com.

RS No. 312

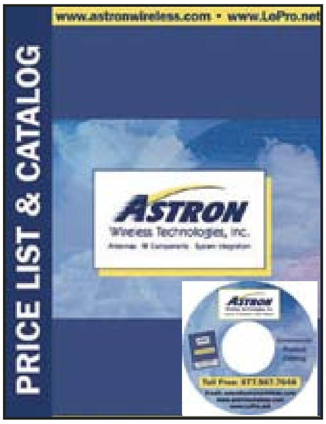

RoHS Compliant Products Catalog

The commercial product catalog showcases the company's range of RoHS compliant products and services, including, but not limited to: OEM consulting and manufacturing, custom antenna design, low profile disc antennas, microcell hemi antennas, omnidirectional antennas, yagi antennas, Enviro-Sealed Protected (ESP) yagi antennas, PCD subscriber series antennas, dual-band and tri-band antennas as well as power dividers, mounting hardware and cable assemblies.

Astron Wireless Technologies Inc., Sterling, VA (703) 450-5517, www.astronwireless.com.

RS No. 313

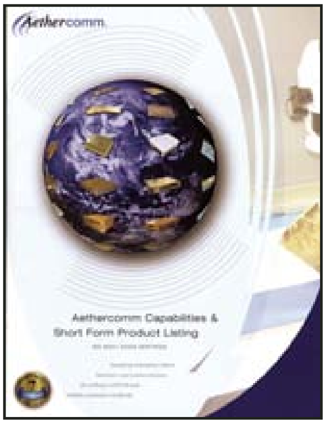

Capabilities and Short Form Product Listing

This catalog features the company's supply of innovative, robust hardware and system solutions for military, SATCOM and wireless customers worldwide. The company designs and manufactures military hardware with frequencies ranging from 10 MHz to 40 GHz. Many of these products are combat-proven and operate in the harshest of environments. The company offers extensive manufacturing capabilities using the latest manufacturing and test aids to help meet strict quality standards.

Aethercomm Inc., San Marcos, CA (760) 598-4340, www.aethercomm.com.

RS No. 314

Accessories Brochure

The revised accessories brochure from AR Worldwide RF/Microwave Instrumentation highlights a new signal generator, tubular wave couplers, system controllers, directional couplers, software, test systems and a complete line of field monitoring equipment, including three laser powered probes. Product photographs, descriptions and specifications are included for each model.

AR Worldwide RF/Microwave Instrumentation, Souderton, PA (215) 723-8181, www.ar-worldwide.com.

RS No. 315

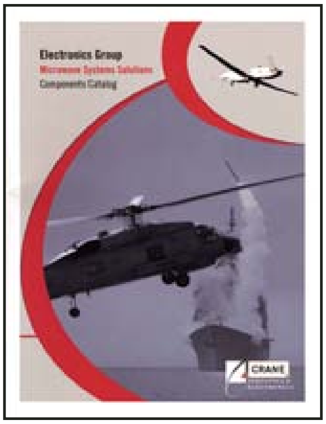

Components Catalog

The 40-page microwave systems solutions components catalog provides easy selection of high reliability microwave components: isolators, circulators, passive components, mixers, limiters and detectors. Data includes frequency range, isolation and insertion loss, as applicable, plus temperature, weight and dimensions.

Crane Aerospace & Electronics, Electronics Group, Microwave Systems Solutions, Chandler, AZ (480) 961-6269, www.craneae.com.

RS No. 317

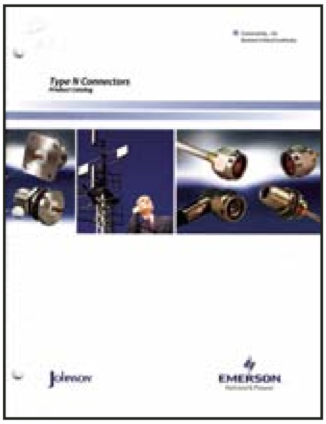

Product Catalog

This catalog features the company's Johnson® Type N connectors that meet or exceed the performance requirements of MIL-PRF-39012. All designs are based on 50 Ω system impedance per MIL-STD-348 and operate at frequencies up to 11 GHz minimum. All contacts are plated with 50 micro-inches of gold for good durability and high frequency performance. Applications include: antennas, base stations, cable assemblies, microwave radio, RF and microwave components.

Emerson Network Power Connectivity Solutions, Johnson Division, Waseca, MN (800) 247-8256, www.emersonnetworkpower.com/connectivity.

RS No. 318

Product Selection Guide

This Guide summarizes over 450 products including 30 products new to this latest edition. The selection guide organizes the company's portfolio by product line as well as by market applications including: automotive, broadband, cellular, microwave and mm-wave, test and measurement equipment, fiber optic, military and space. With redesigned sections for connectorized modules, designer's kits and application circuits, this guide contains over 60 new products released in 2006 that are not included in the 2006 Designer's Guide Catalog.

Hittite Microwave Corp., Chelmsford, MA (978) 250-3343, www.hittite.com.

RS No. 319

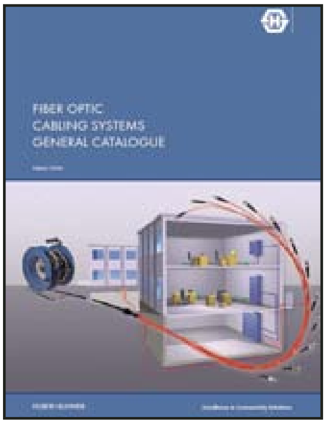

Fiber Optics Cabling Systems Catalog

This new catalog contains detailed information about the company's fiber optic cabling systems. Masterline, Smartline, Mobile Cabling Systems and Connecting Systems are introduced as well as cables, connectors and assembly classes. Together with a short introduction about the fiber management system LISA, this catalog provides a clear overview for FTTx-solutions and also for fixed and mobile networks.

HUBER+SUHNER AG, Herisau, Switzerland +41 (0)71 353 41 11, www.hubersuhner.com.

RS No. 320

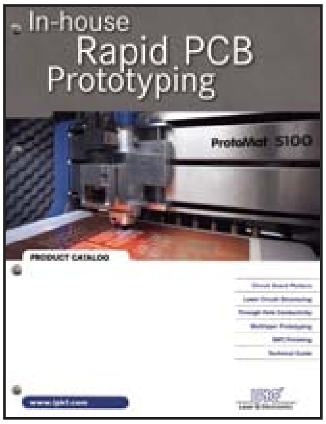

Product Catalog

This catalog contains the latest data and information to help a reader review and choose the best technological solution to all rapid prototyping needs: machines, tools, applications, consumables, accessories and software. This new catalog also contains a Technical Guide, a collection of tips and tricks for using LPKF hardware and software to achieve the best results.

LPKF Laser and Electronics AG, Garbsen, Germany +49 (0) 5131-7095-0, www.lpkf.com.

RS No. 321

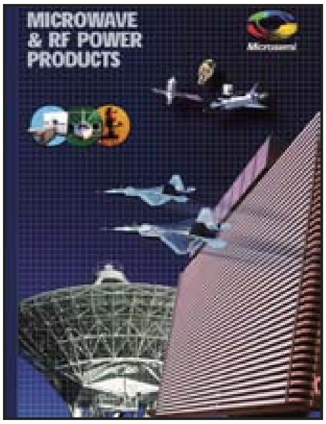

Power Products Brochure

This 36-page brochure features the company's line of microwave PIN diodes and modules for small signal/high speed switching, large signal switching/attenuators, limiters and Schottky mixers in a variety of surface-mount and high-rel packages, plus its new line of RF power semiconductors for avionics, radar, microwave, broadband, HF/VHF/UHF communications and high voltage MOSFETs. Includes useful selector guides and case style outlines.

Microsemi Corp., Irvine, CA (949) 221-7100, www.microsemi.com.

RS No. 322

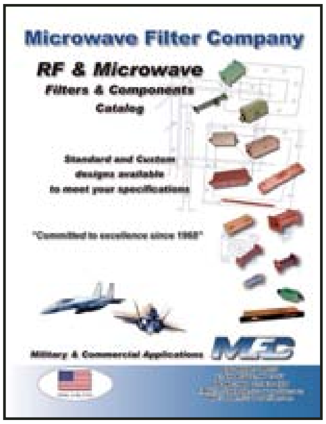

Product Catalog

This catalog features a sampling of the company's RF and microwave filters and components that cover the frequency range from 5 Hz to 50 GHz. These high quality designs include surface-mount, waveguide, stripline/microstrip, lumped element and cavity/coaxial topologies. Filter types and accessories include bandpass, bandstop, combiners, couplers, diplexers, high pass, low pass and adapters.

Microwave Filter Co. Inc., East Syracuse, NY (800) 448-1666, www.microwavefilter.com.

RS No. 323

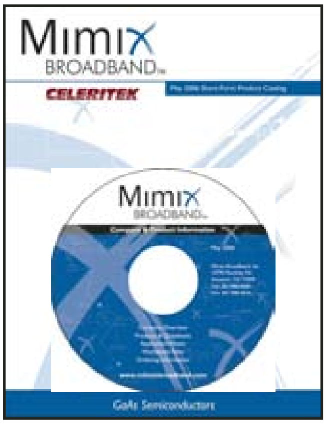

Short Form Catalog/CD-ROM

This updated short-form catalog and product catalog on CD-ROM includes new product highlights, updated data sheets with more comprehensive information and measurement curves, RoHS Program information, application notes, company and facility overviews, ordering information and a complete listing of international sales representative and distribution networks. In addition, the CD-ROM is hyperlinked to the company's web site to facilitate the collection of additional information.

Mimix Broadband Inc.,
Houston, TX (281) 988-4600, www.mimixbroadband.com.

RS No. 324

CD Catalog

This CD Components Catalog offers a comprehensive display of the company's standard and custom capabilities. The CD includes product specifications, outline drawings, test data, manufacturing flow diagrams and a wide assortment of technical application notes. The company designs and manufactures state-of-the-art microwave components such as UHF to millimeter-wave low noise and medium power amplifiers, mixers, multipliers, switches, frequency sources, IF signal processing equipment and integrated microwave subsystems. Emphasis is on high performance, custom engineering driven applications.

MITEQ Inc.,
Hauppauge, NY (631) 436-7400, www.miteq.com.

RS No. 325

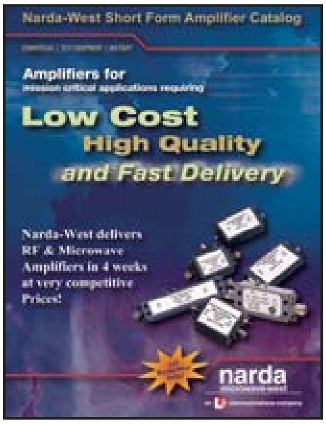

Short Form Amplifier Brochure

This catalog highlights the company's new amplifier product line that offers low cost, high quality and quick turnaround ("off the shelf" on some products and four weeks from time of order in most cases). These amplifiers are suitable for use in commercial, military, test equipment, prototype and laboratory applications. These new amplifiers broaden the already extensive line of amplifiers from Narda Microwave-West.

Narda Microwave-West,
Folsom, CA (916) 351-4500, www.nardamicrowave.com.

RS No. 326

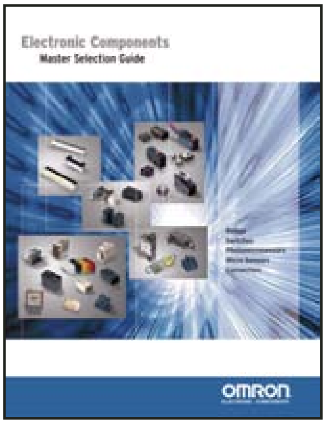

Electronic Components Master Selection Guide

This new 40-page short form catalog provides the latest in product information and a comprehensive, easy-to-use specifying tool for the company's high quality relays, switches, photomicrosensors, microsensors and connectors. It also offers key sales contact details and company information. To request a complimentary copy, e-mail: components@omron.com.

Omron Electronic Components LLC,
Schaumburg, IL (847) 882-2288, www.components.omron.com.

RS No. 327

Cosite Communication Solutions

The 2007 catalog features a comprehensive suite of RF interference mitigation products including tunable filters, Integrated Cosite Equipment (ICE), low noise amplifiers, cosite power amplifiers and other products that are ideal for solving communication problems caused by various types of RF interference.

Pole/Zero,
West Chester, OH (513) 870-9060, www.polezero.com.

RS No. 328

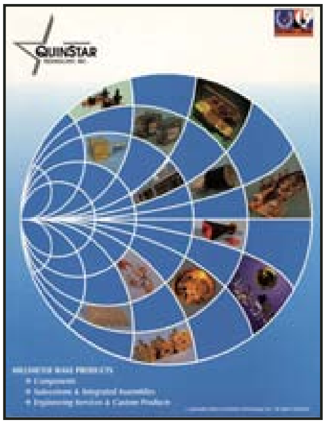

Product Catalog

This catalog features the company's millimeter-wave products that range from standard catalog components to specialized high performance RF signal generating, amplifying and conditioning components to fully integrated and customized assemblies and subsystems for digital and analog sensor, communications and test applications. These products serve established as well as emerging markets and system applications in the commercial, scientific and defense arenas.

QuinStar Technology Inc.,
Torrance, CA (310) 320-1111, www.quinstar.com.

RS No. 329

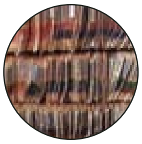

Catalog Update

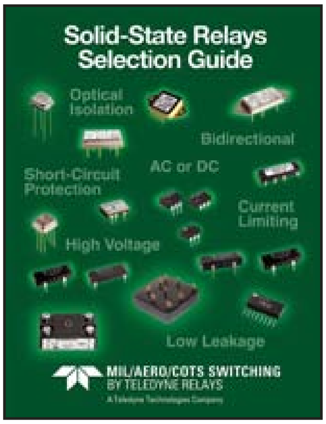

Selection Guide

The solid-state relays selection guide is designed for military, aerospace and COTS applications. The catalog features 74 families in a tabular format designed in an easy to use format to quickly assist engineers in choosing a product. The 20-page digest provides detailed information about the relays, which include AC, DC and bi-directional relays with output ranging from 0.25 to 10 amps. The digest includes parameters such as load voltage, load current, ON-state voltage drop, isolation type and input voltage.

Teledyne Relays,
Hawthorne, CA (800) 284-7007, www.teledynerelays.com.

RS No. 330

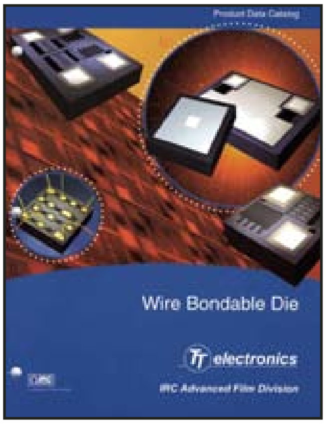

Product Data Catalog

This catalog features the company's tantalum nitride thin film technology in ultra-miniature silicon or ceramic-based wire bondable die, offering space savings, precision and reliability. Features include: single chips, center-tapped dual chips, networks and capacitors with multiple pads for wire bonding; resistor chips at 20 mil square; two-resistor networks at 30-mil square with six pads for shortest available wire bonds; tolerances to ±0.1%; and TCR tracking to ±2 ppm/°C and capacitors at 60 mil square with values from 10 to 700 pF.

TT electronics, IRC Advanced Film Division,
Corpus Christi, TX (361) 992-7900, www.irctt.com.

RS No. 331

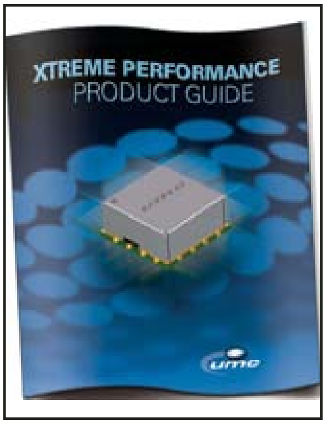

Product Guide

The Xtreme Product Guide features the company's Xtreme frequency solutions. Contents include product description tables, application notes and outline drawings for all UMC VCO and synthesizer products. Visit www.vco1.com to order today.

Universal Microwave Corp.,
Tempe, AZ (877) 862-9873, www.vco1.com.

RS No. 332

Ka-band SATCOM LNA

The model APTW4-18002650-2510-42 is a waveguide (WR-42) amplifier that operates in a frequency range from 18 to 26.5 GHz. This model offers an ultra low noise figure of 2.2 dB (191.3 K) maximum and a minimum output power of +10 dBm (+20 dBm IP3). Optimized bandwidth from 17.8 to 21.3 GHz can also be provided with a noise figure as low as 135 K. Its design is a two-piece modular system that helps in the assembly, troubleshooting and field repairs of the amplifier. This model is unconditionally stable and can operate with the most intense weather conditions, temperatures (–55° to +85°C), shock and vibrations.

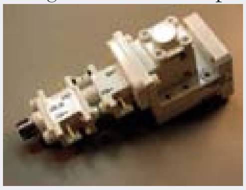

AmpliTech Inc.,
Hauppauge, NY (631) 435-0603,
www.amplitechinc.com.

RS No. 216

500 to 2700 MHz Power Amplifier

The model KMS1030 is a new broadband solid-state GaAs FET power amplifier module that has been added to the company's family of wireless communication amplifiers. Model KMS1030 delivers 5 W across the 500 to 2700 MHz frequency range and is designed to cover UHF, L and S bands for a wide range of applications requiring instantaneous ultra broadband. This 37 dBm linear power amplifier also offers a minimum gain of 45 dB and meets all types of modulation protocols.

AR Worldwide Modular RF,
Bothell, WA (425) 485-9000,
www.ar-worldwide.com.

RS No. 217

70 and 120 W TWT Amplifiers

This expanded line of broadband traveling wave tube (TWT) amplifiers provide even more power/frequency options to its customers. The newest models include the 70T40G45, delivering 70 W of power and model 120T40G45 providing 120 W. Both units operate in a frequency range from 40 to 45 GHz and are designed for applications where wide instantaneous bandwidth, high gain and moderate power output are required.

AR Worldwide RF/Microwave Instrumentation,
Souderton, PA (215) 723-8181,
www.ar-worldwide.com.

RS No. 218

2 to 18 GHz Down Converter

This down converter module operates in a frequency range from 2 to 18 GHz, making it ideally suited for Electronic Warfare (EW) and Electronic Counter Measures (ECM). The module downconverts the broadband RF input signal to a UHF frequency on the IF output. A high isolation buffer amplifier at the LO input, along with tight filtering on RF, LO and IF ports, helps to minimize spurious signals at all inputs and outputs. A broadband limiter is incorporated on the RF front-end for receiver protection, and temperature compensation is used to provide a stable RF-IF gain response over an extended military operating temperature range.

Endwave Defense Systems,
Sunnyvale, CA (408) 522-3180,
www.endwave.com.

RS No. 219

AC/DC Transfer Standard

After years of research and development, the company has developed a new process for manufacturing thermal converters. Each unit is now being manufactured with Evanohms' heater wire and cold bead, which results in lower AC/DC and reversal errors. This unit has been tested by national labs and proven to have low errors. The versatility of the new process allows the use of platinum leads for Evanohm leads for heater wire, which results in extremely flat response to 100 MHz and beyond.

MeasureTech Inc.,
formerly Precision Measurements,
Sun Valley, CA (818) 504-2721,
www.measure-tech.com.

RS No. 220

Amplifier Integrated Microwave Assembly

Model 3703A offers a unique combination of power, bandwidth and harmonic suppression in a highly integrated microwave assembly. This model offers a minimum power output of 5 W CW over the frequency range of 0.5 to 18 GHz while suppressing harmonics to a level of –60 dBc minimum. The assembly employs a tandem connection of switches, medium power amplifiers, filters and combining switches to achieve broadband coverage. The implementation shown utilizes mechanical switches to achieve the maximum output power with a band switching speed of 10 milliseconds. The model 3703B is available with PIN diode switches and 1 microsecond switching speed, but maximum output power is limited to 1 W CW. These products were developed to meet flightline military requirements.

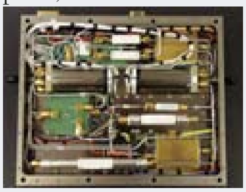

Rodelco Electronics Corp.,
Ronkonkoma, NY (631) 981-0900,
www.rodelcocorp.com.

RS No. 221

5 W High Linearity Amplifier

The model SM2040-37 is a high linearity amplifier designed for multipurpose use in military and commercial applications. The unit operates from 2 to 4 GHz with a P1dB of +37 dBm and OIP3 of +47 dBm. Gain is 37 dB with a flatness of ±0.75 dB across the band. Standard features include a single +12 VDC supply, thermal protection with auto reset and over/reverse voltage protection. In module form, the unit measures 5" × 2.5" × 0.056"; an integral heatsink is also available.

Stealth Microwave Inc.,
Trenton, NJ (609) 538-8586,
www.stealthmicrowave.com.

RS No. 222

SMA Male Termination

The commercial grade 2001-7017-80 is a 10 W SMA male termination that operates in a frequency range from DC to 18 GHz. This model features a lightweight, passivated stainless steel body and coupling nut, gold plated beryllium copper center contact, and a black anodized aluminum heat sink. This product is ideal for test and measurement as well as both military and telecommunications volume production applications that require good long-term performance and low cost.

XMA Corp.,
Manchester, NH (603) 222-2256,
www.xmacorp.com.

RS No. 223

43 dB Dual-directional Coupler

The model C7734 is a low loss, 80:1 bandwidth coupler that covers the entire frequency band from 30 to 2500 MHz, making it ideal for wideband military and commercial applications. This model is rated at 100 W CW, with an insertion loss of 0.35 dB, VSWR (ML) of 1.25, coupling flatness of 40 dB ±1.5 dB and directivity of 18 dB. Size: 3.5" × 2.6" × 0.7".

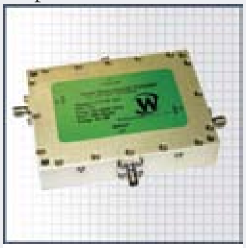

Werlatone Inc.,
Brewster, NY (845) 279-6187,
www.werlatone.com.

RS No. 224

COMPONENTS

Absorptive Switch

The SP3T, absorptive PIN diode switch operates in a frequency range from 2 to 6 GHz.

The isolation is 70 dB with an insertion loss of 3.5 dB and a VSWR of 2.0. The switching speed is 15 ns rise/fall and 100 ns on/off at +20 dBm maximum RF input power. The switch offers TTL control and a DC power supply of +5 VDC at 150 mA maximum and –5 VDC at 100 mA maximum.

American Microwave Corp., Frederick, MD (301) 662-4700, www.americanmicrowavecorp.com.

RS No. 225

Coaxial Attenuators

The EI7004-xx series is RoHS compliant N type, stainless steel, 2 W compact coaxial attenuators.

This series is low in price and covers wireless applications over the DC to 18 GHz frequency range and is available in attenuation values from 1 to 40 dB value. Standard attenuation values include 3, 6, 10, 20 and 30 dB. Standard and custom attenuator kits are also available and are in stock for immediate delivery.

Electronika International Inc., Cleveland, OH (440) 743-7034, www.electronikainc.com.

RS No. 226

Chip and Coaxial Equalizers

These surface-mount chip and coaxial equalizers are designed to compensate frequency variations in RF and microwave subsystems.

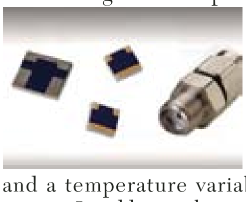

These equalizers are available in a fixed frequency response version and a temperature variable frequency response. In addition, the company can develop custom variations specific to the frequency band and temperature slope characteristics of a customer's application. All EMC equalizers are available with both negative and positive slope coefficients. The CE chip equalizer (1.30 sq in) offers linear broadband fixed slope frequency compensation from 2 to 18 GHz in 1 to 5 dB values.

EMC Technology, Stuart, FL (772) 286-9300, www.emct.com.

RS No. 227

Logarithmic Detector/Controller

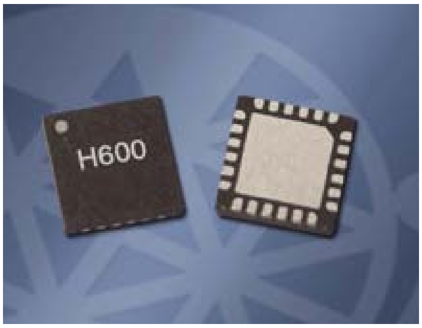

The model HMC600LP4 (E) is a logarithmic detector/controller that is ideal for RF power measurement and control in cellular/3G, telematic, WiMAX and WiBro applications over the 50 MHz to 4 GHz frequency range. This model is fabricated in a SiGe BiCMOS process, and converts RF signals at its differential input to a proportional output DC voltage. The HMC600LP4 (E) delivers an extremely high ±3 dB dynamic range of up to 75 dB, with good accuracy and temperature stability from 50 to 4000 MHz.

Hittite Microwave Corp., Chelmsford, MA (978) 250-3343, www.hittite.com.

RS No. 228

750 MHz to 15 GHz Mixers

The SIM series of frequency mixers operates in broadband and multi-band RF applications

over the frequency range from 750 MHz to 15 GHz. Because of their expansive bandwidth, these double-balanced mixers are also useful for both up and down converting. The low temperature co-fired ceramic (LTCC) leadless package delivers good temperature stability, repeatable performance, high ESD capability and meets the need for high speed automated manufacturing. Price: from $4.95 each (1000). In stock.

Mini-Circuits, Brooklyn, NY (718) 934-4500, www.minicircuits.com.

RS No. 229

10 dB Directional Coupler

The model RFOC-811-QRC-dc-10 is a 10 dB directional coupler with field replaceable SMA

connectors that operates in a frequency range from 8 to 11 GHz. By using the technology of microstripline to stripline transitions, all the feedthrus of input and output ports can be soldered directly to the mechanical housing to have better mechanical support. The coupler is suitable for RF and microwave subsystem integration. The maximum true insertion loss and the minimum directivity of the coupler are 1.6 and 10 dB, respectively. Size: 1" × 0.6" × 0.38".

Planar Monolithics Industries Inc., Frederick, MD (301) 631-1579, www.planarmonolithics.com.

RS No. 231

High Power Transmitter Combiner

These high power transmitter combiners are designed for base station systems including GSM, DCS, PCS and UMTS. Field-tested for true high performance, these combiners have shown excellent low operation temperature and stability for maximum reliability and energy efficiency. Features include: high isolation, low operating temperatures, two separately fused fan banks for redundancy, long life span and a standard 19" – 2U rack size.

Renaissance Electronics Corp., Harvard, MA (978) 772-7774, www.rec-usa.com.

RS No. 234

Two-way Power Divider

The model PS2-52-450/8S is a two-way power divider that operates in a frequency range from

5 to 40 GHz. This model offers a 2.2 dB insertion loss, 13 dB isolation and 1.90 maximum VSWR. Amplitude and phase balance are 0.8 dB and ±10°, respectively. Power rating is 1 W and 2.92 female connectors are utilized.

Pulsar Microwave Corp., Clifton, NJ (973) 779-6262, www.pulsarmicrowave.com.

RS No. 232

Slide Rule Calculator

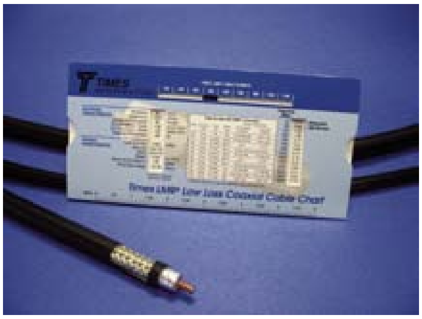

The *LMR*® slide rule calculator has been updated to include new connectors and tools as well as more frequencies. The calculator has a handy chart on one side showing the attenuation in dB/100 feet of each *LMR* cable size at various common frequencies and the key electrical and physical characteristics of each cable. The other side shows the most common *LMR* connectors as well as a listing of the prep and installation tools for use with *LMR* cables and connectors.

Times Microwave Systems, Wallingford, CT (203) 949-8400, www.timesmicrowave.com.

RS No. 236

New Products

GPS Notch Filter

The part number 6R7-1575.42-X15N11 is a highly selective cavity notch filter. This unit is centered at the GPS frequency of 1575.42 MHz and offers a nominal 3 dB bandwidth of 15 MHz. The notch depth is greater than 70 dB at the center frequency ±1 MHz, and has an insertion loss measuring less than 1.25 dB.

Reactel Inc.,
Gaithersburg, MD (301) 519-3660,
www.reactel.com.

RS No. 233

WiMAX Bandpass Filter

This high performance bandpass filter was designed for use in WiMAX base stations filtering broadband information in the 2.5 GHz band. This model offers a maximum 0.7 dB of insertion loss and provides over 30 dB of band rejection at DC to 2.45 GHz and at 2.74 GHz during operation. In addition, this bandpass filter is compact in size with 120 × 90 × 40 mm (4.72" × 3.54" × 1.57"). The bandpass filter is also available with 3.5 GHz frequency band.

Universal Microwave Technology Inc.,
Taipei, Taiwan +886 2 2698 9969,
www.umt-tw.com.

RS No. 237

AMPLIFIERS

Low Noise Amplifiers

The AMFW catalog line of SATCOM waveguide amplifiers utilizes PHEMTs offering low noise figures in the various frequency bands associated with S- and Ka-band satellite communication. Achieving noise temperatures as low as 30 K, these amplifiers have been designed using state-of-the-art technology and can be used in either fixed or transportable applications. The high reliability design of these amplifiers allows the company to offer a standard two-year warranty on units that consistently experience the harsh environments involved with satellite base station operation.

MITEQ Inc.,
Hauppauge, NY (631) 436-7400,
www.miteq.com.

RS No. 239

Low Noise Amplifier

The model PE10WR137-34-68R2-12 is a low noise amplifier that features a removable WR-137 waveguide input and SMA female output connector. This model offers 34 dB typical gain while maintaining a typical noise figure of 0.7 dB (51 K). The output power at 1 dB compression is greater than +2 dBm. Other options are also available.

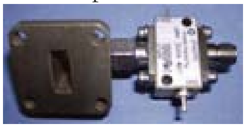

Planar Electronics Technology,
Frederick, MD (301) 662-5019,
www.planarelec.com.

RS No. 240

Low Noise Mixer Preamplifier

The model PKKa-5B is a low noise mixer preamplifier that operates at an LO and RF input frequency from 18 to 40 GHz in WRD-180 waveguide. This mixer-preamplifier offers a double sideband noise figure of only 4 dB typical and 8 dB maximum using an LO input power of 0 to +4 dBm. The PKKa-5B has an IF output frequency of 10 to 500 MHz in SMA(F). RF to IF gain is 25 dB typical. Bias is +15 VDC at 50 mA.

Spacek Labs Inc.,
Santa Barbara, CA (805) 564-4404,
www.spaceklabs.com.

RS No. 241

INTEGRATED CIRCUIT

GaAs MMIC Receivers

These gallium arsenide (GaAs) monolithic microwave integrated circuit (MMIC) receivers are available in RoHS compliant, surface-mount technology packages and operate in a frequency range from 11 to 45 GHz. Features of these parts include high linearity, low noise and broadband performance provided in low cost, standard QFN packages. These receivers are ideal for wireless communications applications such as millimeter-wave point-to-point radio, local multipoint distribution services, SATCOM and VSAT applications.

Mimix Broadband Inc.,
Houston, TX (281) 988-4600,
www.mimixbroadband.com.

RS No. 243

SOURCES

Oven-controlled Crystal Oscillators

These oven-controlled crystal oscillators (OCXO) exhibit a low phase noise of –160 dBc/Hz at 10 kHz. The 9325D has a nominal frequency of 100 MHz improving system phase noise for high frequency applications by lessening the multiplication factor. The device also has tight frequency stability of ±50 ppb maximum over the operating temperature range of –20° to +70°C, and low harmonic distortion of –60 dB typical. It operates on +12 VDC, with an output level of 3 dBm minimum and an output load of 50 Ω. Size: 25.4 × 25.4 mm 5-pin through-hole package with a height of 12.7 mm.

NDK America Inc.,
Belvidere, IL (800) 635-9825, www.ndk.com.

RS No. 245

Temperature-compensated Crystal Oscillator

The model IT5300D is a high stability temperature-compensated crystal oscillator (TCXO) in a 5 × 3.2 mm package. The IT5300D employs an analog IC for temperature compensation providing ±0.16 ppm temperature stability and is available within an operating temperature range from –20° to 70°C. Frequencies are available from 10 to 52 MHz, with either clipped sinewave or HCMOS output. The unit also offers superior phase noise performance and can operate on any supply voltage between 2.7 and 5.5 V.

Rakon Ltd.,
Auckland, New Zealand +64 (9) 573 5554,
www.rakon.com.

RS No. 246

C-band Coaxial Resonator Oscillator

The model CRO3375A-LF is a lead-free, RoHS compliant, coaxial resonator oscillator that operates in C-band (3370 to 3380 MHz) and features low phase noise performance of –113 dBc/Hz at 10 kHz offset from the carrier. The design offers good tuning linearity with a typical tuning sensitivity of 7 MHz/V. It is designed to operate at 5 VDC supply while drawing 21 mA (typical) over the extended operating temperature range of –40° to 85°C. This model is ideally suited for applications that require signal stability, tuning linearity and low phase noise performance. Size: 0.50" × 0.50" × 0.22". Price: \$29.95/VCO (5). Delivery: four weeks.

Z-Communications Inc.,
San Diego, CA (858) 621-2700,
www.zcomm.com.

RS No. 247

TEST EQUIPMENT

Wireless Communications Test Set

This wireless communications test set platform is an ideal solution for calibrating mobile phones in high volume manufacturing. The E6601A is an integrated test system in one box. It features a built-in open Windows® XP PC, which allows test programs to be developed, downloaded and executed directly in the system—eliminating the test system PC and saving system space and cost. With a completely new measurement architecture designed for high speed measurements and good accuracy, repeatability and measurement integrity, the E6601A significantly lowers the cost of mobile phone manufacturing testing.

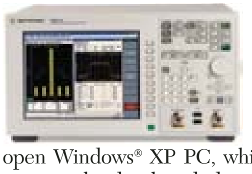

Agilent Technologies Inc.,
Palo Alto, CA (800) 829-4444,
www.agilent.com.

RS No. 248

VNA Hardware and Software

The NM100 VNA+ is a combination of software and hardware, running on top of a VNA and allows the characterization of the harmonic behavior of high frequency components, including diodes, transistors and power amplifiers. On top of the regular capabilities of the VNA, the NM100 measures, in a calibrated way, the incident and reflected waves or voltages and currents at the ports of a component. During measurements, it is submitted to 'realistic conditions' via a periodic harmonic-related stimulus, possibly in combination with tuners. The software includes a user-friendly graphical interface that allows visualization of data in time as well as in the frequency domain. The NM100 supports a frequency range from 600 MHz up to 20 GHz.

NMDG Engineering,
Bornem, Belgium +32 3 890 46 12,
www.nmdg.be.

RS No. 249

Real-time Spectrum Analyzer

The RSA6100A series of real-time spectrum analyzers provides an excellent combination of real-time performance, capture bandwidth and dynamic range to meet the needs of a broad range of digital RF applications. DPX™ waveform image processor technology transforms volumes of real-time data to produce a live RF spectrum presentation that reveals previously unseen RF signals and signal anomalies. Test instruments for digital RF require wide bandwidth with high dynamic range, fast signal capture, and the ability to fully correlate the time, frequency and modulation domains. The first offerings in the RSA6100A series of real-time spectrum analyzers provide 110 MHz real-time bandwidth simultaneous with 73 dB spurious-free dynamic range.

Tektronix Inc.,
Beaverton, OR (800) 835-9433,
www.tektronix.com.

RS No. 250

Microwave Metrics

MEMS Market to Reach $12.5 B in 2010

According to BCC Research, the global market for microelectromechanical systems (MEMS) devices and production equipment was worth an estimated $5 B in 2005, and will increase to $12.5 B through 2010, an average annual growth rate (AAGR) of more than 20%.

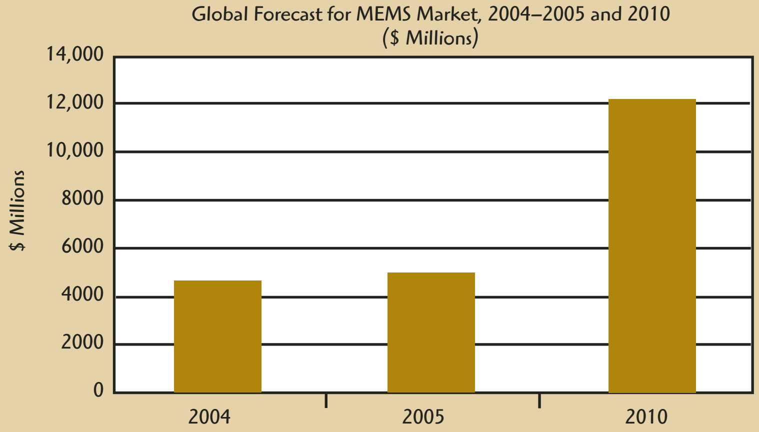

Source: BCC Research, 40 Washington Street, Suite 110, Wellesley, MA 02481 (www.bccresearch.com)

Silicon Carbide Electronics Market to Exceed $50 M by 2009

The market for Silicon Carbide (SiC) devices will exceed $50 M by 2009, according to a new study by WTC, a market research company located in Munich, Germany. The new survey forecasts that the world market for Schottky diodes and power transistors will grow from $13 M in 2004 to over $53 M in 2009, a CAGR of 32%. Schottky diodes will penetrate the microelectronics market at a much higher rate than transistors, which are less mature.

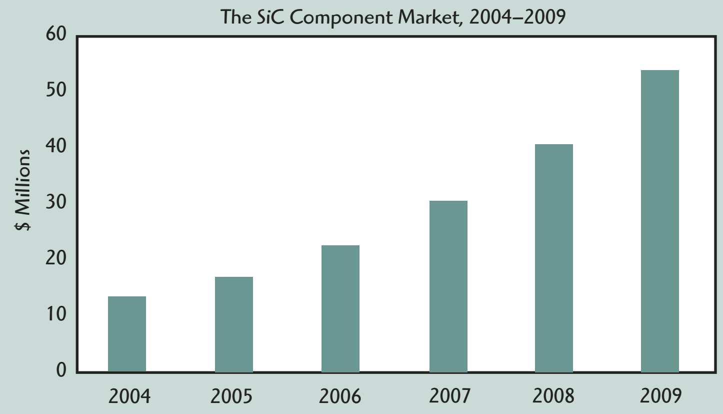

Source: Wicht Technologie Consulting, Frauenplatz 5, D-80331 Munich, Germany (www.wtc-consult.de)

Ultra Wideband Signals and Systems in Communication Engineering

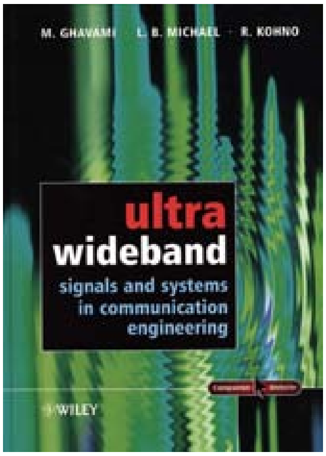

M. Ghavami, L.B. Michael and R. Kohno
John Wiley & Sons Ltd. • 275 pages; $90
ISBN: 0-470-86751-5

This book focuses on the basic signal processing that underlies current and future ultra wideband (UWB) systems. The introduction offers a brief look at why UWB is considered to be such an exciting wireless technology for the near future. Chapter 1 presents the basic properties of UWB. The power spectral density, basic pulse shape and spectral shape of these pulses are examined. Chapter 2 examines in detail how to generate pulse waveforms for UWB systems for both simple cases, such as the Gaussian pulse shape, and more complex orthogonal pulses. Chapter 3 looks at different signal processing techniques for UWB systems. It begins with a review of basic signal processing techniques, including both frequency and time domain. The Laplace, Fourier and z-transform are reviewed and their application to UWB is discussed. The wireless indoor channel and how it should be modeled for UWB communications is considered in Chapter 4. Chapter 5 takes a look at some of the fundamental communication concepts and how they should be applied to UWB. A basic communication system consisting of transmitter, receiver and channel is discussed. Chapter 6 is concerned with ultra wideband antennas and arrays of antennas. This is considered one of the most difficult problems that must be overcome before the widespread commercialization of UWB devices takes place. Positioning and location using both traditional techniques and UWB is discussed in Chapter 7. The advantages of UWB, particularly the extremely precise positioning that is theoretically possible, are examined. Chapter 8 concludes the book with a brief look at some current applications that use UWB technology as well as an overview of current chipsets and possible future UWB products.

To order this book, contact:
John Wiley & Sons Ltd.
The Atrium, Southern Gate
Chichester, West Sussex,
PO19 8SQ, England
+44 1243 779777

Lumped Element Quadrature Hybrids

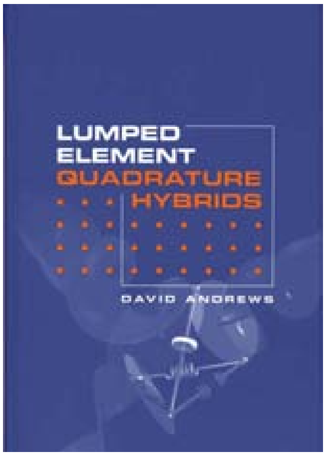

David Andrews
Artech House • 225 pages; $119, £70
ISBN: 1-58053-601-8

Quadrature hybrids find wide applications in radio frequency (RF) and microwave circuits and systems. In answer to this need, considerable attention has been paid to distributed circuits with quadrature properties, particularly for microwave applications. RF engineers too find quadrature hybrids useful, although they prefer lumped element circuits for reasons of size. Microwave engineers will be surprised by the breadth of applications for lumped element quadrature hybrids, which offer the prospects of reduction in circuit size, ease of fabrication and remarkable performance. RF engineers will also find useful the material presented. This book is structured in a similar manner to the treatment of filter theory because the subjects have much in common. Chapter 1 gives an overview of the various forms of quadrature hybrids and their applications, and then shows a method for assessing the relative performance of a particular design. Chapter 2 examines the constraints that theory places on quadrature hybrid circuits, and more particularly, lumped element forms. Chapter 3 is a treatment of the subject of approximation, a concept familiar to the filter designer. Quadrature hybrids are also filter circuits and their performance is one of optimization rather than perfection. Chapter 4 deals with the subject of circuit synthesis and shows how the various approximation functions can be given their expression in electrical networks. Chapter 5, titled "Practical Design," might also be titled "Realizations" and shows how the theoretical circuits can be made in practice. A number of concept circuits are described, illustrating most of the aspects described in the theoretical chapters. The final chapter, "Special Topics," shows how the theory and application of quadrature hybrids can be extended to related matters, which are of themselves also useful.

To order this book, contact:
Artech House
685 Canton St.
Norwood, MA 02062
(781) 769-9750 ext. 4030; or
46 Gillingham St.
London SW1V 1HH UK
+44 (0) 207-8750

Advertising Index

RS No.	Advertiser	Page No.	Phone	Fax	Web Address
1	AA MCS	211	+33(0)8 11 09 76 76	+33(0)1 76 91 50 31	http://mwj.hotims.com/7964-1
2	Advanced Control Components Inc.	193	732-460-0212	732-460-0214	http://mwj.hotims.com/7964-2
3	Advanced Switch Technology	213	613-384-3939	613-384-5026	http://mwj.hotims.com/7964-3
4	Aeroflex	39	516-694-6700	516-694-2562	http://mwj.hotims.com/7964-4
5	Aeroflex/Inmet, Inc.	90	734-426-5553	734-426-5557	http://mwj.hotims.com/7964-5
6	Aeroflex/Weinschel, Inc.	95	800-638-2048	301-846-9116	http://mwj.hotims.com/7964-6
7	Aethercomm	36	760-598-4340	760-598-4342	http://mwj.hotims.com/7964-7
	Agilent Technologies, Inc.	33,41,81,83,85	800-829-4444	415-857-5518	www.agilent.com
8	Allwin Technology, Inc.	192	+86-25-84304950	+86-25-84304959	http://mwj.hotims.com/7964-8
9	American Microwave Corporation	38	301-662-4700	301-662-4938	http://mwj.hotims.com/7964-9
10,11	American Technical Ceramics	84,93	631-622-4700	631-622-4748	http://mwj.hotims.com/7964-10
12	AML Communications Inc.	79	805-388-1345	805-484-2191	http://mwj.hotims.com/7964-12
13	Amphenol RF	82	800-627-7100	203-796-2032	http://mwj.hotims.com/7964-13
14	Anaren Microwave	75	800-411-6596	315-432-9121	http://mwj.hotims.com/7964-14
15	Ansoft Corporation	87	412-261-3200	412-471-9427	http://mwj.hotims.com/7964-15
16	Applied Computational Sciences	104			http://mwj.hotims.com/7964-16
17	Applied Wave Research, Inc.	186	310-726-3000		http://mwj.hotims.com/7964-17
18,19	AR Worldwide	60,69	215-723-8181	215-723-5688	http://mwj.hotims.com/7964-18
20	Arlon-Materials for Electronics Division	171	800-635-9333	302-834-2574	http://mwj.hotims.com/7964-20
22	Association of Old Crows	210	703-549-1600	703-549-2589	http://mwj.hotims.com/7964-22
23	Aviel Electronics, a Division of RF Industries	64	702-739-8155	702-739-8161	http://mwj.hotims.com/7964-23
24	B&Z Technologies	20–21	631-331-0101	631-331-0117	http://mwj.hotims.com/7964-24
8	Caiqin Electronics Elements Co., Ltd.	192	+86-512-58339888	+86-512-58331196	http://mwj.hotims.com/7964-8
25	Chelton & Telecom Microwave, a Cobham company	117	+33 (0) 1 69 02 25 60	+33 (0) 1 69 02 25 99	http://mwj.hotims.com/7964-25
26	Ciao Wireless, Inc.	44	805-389-3224	805-389-3629	http://mwj.hotims.com/7964-26
27	Cobham Defense Electronic Systems – Sensor & Antenna Systems	111	410-542-1700	410-542-9184	http://mwj.hotims.com/7964-27
28	Comtech PST Corp.	205	631-777-8900	631-777-8877	http://mwj.hotims.com/7964-28
29	CPI Beverly Microwave Division	30	978-922-6000	978-922-2736	http://mwj.hotims.com/7964-29
30	Crane Aerospace & Electronics	46	480-961-6269		http://mwj.hotims.com/7964-30
31	CST of America, Inc.	29	781-416-2782	781-576-5702	http://mwj.hotims.com/7964-31
32	CTT Inc.	65	408-541-0596	408-541-0794	http://mwj.hotims.com/7964-32
33	Cuming Microwave Corporation	197	800-432-6464	508-584-2309	http://mwj.hotims.com/7964-33
34	Daico Industries, Inc.	37	310-507-3242	310-507-5701	http://mwj.hotims.com/7964-34
35	Damaskos Inc.	213	610-358-0200	610-558-1019	http://mwj.hotims.com/7964-35
36	Delta Electronics Mfg. Corp.	185	978-927-1060	978-922-6430	http://mwj.hotims.com/7964-36
37	Dynawave Incorporated	101	978-469-0555	978-521-4589	http://mwj.hotims.com/7964-37
38	Eastern Wireless TeleComm, Inc.	142	410-749-3800	410-749-4852	http://mwj.hotims.com/7964-38
39	Electronika International Inc.	213	440-743-7034	440-743-7035	http://mwj.hotims.com/7964-39
40	Elisra Electronic Systems Ltd. (Microwave Division)	31	972(3)6175655	972(3)6175299	http://mwj.hotims.com/7964-40
41	EMC Technology Inc.	17	772-286-9300	772-283-5286	http://mwj.hotims.com/7964-41
42	Emerson Network Power	183	800-247-8256		http://mwj.hotims.com/7964-42
43	Emhiser Micro-Tech	140	775-345-0461	775-345-1152	http://mwj.hotims.com/7964-43
44	Empower RF Systems, Inc.	151	310-412-8100	310-412-9232	http://mwj.hotims.com/7964-44
45	Endwave Defense Systems	27	408-522-3180	408-522-3181	http://mwj.hotims.com/7964-45
46	ET Industries	64	973-394-1719	973-394-1710	http://mwj.hotims.com/7964-46
47	EuMW 2006	123	+ 44 20 7596 8742	+ 44 20 7596 8749	http://mwj.hotims.com/7964-47
48	Filtronic Compound Semiconductors, Ltd.	179	408-850-5740	831-621-8074	http://mwj.hotims.com/7964-48
41	Florida RF Labs Inc.	17	800-544-5594		http://mwj.hotims.com/7964-41
49	Freescale Semiconductor, Inc.	23			http://mwj.hotims.com/7964-49
50	GGB Industries, Inc.	3	239-643-4400	239-643-4403	http://mwj.hotims.com/7964-50
51	Greenray Industries, Inc.	130	717-766-0223	717-790-9509	http://mwj.hotims.com/7964-51
53	Herotek, Inc.	15	408-941-8399	408-941-8388	http://mwj.hotims.com/7964-53
54,13	Huber + Suhner AG	153,82	+41 71 353 41 11	+41 71 353 44 44	http://mwj.hotims.com/7964-54
21	IEEE Boston Section	180	781-245-5405	781-245-5406	http://mwj.hotims.com/7964-21
	IEEE MTT-S International Microwave Symposium – Hawaii	99	781-769-9750	781-769-5037	www.ims2007.org
	IEEE Radio and Wireless Symposium	215	781-769-9750	781-769-5037	www.radiowireless.org
	IEEE RFIC Symposium	191			www.rfic2006.org
55	Ingun Prufmittelbau GmbH	71	+49 7531 8105-0	+49 7531 8105-65	http://mwj.hotims.com/7964-55
52	Innovative Concepts, Inc., A Herley Company	72	703-893-2007	703-991-0432	http://mwj.hotims.com/7964-52
56	Insulated Wire Inc.	173	203-791-1999	203-748-5217	http://mwj.hotims.com/7964-56
57	Integra Technologies, Inc.	80	310-606-0855	310-606-0865	http://mwj.hotims.com/7964-57
58	Ion Beam Milling, Inc.	146	603-644-2326	603-647-6889	http://mwj.hotims.com/7964-58
59	Isola Corp.	201	800-845-2904		http://mwj.hotims.com/7964-59
60	ITT Corporation	139	978-441-0200		http://mwj.hotims.com/7964-60
61,62,63	J microTechnology	213	503-614-9509	503-531-9325	http://mwj.hotims.com/7964-61
64	K&L Microwave, Inc.	7	410-749-2424	443-260-2268	http://mwj.hotims.com/7964-64
65	KOR Electronics	167	714-898-8200	714-895-7526	http://mwj.hotims.com/7964-65
66	L-3 Communications Electron Devices	103	650-591-8411 x 2285		http://mwj.hotims.com/7964-66
67	LNX Corporation	102	603-898-6800	603-898-6860	http://mwj.hotims.com/7964-67

ADVERTISING INDEX

RS No.	Advertiser	Page No.	Phone	Fax	Web Address
68	Locus Microwave, Inc.	108	814-466-6275	814-466-1104	http://mwj.hotims.com/7964-68
69	Logus Microwave Corporation	159	561-842-3550	561-842-2196	http://mwj.hotims.com/7964-69
70	Lorch Microwave	47	800-780-2169	410-860-1949	http://mwj.hotims.com/7964-70
71	M/A-COM, Inc.	11	800-366-2266	978-442-5350	http://mwj.hotims.com/7964-71
72	Marki Microwave, Inc.	107	408-778-4200	408-778-4300	http://mwj.hotims.com/7964-72
73	Maury Microwave Corporation	9	909-987-4715	909-987-1112	http://mwj.hotims.com/7964-73
74	MECA Electronics, Inc.	120	973-625-0661	973-625-9277	http://mwj.hotims.com/7964-74
75	Micro-Coax Components	195	800-223-2629	610-495-6656	http://mwj.hotims.com/7964-75
76	MicroMetrics Inc.	105	603-641-3800	603-641-3500	http://mwj.hotims.com/7964-76
77	Microsemi	76	408-986-8031	408-986-8120	http://mwj.hotims.com/7964-77
78	Microwave Circuit Technology Inc.	106	631-845-1041		http://mwj.hotims.com/7964-78
79	Microwave Communications Laboratories Inc. (MCLI)	13	800-333-6254	727-381-6116	http://mwj.hotims.com/7964-79
80	Microwave Development Laboratories	109	781-292-6680/6684	781-453-8629	http://mwj.hotims.com/7964-80
81	Microwave Filter Company, Inc.	134	800-448-1666	315-463-1467	http://mwj.hotims.com/7964-81
	Microwave Journal	182,217,221	800-225-9977	781-769-5037	www.mwjournal.com
82	Milmega Limited	155	+44 (0) 1983 618004	+44 (0) 1983 811521	http://mwj.hotims.com/7964-82
83	Mimix Broadband, Inc.	COV 3	281-988-4600	281-988-4615	http://mwj.hotims.com/7964-83
84,85,86, 87,88,89, 90,91,92, 93,94,95	Mini-Circuits	4–5,16,35, 51,52,66–67, 91,121,161, 175,207,219	718-934-4500	718-332-4661	http://mwj.hotims.com/7964-84
96	Mini-Systems, Inc.	122	508-695-0203	508-695-6076	http://mwj.hotims.com/7964-96
97,98	MITEQ Inc.	42–43,143	631-436-7400	631-436-7430	http://mwj.hotims.com/7964-97
99	Modular Components National, Inc.	147	410-879-6553	410-638-7356	http://mwj.hotims.com/7964-99
100	MTI Wireless Edge	28	+972-3-9025050	+972-3-9025051	http://mwj.hotims.com/7964-100
101	Narda Microwave-East, an L3 Communications Co.	6	631-231-1700	631-231-1711	http://mwj.hotims.com/7964-101
102	Narda Microwave-West, an L3 Communications Co.	48	916-351-4500	916-351-4550	http://mwj.hotims.com/7964-102
103	Networks International Corporation	172	913-685-3400	913-685-3732	http://mwj.hotims.com/7964-103
104	Nexyn Corporation	18	408-982-9339	408-982-9275	http://mwj.hotims.com/7964-104
105	Noisecom	19	973-386-9696	973-386-9191	http://mwj.hotims.com/7964-105
106	NoiseWave Corp.	8	973-386-1119	973-386-1131	http://mwj.hotims.com/7964-106
107	OML Inc.	177	408-779-2698	408-778-0491	http://mwj.hotims.com/7964-107
108	Pascall Electronics Limited	164,212	+44(0) 1983 817300	+44(0) 1983 564708	http://mwj.hotims.com/7964-108
109	Phase One Microwave Inc.	62	916-784-9072	916-784-9074	http://mwj.hotims.com/7964-109
110	Picosecond Pulse Labs Inc.	73	303-209-8100	303-447-2236	http://mwj.hotims.com/7964-110
111	Planar Monolithic Industries, Inc.	40	301-631-1579	301-662-2029	http://mwj.hotims.com/7964-111
112	Pole/Zero Corporation	89	513-870-9060	513-870-9064	http://mwj.hotims.com/7964-112
113	QuinStar Technology, Inc.	174	310-320-1111		http://mwj.hotims.com/7964-113
114,13,115	Radiall	70,82,162	33-1-49-353535	33-1-48-546363	http://mwj.hotims.com/7964-114
116	Radio Research Instrument Co., Inc.	214	203-753-5840	203-754-2567	http://mwj.hotims.com/7964-116
117	Reactel, Incorporated	14	301-519-3660	301-519-2447	http://mwj.hotims.com/7964-117
118	REMEC Defense & Space	34	858-560-1301		http://mwj.hotims.com/7964-118
119	Renaissance Electronics Corporation	50	978-772-7774	978-772-7775	http://mwj.hotims.com/7964-119
120	RF Micro Devices	77	336-678-5570	336-931-7454	http://mwj.hotims.com/7964-120
121	RFHIC	128	82-31-250-5011	82-31-250-5089	http://mwj.hotims.com/7964-121
122	Richardson Electronics, Ltd.	113	800-737-6937	630-208-2550	http://mwj.hotims.com/7964-122
123	RLC Electronics, Inc.	25	914-241-1334	914-241-1753	http://mwj.hotims.com/7964-123
124	Rogers Corporation	125	480-961-1382	480-961-4533	http://mwj.hotims.com/7964-124
125	Rohde & Schwarz GmbH	59	+49-1805-124242	+49-89-412913777	http://mwj.hotims.com/7964-125
126,13	Rosenberger	129,82	+49-8684-18-0	+49-8684-18-499	http://mwj.hotims.com/7964-126
127	Roswin Inc.	160	+82-41-621-4450	+82-41-621-4451	http://mwj.hotims.com/7964-127
128	RTx Technology Co., LTD.	126	82-31-743-6275~7	82-31-743-6278	http://mwj.hotims.com/7964-128
129	San-Tron Inc.	COV 2	978-356-1585	978-356-1573	http://mwj.hotims.com/7964-129
130	Sarnoff Corporation	110	609-734-2553		http://mwj.hotims.com/7964-130
131	Satellink, Inc.	213	972-487-1434	972-487-1204	http://mwj.hotims.com/7964-131
132	Sector Microwave Industries, Inc.	213	631-242-2300	631-242-8158	http://mwj.hotims.com/7964-132
133	SGMC Microwave	145	321-409-0509	321-409-0510	http://mwj.hotims.com/7964-133
134	Skyworks Solutions, Inc.	55	781-376-3000		http://mwj.hotims.com/7964-134
135	Sonnet Software, Inc.	203	315-453-3096	315-451-1694	http://mwj.hotims.com/7964-135
136	Sophia Wireless Inc.	148	703-961-9573	703-961-9576	http://mwj.hotims.com/7964-136
137	Spacek Labs Inc.	152	805-564-4404	805-966-3249	http://mwj.hotims.com/7964-137
138	Special Hermetic Products, Inc.	182	603-654-2002	603-654-2533	http://mwj.hotims.com/7964-138
139	Spectrum Elektrotechnik GmbH	119	+49-89-3548-040	+49-89-3548-0490	http://mwj.hotims.com/7964-139
140	State of the Art, Inc.	150	800-458-3401	814-355-2714	http://mwj.hotims.com/7964-140
141	Stealth Microwave, Inc.	63	888-772-7791	609-538-8587	http://mwj.hotims.com/7964-141
142	Storm Products Company	141	630-754-3300	630-754-3500	http://mwj.hotims.com/7964-142
143	SV Microwave, Inc.	97	561-840-1800	561-842-6277	http://mwj.hotims.com/7964-143
144	Swift & Associates	115	818-989-1133	818-989-4784	http://mwj.hotims.com/7964-144
145	Symmetricom	32	978-232-1497		http://mwj.hotims.com/7964-145
146,147,148	Synergy Microwave Corporation	57,137,209	973-881-8800	973-881-8361	http://mwj.hotims.com/7964-146
149	Tampa Microwave	96	813-855-2251		http://mwj.hotims.com/7964-149
150	Teledyne Cougar	199	408-522-3838	408-522-3839	http://mwj.hotims.com/7964-150
151	Temp-Flex Cable Inc.	170	508-839-5987		http://mwj.hotims.com/7964-151

ADVERTISING INDEX

RS No.	Advertiser	Page No.	Phone	Fax	Web Address
152	Terabeam/HXI	135	978-521-7300	978-521-7301	http://mwj.hotims.com/7964-152
153	Thermax/CDT	131	888-761-7800	718-746-4190	http://mwj.hotims.com/7964-153
154	Tiger Micro-Electronics Institute	114	+86-28-66070208	+86-28-66070496	http://mwj.hotims.com/7964-154
155	TRAK Microwave Corporation	163	813-901-7200		http://mwj.hotims.com/7964-155
156	Trilithic Inc.	54	800-874-5484	317-895-3612	http://mwj.hotims.com/7964-156
157	TriQuint Semiconductor, Inc.	61	503-615-9000	503-615-8900	http://mwj.hotims.com/7964-157
158	T-Tech, Inc.	132	800-370-1530	770-455-0970	http://mwj.hotims.com/7964-158
159	Tusonix	127	520-744-0400	520-744-6155	http://mwj.hotims.com/7964-159
160	Universal Microwave Components Corporation	214	703-642-6332	703-642-2568	http://mwj.hotims.com/7964-160
161	UTE Microwave Inc.	181	732-922-1009	732-922-1848	http://mwj.hotims.com/7964-161
162	ValueTronics International, Inc.	213	847-468-8258		http://mwj.hotims.com/7964-162
163	Vectron International	133	1-88-VECTRON1	888-FAX-VECTRON	http://mwj.hotims.com/7964-163
164	ViaSat, Inc.	204			http://mwj.hotims.com/7964-164
165	Voltronics Corporation	165	973-586-8585	973-586-3404	http://mwj.hotims.com/7964-165
166	W.L. Gore & Associates, Inc.	196	800-445-GORE		http://mwj.hotims.com/7964-166
167	Weinschel Associates	118	877-948-8342	301-963-8640	http://mwj.hotims.com/7964-167
168	Wenzel Associates, Inc.	88	512-835-2038	512-719-4086	http://mwj.hotims.com/7964-168
169	Werlatone, Inc.	COV 4	845-279-6187	845-279-7404	http://mwj.hotims.com/7964-169
170	Wide Band Systems, Inc.	154	973-586-6500	973-627-9190	http://mwj.hotims.com/7964-170
171	Win Semiconductors Corp.	149	310-530-8485	310-530-8499	http://mwj.hotims.com/7964-171
172	Winchester Electronics	94	203-741-5400	203-741-5500	http://mwj.hotims.com/7964-172
173	Wisewave Technologies, Inc.	169	310-539-8882	310-539-8862	http://mwj.hotims.com/7964-173
174	WV Communications	98	805-376-1820	805-376-1840	http://mwj.hotims.com/7964-174
175	Z~Communications, Inc.	157	858-621-2700	858-621-2722	http://mwj.hotims.com/7964-175

Visit **Microwave Journal** *on the Web at* **www.mwjournal.com**

Visit mwjournal.com/info and enter RS# to request information from our advertisers

SALES REPRESENTATIVES

microwave journal

CARL SHEFFRES, PUBLISHER | **ED JOHNSON, ASSOCIATE PUBLISHER** | **KEN HERNANDEZ, TRAFFIC ADMINISTRATOR**

Eastern and Central Time Zones
Chuck Curley
Eastern Reg. Sales Mgr.
685 Canton Street
Norwood, MA 02062
Tel: (781) 769-9750
FAX: (781) 769-5037
ccurley@mwjournal.com

Michael Hallman
Eastern Reg. Sales Mgr.
4 Valley View Court
Middletown, MD 21769
Tel: (301) 371-8830
FAX: (301) 371-8832
mhallman@mwjournal.com

Eastern and Central Time Zones
Ed Johnson
Associate Publisher
PO Box 5962
Ocala, FL 34478-5962
Tel: (352) 620-2442
FAX: (352) 620-2443
ejohnson@mwjournal.com

Pacific and Mountain Time Zones
Wynn Cook
Western Reg. Sales Mgr.
PO Box 23200
San Jose, CA 95153
Tel: (408) 224-9060
FAX: (408) 224-6106
wcook@mwjournal.com

International Sales
Richard Vaughan
International Sales Manager
Tel: +44 207 596 8742
rvaughan@horizonhouse.co.uk

Michel Zoghob
Deputy Publisher
Tel: +44 207 596 8741
mzoghob@horizonhouse.co.uk

46 Gillingham Street
London SW1V 1HH, England
Tel: +44 207 596 8740
FAX: +44 207 596 8749

Germany, Austria, and Switzerland (German-speaking)
Juergen Wissling
Wissling Marketing Services
Riedstrasse 5
72813 St. Johann-Wuertingen
Germany
Tel: +49 7122 828140
FAX: +49 7122 828145
jwissling@horizonhouse.com

Israel
Oreet Ben Yaacov
Oreet International Media
15 Kineret Street
51201 Bene-Berak, Israel
Tel: +972 3 570 6527
FAX: +972 3 570 6526
obenyaacov@horizonhouse.com

Korea
Young-Seoh Chinn
JES Media International
2nd Floor, ANA Bldg.
257-1, Myungil-Dong
Kangdong-Gu
Seoul, 134-070 Korea
Tel: +82 2 481-3411
FAX: +82 2 481-3414
yschinn@horizonhouse.com

Japan
Katsuhiro Ishii
Ace Media Service Inc.
12-6, 4-Chome,
Nishiiko, Adachi-Ku
Tokyo 121-0824, Japan
Tel: +81 3 5691 3335
FAX: +81 3 5691 3336
amskatsu@dream.com